

A
F
T
ACTA
FACULTATIS
TECHNICAE



TECHNICAL UNIVERSITY IN ZVOLEN

1

ISSUE: XXV
ZVOLEN 2020

Medzinárodný zbor recenzentov / International Reviewers Board

Witold Bialy (PL)

Silesian University of Technology, Faculty of Organization and Management

Igor Đukić (HR)

University of Zagreb, Faculty of Forestry

Jiří Dvořák (CZ)

Czech University of Life Sciences Prague, Faculty of Forestry and Wood Sciences

Ladislav Dzurenda (SK)

Technical University in Zvolen, Faculty of Wood Sciences and Technology

Roman Gálik (SK)

Slovak University of Agriculture in Nitra, Faculty of Engineering

Zhivko Gochev (BG)

University of Forestry, Faculty of Forest Industry

Radek Knoflíček (CZ)

Brno University of Technology, Faculty of Mechanical Engineering)

Zdeněk Kopecký (CZ)

Mendel University in Brno, Faculty of Forestry and Wood Technology

Ján Kosiba (SK)

Slovak University of Agriculture in Nitra, Faculty of Engineering

Dražan Kozak (HR)

Josip Juraj Strossmayer University of Osijek, Mechanical Engineering Faculty

Antonín Kříž (CZ)

University of West Bohemia, Faculty of Mechanical Engineering

Stanisław Legutko (PL)

Poznan University of Technology

Oleg Machuga (UA)

National Forestry University of Ukraine, Lviv

Milan Malcho (SK)

University of Zilina, The Faculty of Mechanical Engineering

Stanislav Marchevský (SK)

Technical University of Košice, Faculty of Electrical Engineering and Informatics

Ján Mihalík (SK)

Technical University of Košice, Faculty of Electrical Engineering and Informatics

Miroslav Müller (CZ)

Czech University of Life Sciences Prague, Faculty of Engineering

Nataša Náprstková (CZ)

UJEP in Ustí nad Labem, Faculty of Production Technology and Management

Jindřich Neruda (CZ)

Mendel University in Brno, Faculty of Forestry and Wood Technology

Alena Očkajová (SK)

Matej Bel University, Faculty of Natural Sciences

Marián Peciar (SK)

Slovak University of Technology in Bratislava, Faculty of Mechanical Engineering

Krzysztof Zbigniew Rokosz (PL)

Koszalin University of Technology, Faculty of Mechanical Engineering

Juraj Ružbarský (SK)

Technical University of Košice, Faculty of Manufacturing Technologies

Ruslan Safin (RU)

Kazan National Research Technological University

Sergey Spiridonov (RU)

State Institution of Higher Professional Education, Saint Petersburg State

Dana Stančeková (SK)

University of Žilina, Faculty of Mechanical Engineering

Vladimír Štollmann (SK)

Technical University in Zvolen, Faculty of Forestry

Marian Šušniar (HR)

University of Zagreb, Faculty of Forestry

Paweł Tylek (PL)

University of Agriculture in Krakow, Faculty of Forestry

Valery Zhylinski (BY)

Belarusian State Technological University

TABLE OF CONTENTS

SCIENTIFIC PAPERS

EFFECT OF TEMPERATURE OF HEAT TREATMENT OF OAK WOOD AND TECHNOLOGICAL PARAMETERS OF MILLING ON ENERGETIC EFFICIENCY WHEN PLANAR MILLING VPLYV TEPLoty TEPELNEJ MODIFIKÁCIE DUBOVÉHO DREVA A TECHNOLOGICKÝCH PARAMETROV FRÉZOVANIA NA ENERGETICKÚ ÚČINNOSŤ PRI ROVINNOM FRÉZOVANÍ Peter Koleda, Štefan Barcík, Michal Korčok, Zuzana Jamberová	9
COMPARING THE VARIOUS METHODS FOR MACHINE WRITTEN CHARACTER RECOGNITION POROVNANIE RÔZNYCH METÓD NA ROZPOZNÁVANIE STROJOM PÍSANÝCH ZNAKOV Ladislav Karrach, Elena Pivarčiová	21
METHOD FOR WOOD COLOUR DETERMINING IN DIGITAL IMAGE METÓDA URČOVANIA FARBY DREVA V DIGITÁLNO M OBRAZE Pavol Koleda	35
CONSTRUCTION OF THE LOADED HANDLING PART OF A PNEUMATIC MANIPULATOR KONŠTRUKCIA ZAŤAŽENEJ MANIPULAČNEJ ČASTI PODTLAKOVÉHO MANIPULÁTORA Mária Vargovská, Martin Mokryš, Ľubomír Javorek, Ján Svoreň	43
EFFECT OF FEED SPEED AND TYPE OF ROUTING TO TOTAL FORCE EFEKT POSUVNEJ RÝCHLOSTI A SPÔSOBU FRÉZOVANIA NA CELKOVÚ SILU Ľubomír Javorek	55
APPLICATION OF SELECTED REVERSE ENGINEERING TECHNIQUES IN THE CREATION OF CAD MODEL OF A PART WITH A COMPLEX SHAPE APLIKÁCIA VYBRANÝCH POSTUPOV REVERZNÉHO INŽINIERSTVA PRI TVORBE CAD MODELU TVAROVO ZLOŽITEJ SÚČIASTKY Mária Hrčková, Pavol Koleda, Marek Kassai	63
ELIMINATING THE MALFUNCTION OF THE VEHICLE COOLING SYSTEM BY USING THERMO DIAGNOSTICS METHODS ODSTRÁNENIE PORUCHY CHLADIACEHO SYSTÉMU VOZIDLA POMOCOU TERMODIAGNOSTICKÝCH METÓD Pavol Harvánek, Ján Kováč, Ján Melicherčík	75

COMPARISON OF CASE STUDIES OF VIBRO, THERMAL AND ACOUSTIC DIAGNOSTICS METHODS POROVNANIE PRÍPADOVÝCH ŠTÚDII VIBRAČNEJ, TEPELNEJ A AKUSTICKEJ DIAGNOSTIKY Silvia Kopčanová, Marián Kučera	85
ANALYSIS OF TECHNICAL PARAMETERS OF HARVESTER HEADS IN FORESTRY ANALÝZA TECHNIKÝCH PARAMETROV HARVESTEROVÝCH HLAVÍC V LESNÍCTVE Ján Melicherčík, Jozef Krilek, Pavol Harvánek	95
INVESTIGATION ON HEAT TRANSFER AND TEMPERATURE PROFILE OF COUNTERCURRENT AND PARALLEL FLOW ARRANGEMENT IN A PLATE HEAT EXCHANGER VYŠETROVANIE PRENOSU TEPLA A TEPLOTNÉHO PROFILU V PROTIPRÚDOVOM A PARALELNOM DOSKOVOM VÝMENNÍKU TEPLA Mohammad Emal Qazizada, Elena Pivarčiová	103

SCIENTIFIC PAPERS

EFFECT OF TEMPERATURE OF HEAT TREATMENT OF OAK WOOD AND TECHNOLOGICAL PARAMETERS OF MILLING ON ENERGETIC EFFICIENCY WHEN PLANAR MILLING

VPLYV TEPLoty TEPELNEJ MODIFIKÁCIE DUBOVÉHO DREVA A TECHNOLOGICKÝCH PARAMETROV FRÉZOVANIA NA ENERGETICKÚ ÚČINNOSŤ PRI ROVINNOM FRÉZOVANÍ

Peter Koleda, Štefan Barčík, Michal Korčok, Zuzana Jamberová

Department of Manufacturing and Automation Technology, Technical University in Zvolen, T. G. Masaryka 24, 960 01 Zvolen, Slovakia, peter.koleda@tuzvo.sk

ABSTRACT: Woodworking is an interest in scientific studies from the perspective of the final product quality and the machining process itself. Thermally modified wood is increasingly used in interior and exterior spaces, where its properties make it more resistant to natural wood. The article deals with the energy intensity of milling of thermally modified oak wood (*Quercus petraea.*) by ThermoWood® technology. The investigated technological parameters are the thermal modification temperatures (160, 180, 200 and 220 °C) and the material of the cutting tool. As the temperature of the thermal modification increases, the cutting power decreases due to a decrease in the density of the wood. The lowest energy consumption is at the milling of wood modified at 220 °C, cutting speed of 20 m.s⁻¹ and rake angle of 30 °C.

Keywords: Milling, energetic efficiency, ThermoWood®, *Quercus petraea.*

ABSTRAKT: Obrábanie dreva je vo vedeckom záujme z hľadiska kvality finálneho produktu a samotného procesu obrábania. Termicky modifikované drevo má stále väčšie využitie v interiéri aj exteriéri, kde má lepšie vlastnosti oproti prírodnému drevu. Článok sa zaoberá energetickou účinnosťou termicky modifikovaného dubového dreva (*Quercus petraea.*) technológiou ThermoWood®. Skúmané parametre sú teplota termickej modifikácie (160, 180, 200 a 220 °C) a materiál rezného nástroja. Zvyšovaním teploty termickej modifikácie sa rezný príkon znižuje, zvyšovaním reznej rýchlosti sa znižuje. Najnižšie hodnoty rezného príkonu boli namerané pri uhle reznej hrany 30°, teplote termickej modifikácie 220 °C a reznej rýchlosti 20 m.s⁻¹.

Kľúčové slová: Frézovanie, energetická účinnosť, ThermoWood®, *Quercus petraea.*

INTRODUCTION

A large number of wood products are produced in the industry so that one of the production processes is also the plane milling. This process can be considered by the size

of the cutting capacity, quality of machined surface, the wear of the cutter blade, safety and ambient noise load. The first three criteria, which form a significant part of costs in financial balance, are of interest to every company from the point of view of economy. The reduction of costs is possible only based on a deeper knowledge of the process, which justifies further research. Unfortunately, only a limited number of research papers are focused on the issue of energy consumption of thermally modified wood woodworking or its optimisation (Moura *et al.* 2011; Barcik and Gašparík 2014; Tu *et al.* 2014; Koleda *et al.* 2018).

(Mandic *et al.* 2010) examined the impact of feed speed on cutting power during plane milling beech samples. Cutting power significantly increased at the feed speed $v_f > 8$ m.min⁻¹. (Kubš *et al.* 2016, 2017), based on their research of the beech and pine wood machining, have shown, that the most important factors affecting the cutting power during plane milling are: cutting speed, face angle of the milling cutter face and feed speed. Larger differences in power have been demonstrated at different face angles of the milling cutter.

(Ispas *et al.* 2016) examined the impact of cut depth (1, 2 and 3 mm) of beechwood samples on cutting power during plane milling. The results of the experimental measurements showed that the cutting power increased at all samples with increasing cut depths, revolutions (3300 and 4830 min⁻¹) and feed speeds (4.5, 9, 13.5, 18 and 22.5 m.min⁻¹).

(Krauss *et al.* 2016) carried out a research in which they analysed the impact of cut depth (0.5, 1.0 and 2.0 mm) of the pine samples on the cutting power during the plane milling. The results of the research have shown that cutting power at plane milling of wood increases with the increasing depth of cut.

(Koleda and Hřčková 2018) measured dimensions of fractional particles resulting from the milling with prediction of the tool wear.

Heat-treated wood has been extensively manufactured for more than 10 years, and its production has been introduced to many Western European countries in response to changing chemical wood treatment legislation (International ThermoWood Association 2003). Finland pioneered the production of thermally modified wood called ThermoWood® in 1990. Later, ThermoWood® began to be produced in the Netherlands, Germany, Austria, and France (International ThermoWood Association 2003; Gaff *et al.* 2015).

Heat treatment is a method of modifying the wood structure by means of high temperature, humidity or a bath of oil. The technology itself depends on the country where it was developed. The main differences between these methods are based on the materials (e.g. wood species, fresh or dried wood, moisture content, dimensions), process conditions applied (e.g. one or two process stages, wet or dry process, heating medium, oxygen or nitrogen as sheltering gas, heating and cooling down velocity) and the equipment necessary for treatment (e.g. process vessel, kiln) (Boonstra *et al.* 2007; Boonstra 2008). This has a positive effect on wood's properties. The primary aim of thermally modifying wood is to prepare a material that balances the following benefits: a lower hygroscopicity; higher dimensional stability; higher resistance to wood-decaying and discolouring fungi, moulds, and ligniperdous insects; maintaining or improving the aesthetics (colour, minimal cracks, gloss, texture, etc.); and preservation or improvement of the mechanical properties (strength hardness, stiffness, etc.) (Požgaj *et al.* 1997; Bengtsoon *et al.* 2003; Niemz *et al.* 2010; Barcik and Gašparík 2014).

The aim of article is to evaluate the effect of technology (temperature) of heat treatment, rake angle and cutting speed on energetic efficiency when planar milling oak wood.

MATERIAL AND METHODS

Samples of *Quercus petraea* wood with an average age of 107 years from locality Vlčí jarok (Budča, Slovakia) were used in the experimental tests. The samples were made via ThermoWood® technology at the Arboretum of the Faculty of Forestry and Wood Sciences (Czech University of Life Sciences in Prague) in Kostelec nad Černými lesy in the chamber LAC S400/03 type manufactured by KATRES s.r.o.(Ltd.). The mechanical woodworking of samples with the dimensions of 500 mm × 110 mm × 20 mm and their subsequent heat treatment at temperatures of 160, 180, 200, and 220 °C were performed using the technologies described in (Hrčková *et al.* 2018). The samples were stored at a temperature of 10 °C. The samples remained in the chamber until they cooled to 60°C; then, they were taken out. The process of temperature change itself (heating, temperature exposure, cooling) in time is illustrated in Fig. 1. The density measurements and cutting conditions were as in (Koleda *et al.* 2018). The samples were milled on a lower spindle milling machine FVS (Czechoslovakia Music Instruments, Hradec Králové, Czech Republic) and feeding mechanism ZMD 252/137 (Frommia, Fellbach, Germany) at Technical University in Zvolen, Slovakia. Table 1 shows the technical parameters of the milling machine. The device for power consumption measurement at milling consists of a frequency converter that controls the speed of a three-phase asynchronous motor. Another part of the device is a sinusoidal filter that smoothed the impulse voltage from the inverter in such a way as to approximate the ideal sinusoidal phase with a phase shift of 120°. The frequency converter evaluated the active motor input without losses and engine power from the current, voltage and efficiency of the motor. The cutting power was calculated as the difference between power when milling and power when idling.

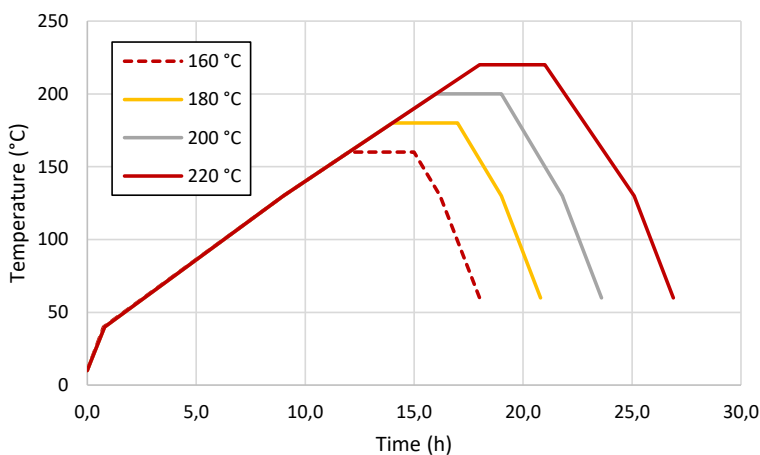


Fig. 1 Times of thermal treatment of oak wood (*Quercus petraea*)
Obr. 1 Časový priebeh termickej modifikácie duba letného (*Quercus petraea*)

Table 1 Technical Parameters of the Lower Spindle Milling Machine FVS and the Feeder
 Tabuľka 1 Technické parametre spodnej vretenovej frézky a podávacieho mechanizmu

Lower Spindle Milling Machine ¹⁾ (FVS)		Feeder ²⁾ (Frommia ZMD 252/137)	
Voltage System ³⁾ (V)	360 and 220	Feed Range ⁶⁾ (m.min ⁻¹)	2.5, 10, 15, 20, and 30
Frequency ⁴⁾ (Hz)	50	Voltage ⁷⁾ (V)	380
Input ⁵⁾ (kW)	4	Speed ⁸⁾ (m.min ⁻¹)	2800

¹⁾Spodná vretenová frézka, ²⁾Podávač, ³⁾Napät'ový systém, ⁴⁾Frekvencia, ⁵⁾Vstupný výkon, ⁶⁾Rozsah posuvov, ⁷⁾Napätie, ⁸⁾Rýchlosť

A double-blade wood cutter block with a rake angle (γ) of 15°, 20°, and 30° and interchangeable blades was used for milling (Fig. 2) with cutting depth of 1 mm. The cutting tool geometry and the cutting speed (20, 40, and 60 m.s⁻¹) and feed rate (6, 10, and 15 m.min⁻¹) were the same as those used in (Koleda *et al.* 2018). Three sets of knives were used when milling:

1. knives induction hardened from material 19 573,
2. knives from steel HSS 18%W with coating AlTiCrN,
3. knives from steel MAXIMUM SPECIAL 55: 1985/5.

Measured data was processed using MS Excel and statistically evaluated by STATISTICA 12.

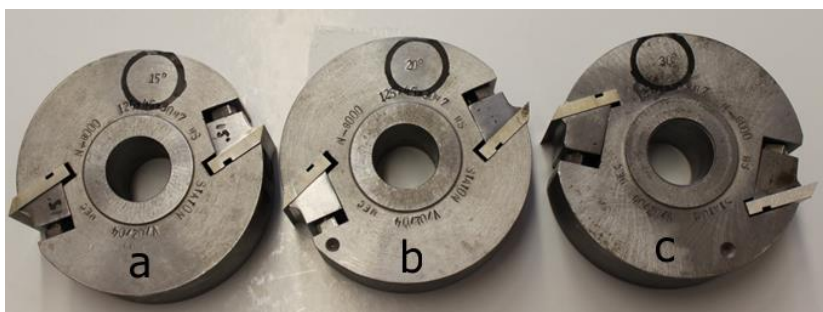


Fig. 2 Milling cutters with rake angles of 15° (a), 20° (b), and 30° (c)
 Obr. 2 Frézovacie hlavy s uhlami 15° (a), 20° (b), and 30° (c)

RESULTS AND DISCUSSION

Table 1 and fig. 3 show the density values of the samples. As the temperature of heat treatment rises, the density decreases. The natural wood sample shows the highest density of 775.85 kg.m⁻³. The thermally treated sample shows the lowest density at the highest temperature of 220 °C, which is a decrease of 21.51 % compared to a sample that has not been heat-treated. Thermal treatment makes wood more fragile. Hydrophilic functional groups begin to disappear in structures of the polysaccharides, lignin and accompanying materials.

Table 2 Density of samples
Tabuľka 2 Hustota vzoriek

Temperature ¹⁾	Density ²⁾ (kg.m ⁻³)	Drop compered with N ³⁾ (%)
N	775.85	–
160	719.73	7,23
180	687.39	11.40
200	617.84	20.37
220	608.96	21.51

¹⁾Teplota, ²⁾Hustota, ³⁾Pokles voči prírodnému drevu (N)

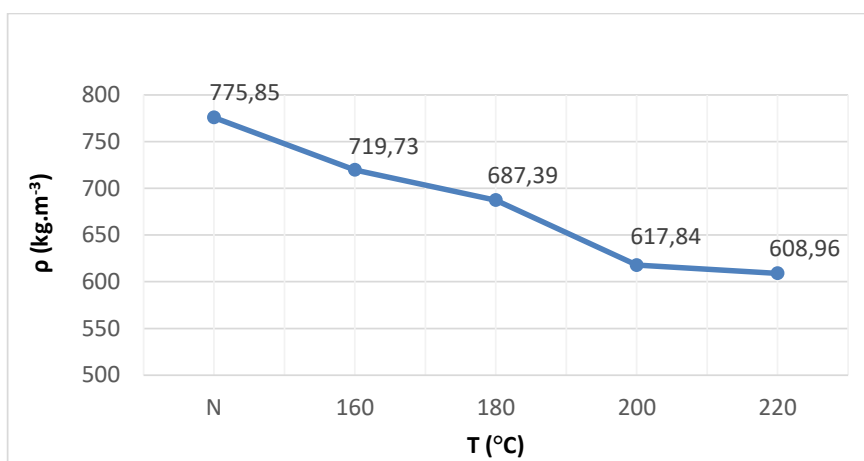


Fig. 3 Dependence of density on temperature of thermal treatment
Obr. 3 Závislosť hustoty vzoriek na teplote termickej úpravy

Table 3 shows the basic cutting power statistics depending on the thermal modification temperature. With increasing temperature, the cutting power decreases. The highest cutting power was measured for the native wood and the lowest for the sample that was thermally modified at 220 °C. The decrease is caused by a change in the structure of the wood and its chemical composition due to temperature, which is also reflected in its lower density. Nociarová (2017) and Il'áš (2018) showed the same decreasing trend of the total power consumption depending on the temperature of the thermal treatment of oak wood.

The structure of the examined samples influenced the power values recorded during milling, as the experimental samples were extracted from different logs and were manipulated from different parts of the trunk. Further research of the heat transfers of thermally modified wood by a holography interferometer could find out the values of the heat transfer coefficients (Černecký *et al.* 2013, 2015).

Table 3 Basic statistic of cutting power depending on temperature
 Tabuľka 3 Základná štatistika závislosti rezného príkonu na teplote

T (°C)	Number ¹⁾	Average power ²⁾ (W)	St. dev. ³⁾ (W)	Error ⁴⁾ (W)	-0.95% interval (W)	+0,95% interval (W)
N	5670	146,76	71,27	0,95	144,90	148,62
160	5670	119,16	62,68	0,83	117,53	120,79
180	5670	103,78	54,80	0,73	102,35	105,20
200	5670	99,63	53,85	0,72	98,23	101,04
220	5670	89,07	48,00	0,64	87,82	90,32

¹⁾Počet údajov, ²⁾Priemerný príkon, ³⁾Smerodajná odchýlka, ⁴⁾Chyba

Fig. 4 shows the influence of the cutting tool on the cutting power depending on the temperature. Cutting tool set No. 2 (HSS 18% W with AlTiCrN coating) shows the lowest energy consumption in all samples, with the cutting power decreasing as the temperature increases. For cutting tool No. 1 (knives induction hardened from material 19 573) and No. 3 (knives made from steel MAXIMUM SPECIAL 55: 1985/5), the values are overlapping. The highest cutting power values were recorded at tool set No. 1 (Knives Surface Induction Hardened 19 573), whereby they overlap with the cutting power values measured at set No. 3 (knives made of steel MAXIMUM SPECIAL 55: 1985/5). The different values are due to the wear and hardness of the material depending on the knife hardening technology 1, the coating of the blades 2 and 3 and their grinding before coating.

From the point of view of heat treatment, the highest cutting power was recorded for the native wood and the lowest for the heat-treated sample at 220 °C, regardless of the type of cutting tool set. As the temperature rises (thermally modified wood), the power decreases when milling. The reduction in milling power consumption is reported in (Krauss *et al.* 2016) when milling of thermally treated pine wood. This is related to a change in the chemical composition and structure of the wood and a change in its density.

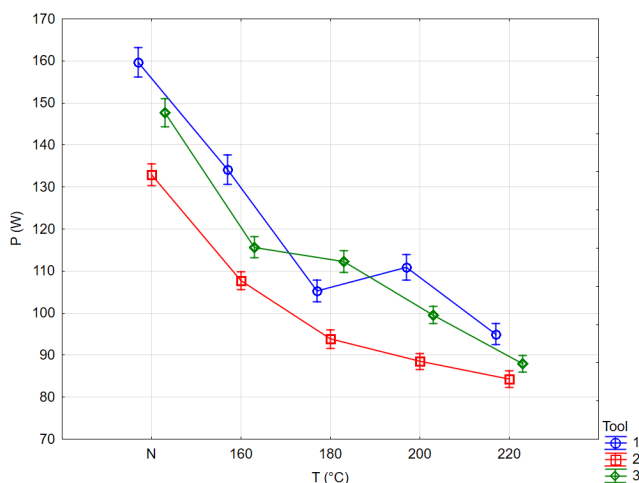


Fig. 4 Analysis of variance of cutting power dependence on temperature of thermal treatment and tool set

Obr. 4 Analýza rozptylu závislosti rezného príkonu na type nástroja a teplote termickej úpravy

Fig. 5 show the basic statistic for cutting power depending on the heat treatment and the tool material. The highest average cutting power value of 159,65 W was at the native wood machined with the tool set No. 1 (19 573 surface induction hardened knives). The lowest average cutting power value of 84.24 W was captured at the thermally treated sample at 220 °C, machined with the tool set No. 2 (HSS 18% W AlTiCrN knives).

Table 4 shows the basic statistics of the dependency of the cutting power on the rake angle. Figures 5 and 6 show the analysis of variance of cutting power versus temperature of thermal modification and rake angle. As the rake angle increased, the cutting power dropped. For all technologies of heat treatment, the lowest cutting power was achieved at rake angle of 30°. Its lowest value (69,1 W) was measured at the rake angle of 30° at the sample treated at the temperature of 220 °C, the highest (183,56 W) at rake angle of 15° at the untreated sample. This is due to a change in the force conditions for chip separation and a reduction in the cutting force required to separate the material.

Table 4 Basic statistic of cutting power depending on rake angle.

Tabuľka 4 Základná štatistika závislosti rezného príkonu na uhle čela

γ (°)	Number ¹⁾	Average power ²⁾ (W)	St. dev. ³⁾ (W)	Error ⁴⁾ (W)	-0,95% interval (W)	+0,95% interval (W)
15	9450	130,37	64,28	0,66	129,08	131,67
25	9450	119,36	66,37	0,68	118,02	120,69
30	9450	85,30	43,46	0,44	84,42	86,17

¹⁾Počet údajov, ²⁾Priemerný príkon, ³⁾Smerodajná odchýlka, ⁴⁾Chyba

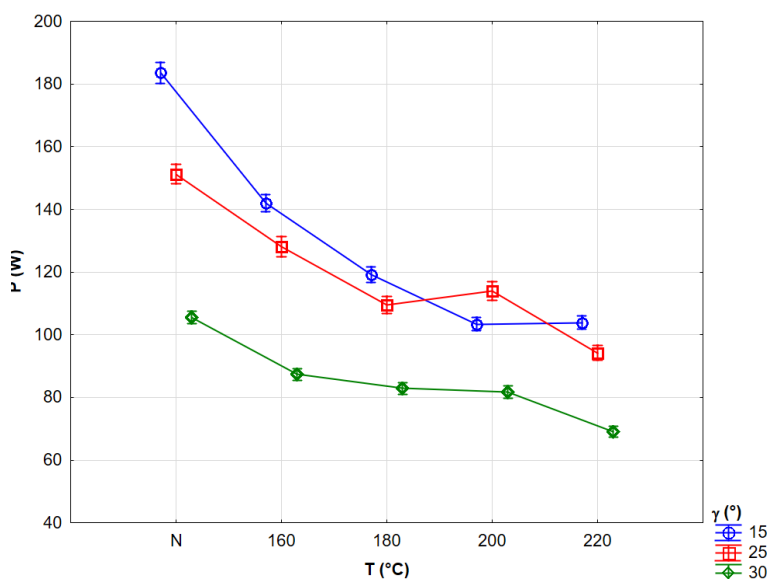


Fig. 5 Analysis of variance of cutting power dependence on temperature of thermal treatment and rake angle

Obr. 5 Analýza rozptylu závislosti rezného príkonu na teplote a uhle čela

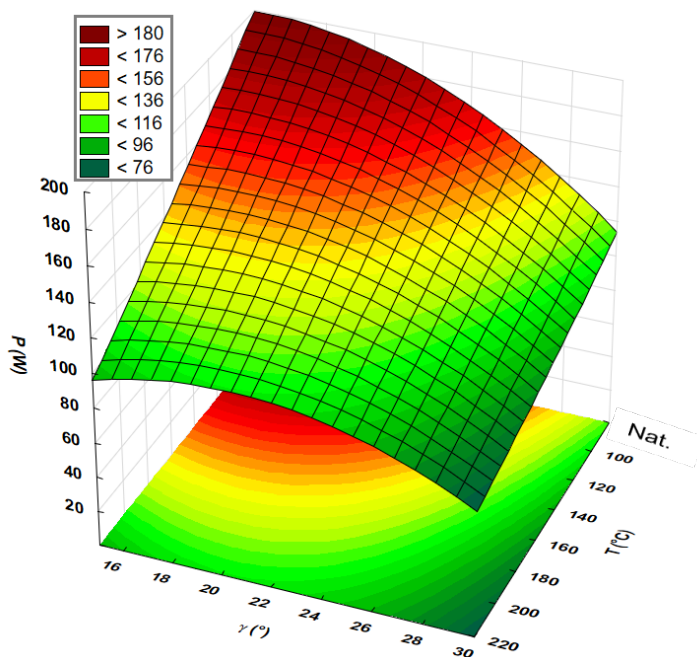


Fig. 6 Two-parameter analysis of variance of cutting power dependence on temperature and rake angle

Obr. 6 Dvojparametrická analýza rozptylu závislosti rezného príkonu na teplote a uhle čela

Table 5 shows the basic statistics of cutting power dependence on cutting speed. With increasing cutting speed, the cutting power increased. Figure 7 and 8 show the analysis of variance of cutting power versus temperature and cutting speed. Increasing cutting speed also increases cutting power, which results from the relation for calculating cutting power as a product of elementary cutting force and cutting speed (Vasilko 2007). The highest cutting power (201,02 W) was measured at native wood and cutting speed of 60 m.s⁻¹, the lowest (47,71 W) at wood treated at 220 and speed 20 m.s⁻¹. For all technologies of heat treatment, the highest cutting power was achieved at cutting speed 60 m.s⁻¹, the lowest at cutting speed 20 m.s⁻¹.

Table 5 Basic statistic of cutting power depending on cutting speed

Tabuľka 5 Základná štatistika závislosti rezného príkonu na reznej rýchlosti

v_c (m.s ⁻¹)	Number ¹⁾	Average Power ²⁾ (W)	St. dev ³⁾ . (W)	Error ⁴⁾ (W)	-0.95% Interval (W)	+0.95% Interval (W)
20	9450	61,15	26,93	0,27	60,61	61,69
40	9450	113,11	45,99	0,47	112,18	114,04
60	9450	160,76	61,04	0,62	159,53	162,00

¹⁾Počet údajov, ²⁾Priemerný príkon, ³⁾Smerodajná odchýlka, ⁴⁾Chyba

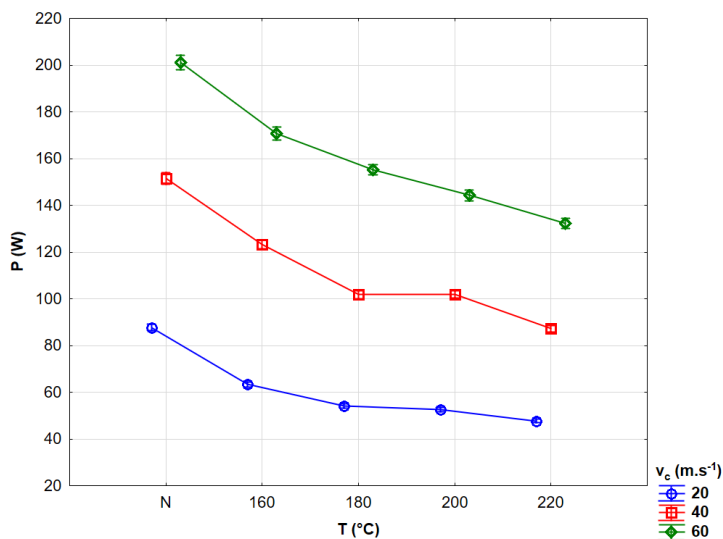


Fig. 7 Analysis of variance of cutting power dependence on temperature of thermal treatment and cutting speed
 Obr. 7 Analýza rozptylu závislosti rezného príkonu na teplote a reznej rýchlosti

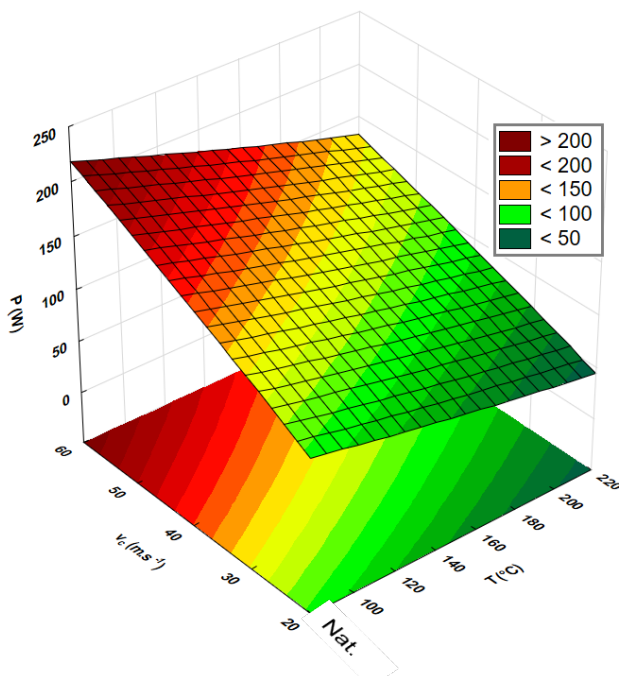


Fig. 8 Two-parameter analysis of variance of cutting power dependence on temperature and cutting speed
 Obr. 8 Dvojparametrická analýza rozptylu závislosti rezného príkonu na teplote a reznej rýchlosti

CONCLUSION

The energy consumption of the machining process is an object of research to optimize production and production costs. When milling thermally modified oak wood, it was confirmed that the cutting power decreases with increasing modification temperature. This is related to a change in the chemical composition and structure of the wood and a change in its density. Therefore, the qualitative parameter of the treated surface and the product should also be considered.

The surface treatment of the cutting tool affects the size of the cutting power. The lowest energy consumption for milling (84.24 W for treatment temperature of 220 °C) was measured using knives from steel HSS 18% W with AlTiCrN coating. The highest values (159.65 W, untreated sample) were recorded for milling with knives induction hardened from material 19 573.

The cutting speed affects the cutting power. Increasing cutting speed also increases cutting power. The rake angle influences cutting power. Raising the rake angle the cutting power decreases. Further research will be focused on the influence of other technological parameters on the cutting power and the quality of the machined surface.

ACKNOWLEDGEMENT

The paper was written within the project VEGA 1/0315/2017: Research of relevant properties of thermally modified wood at a contact effects in the machining process with the prediction of obtaining an optimal surface, and the project of Internal Project Agency No. 2/2019: Impact of selected technological, tool and material factors on the surface finish quality and energetic intensity at plane milling of thermally modified spruce wood.

REFERENCES

- BARCÍK, Š., GAŠPARÍK, M. 2014. Effect of tool and milling parameters on the size distribution of splinters of planed native and thermally modified beech wood. In *BioResources*, vol. 9, no. 1, pp. 1346-1360. doi: 10.15376/biores.9.1.1346-1360.
- BARCÍK, Š., KMINIAK, R., ŘEHÁK, T., KVIETKOVÁ, M. 2010. The influence of selected factors on energy requirements for plain milling of beech wood. *Journal of Forest Science*56(5), 243-250
- BENGTSSON, C., JERMER, J., CLANG, A., EK-OLAUSSON, B. 2003. Investigation of Some Technical Properties of Heat-treated Wood (IRG/WP 03-40266), International Research Group on Wood Protection. Brisbane, Australia.
- BOONSTRA, M. J., VAN ACKER, J., PIZZI, A. 2007. Anatomical and molecular reasons for property changes of wood after full-scale industrial heat-treatment. In *Proceedings of the Third European Conference on Wood Modification*. Cardiff, UK, pp. 343-358.
- BOONSTRA, M. J. 2008. A Two-stage Thermal Modification of Wood, Ph.D. dissertation in cosupervision Ghent University and Université Henry Poincaré - Nancy 1, 297 p.
- ČERNECKÝ, J., KONIAR, J., BRODNIANSKÁ, Z. 2013. The effect of regulating elements on convective heat transfer along shaped heat exchange surfaces. In *Chemical and Process Engineering - Inzynieria Chemiczna i Procesowa*, vol. 34, no. 1, pp. 5-16.
- ČERNECKÝ, J., JANDAČKA, J., MALCHO, M., KONIAR, J., BRODNIANSKÁ, Z. 2015. Effect of the positions of directional tubing towards shaped heating surfaces on the value of local heat

- transfer coefficients. In *JP Journal of Heat and Mass Transfer*, vol. 12, no. 1, pp. 15-30. DOI: 10.17654/JPHMTAug2015_015_030.
- GAFF, M., KVIETKOVÁ, M., GAŠPARÍK, M., KAPLAN, L., BARCÍK, Š. 2015. Effect of selected parameters on the surface waviness in plane milling of thermally modified birch wood. In *BioResources*, vol. 10, no. 4, pp. 7618-7626. DOI: 10.15376/biores.10.4.7618-7626.
- HRČKOVÁ, M., KOLEDA, P., KOLEDA, P., BARCÍK, Š., ŠTEFKOVÁ, J. 2018. Colour change of selected wood species affected by thermal treatment and sanding. In *BioResources*, vol. 13, no. 4, pp. 8956-8975, doi: 10.15376/biores.13.4.8956-8975.
- ILAŠ, Š. 2018. The influence of selected factors on the energy intensity of flat milling thermally modified spruce wood. Technical University in Zvolen. Master thesis.
- International ThermoWood Association. 2003. "ThermoWood handbook," International ThermoWood Association, (<http://www.ThermoWood.fi>), Accessed 12 Aug 2017.
- ISPAS, M., GURAU, L., CAMPEAN M., HACIBEKTASOGLU, M., RACASAN, S. 2016. Milling of heat-treated beech wood (*Fagus sylvatica* L.) and analysis of surface quality. In *BioResources*, vol. 11, no. 4, pp. 9095-9111. doi: 10.15376/biores.11.4.9095-9111.
- KOLEDA, P., BARCÍK, Š., NOCIAROVÁ, A. 2018. Effect of technological parameters of machining on energy efficiency in face milling of heat-treated oak wood. In *BioResources*, vol. 13, no. 3, pp. 6133-6146. DOI: 10.15376/biores.13.3.6133-6146.
- KOLEDA, P., BARCÍK, Š., NOCIAROVÁ A. 2018. Effect of technological parameters of machining on energy efficiency in face milling of heat-treated oak wood. In *BioResources*, vol. 13, no. 3, pp. 6133-6146. doi: 10.15376/biores. 13.3. 6133-6146.
- KOLEDA, P., HRČKOVÁ, M. 2018 Global and Local Thresholding Techniques for Sawdust Analysis. In *Acta Facultatis Technicae*, vol. 23, no. 1, pp. 33-42.
- KRAUSS, A., PIERNIK, M., PINKOWSKI, G. 2016. Cutting Power during Milling of Thermally Modified Pine Wood. In *Drvna Industrija*, vol. 67, no. 3, pp. 215-222. doi: 10.5552/drind.2016.1527.
- KUBŠ, J., GAFF, M., BARCÍK, Š. 2016. Factors affecting the consumption of energy during the milling of thermally modified and unmodified beech wood. In *BioResources*, vol. 11, no. 1, pp. 736-747. doi: 10.15376/biores.11.1.736-747.
- KUBŠ, J., GAŠPARÍK, M., GAFF, M., KAPLAN, L., ČEKOVSKÁ, H., JEŽEK, J., ŠTÍCHA, V. 2017. Influence of thermal treatment on power consumption during plain milling of Lodgepole pine (*Pinus contora* subsp. *Murrayana*). In *BioResources*, vol. 12, no. 1, pp. 407-418. doi: 10.15376/biores. 12.1. 407-418.
- MANDIC, M., TODOROVIC, N., POPADIC, R., DANON G. 2010. Impact of thermal modification and technological parameters of processing on cutting powers in milling wood processing. In *Proceedings of 1st Serbian Forestry Congress – Future with Forest*. Belgrade, Serbia, pp. 1438-1453.
- MOURA, L. F., BRITO, J.O., NOLASCO, A. M., ULIANA, L.R. 2011. Effect of thermal rectification on machinability of *Eucalyptus grandis* and *Pinus caribaea* var. *Hondurensis* woods. In *European Journal of Wood and Wood Products*, vol. 69, no. 4, pp. 641-648. doi: 10.1007/s00107-010-0507-x.
- NIEMZ, P., HOFMANN, T., RÉTFALVI, T. 2010. Investigation of chemical changes in the structure of thermally modified wood. In *Maderas-Cienc. Tecnol.* vol. 12, no. 2, pp. 69-78. DOI: 10.4067/S0718-221x2010000200002.
- NOCIAROVÁ, A. 2017. The influence of technical – technological independent parameters on the energy intensity of planar milling of thermally modified oak wood. Technical University in Zvolen. Master thesis.
- POŽGAJ, A., CHOVANEC, D., KURJATKO, S., BABIAK, M. 1997. *Structure and Properties of Wood*. Bratislava: Príroda, 485 p. ISBN 80-07-00600-1.

TU, D., LIAO, L., YUN, H., ZHOU, Q., CAO, X., HUANG, J. 2014. Effects of heat treatment on the machining properties of *Eucalyptus urophylla* x *E. camaldulensis*. In *BioResources*, vol. 9, no. 2, pp. 2847-2855. doi: 10.15376/biores.9.2.2847-2855.

VASILKO, K. 2007. Analytická teória trieskového obrábania. Prešov: Fakulta výrobných technológií TU v Košiciach so sídlom v Prešove, 2007. ISBN 978-80-8073-759-7

Corresponding author:

Peter Koleda, email: peter.koleda@tuzvo.sk

COMPARING THE VARIOUS METHODS FOR MACHINE WRITTEN CHARACTER RECOGNITION

POROVNANIE RÔZNYCH METÓD NA ROZPOZNÁVANIE STROJOM PÍSANÝCH ZNAKOV

Ladislav Karrach, Elena Pivarčiová

Katedra výrobnjej a automatizačnej techniky, Fakulta techniky, Technická univerzita Zvolen, Študentská 26, 960 01 Zvolen, karrach@zoznam.sk, pivarciova@tuzvo.sk

ABSTRACT: In this article, we present an overview and comparison of various methods and approaches for Latin alphabet characters recognition. We assume that individual characters are already located in an image. To recognize characters and translate them to text, each character must be described by a feature vector, which is then classified into one of 36 classes corresponding to the Latin alphabet letters and numbers. These methods were been tested using a database of Slovak vehicle registration plates. Recognition has been performed with two sets of training samples of different sizes and we have compared recognition rate.

Key words: Vehicle Registration Plate, Optical Character Recognition, Feature Vector, Classification

ABSTRAKT: V článku predkladáme prehľad a porovnanie rôznych metód a prístupov pre rozpoznávanie znakov latinskej abecedy. Predpokladáme, že jednotlivé znaky sú už lokalizované v obraze. Pre rozpoznania znakov a ich prevod na text je nutné každý znak popísať vektorom príznakov, ktorý následne klasifikujeme do jednej z 36 tried zodpovedajúcim číslam a písmenám latinskej abecedy. Tieto metódy boli testované na databáze slovenských evidenčných čísiel vozidiel a dosiahnuté výsledky boli uspokojivé. Rozpoznávanie sme vykonali s dvoma sadami tréningových vzoriek rôznych veľkostí a porovnali sme úspešnosť.

Kľúčové slová: evidenčné číslo vozidla, optické rozpoznávanie znakov, vektor príznakov, klasifikácia

INTRODUCTION

Image recognition methods are used more and more in various fields such as manufacturing technology, robotics, logistics, medicine, quality control, etc. Text recognition – the ability to read – is essential for emerging artificial intelligence applications. As AI systems are often aimed at supporting a human, they must also be able to detect and recognize information presented in textual form that is natural to man. The basis for understanding text is to recognize the individual characters of the alphabet that make up words, sentences, and at the end the final meaning of the text as a whole.

The recognition of the Vehicle Registration Plate (VRP) is one of the classical tasks in recognition of text in real scene images. All vehicles which are in operation on public roads in Slovakia must have the Vehicle Registration Number (VRN), which is formed by letters and digits. The vehicle registration plate (VRP) replaced the previous plates with State Registration Number (SRN).

Recognition of VRP characters can be applied in various traffic systems (e.g. in speed control, in tracing of traffic offences, monitoring of traffic density, parking systems, tolling systems, tracking of stolen cars). However the algorithms and approaches which are applicable to VRP recognition can be generalized and applied in wide variety of image recognition tasks and applications (e.g. support for the visually impaired and blind, digitization of documents, books, check of personal documents).

Recognition of the VRP can be divided into the task of locating the VRP in an image, which can contain many similar objects, and then to the task of detecting the individual characters that make up the VRP and ultimately their recognition as the text which we were looking for. In this article we deal with the second phase of VRP recognition – recognizing of the individual VRP characters – transforming image information to plain text.

MATERIAL AND METHODS

For recognition of the VRP characters, we assume that the individual characters of the VRP are already binarized and segmented (Fig. 1). This assumption meets the algorithm for localization of VRP in the images (Karrach & Pivarčiová 2019), which identifies the VRP as a sequence of 7 characters placed in a row. The algorithm employs adaptive thresholding, joining adjacent foreground pixels into continuous regions (blobs), and searching of 7 regions which are of roughly the same size and are placed in the image approximately in the same Y-position.



Fig. 1 Individual characters in VRP are surrounded by bounding box
Obr. 1 Jednotlivé znaky v EČV sú ohraničené obdĺžnikom

The individual characters of VRP, which are surrounded by the bounding box, must be proportionally resized to the normalized height prior to further processing. Normalized height corresponds to the height of the training samples.

FEATURE VECTOR

The feature vector is an n-dimensional numeric vector that represents the object (in our case, object is a one character in the VRP identified by location phase as continuous region). The goal of feature extracting is to reduce the complexity of an object to a compact feature vector that concisely describes the object. Requirement for a feature vector are (Šikudová et al., 2013):

- two identical objects must have the same descriptors and vice versa, two identical descriptors must describe the same objects,
- descriptor should be invariant, especially under translation, rotation, scaling,
- descriptor should contain the smallest set of information needed to identify the object and distinguish it from objects of other classes.

The choice of features has a major impact on the accuracy of the classification.

Bitmap of character

The values of feature vector correspond directly to the individual pixels of an input image. The white pixel is represented by value 0 and black pixel by value 1 (Fig. 2). The size of feature vector is equal to the width \times height of the character bitmap.

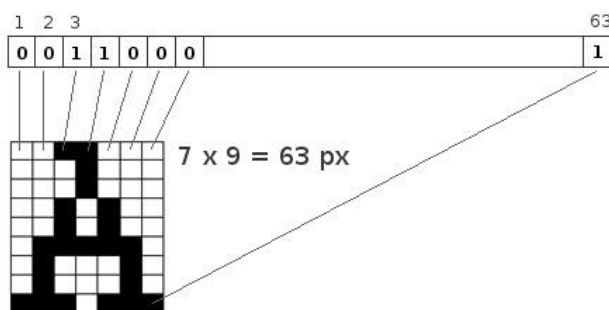


Fig. 2 Feature values corresponds to the pixels of an image
Obr. 2 Hodnoty príznakového vektora zodpovedajú bodom obrázku

Shape features

We used the following properties to describe the VRP characters:

- Aspect Ratio: ratio of the width to the height of a bounding box,
- Extent: ratio of pixels in the region (count of black pixels) to pixels in the total bounding box,
- Roundness: ratio of the area of an object to the area of a circle with the same perimeter,
- Holes: number of holes (1 - Euler number),
- Horizontal Crossing: number of crossings from white to black in a row (computed in 1/3 and 2/3 of height and minimum and maximum computed in 1st third, 2nd third and 3rd third of height),
- Vertical Crossing: number of crossings from white to black in a column (computed in 1/3 and 2/3 of width and minimum and maximum computed in 1st third, 2nd third and 3rd third of width),
- Horizontal Projection: ratio of number of black pixels in a row to the total width for each image row,

- Vertical Projection: ratio of number of black pixels in a column to the total height for each image column.

Table 1 lists these properties on the example of the “A” character shown in Fig. 2 (Area of the character is equal to the number of black pixels which is 23 and perimeter is 50).

Table 1 Shape features describing character “A” in Fig. 2
Tabuľka 1 Príznyky tvaru popisujúce znak “A” v Obr. 2

Feature	Value	Feature	Value	Feature	Value
Aspect Ratio	7/9	H.Cross. 1/3 min, max	1, 1	V. Cross. 2/3 min, max	2, 3
Extent	23/63	H.Cross. 2/3 min, max	1, 2	V. Cross. 3/3 min, max	1, 2
Roundness	$23 \cdot 4 \cdot \pi / 50^2$	H.Cross. 3/3 min, max	2, 2	H. Projection	2/7, 1/7, ...
Holes	1	V. Crossing 1/3	1		
H. Crossing 1/3	1	V. Crossing 2/3	2	V. Projection	1/9, 4/9, ...
H. Crossing 2/3	1	V. Cross. 1/3 min, max	1, 1		

Run-length encoding

The individual rows in a bitmap of a character are expressed as the ratio of the number of consecutive white pixels – black pixels – white pixels – black pixels to bitmap width (Fig. 3). The feature vector size is $4 \times$ height of character bitmap.

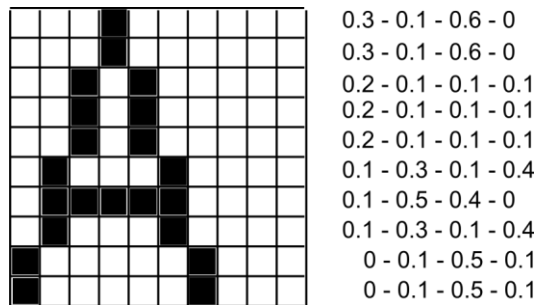


Fig. 3 Run-length encoding
Obr. 3 Run-length kódovanie

Hu and Chebyshev moments

- 8 Hu invariant moments (Hu, 1962). Hu moments are invariant under translation, rotation and scaling and we can calculate them from normalized central geometric moments (Eq. 1):

$$\begin{aligned}
I_1 &= \eta_{20} + \eta_{02} \\
I_2 &= (\eta_{20} - \eta_{02})^2 + 4\eta_{11}^2 \\
I_3 &= (\eta_{30} - 3\eta_{12})^2 + (3\eta_{21} - \eta_{03})^2 \\
I_4 &= (\eta_{30} + \eta_{12})^2 + (\eta_{21} + \eta_{03})^2 \\
I_5 &= (\eta_{30} - 3\eta_{12})(\eta_{30} + \eta_{12})[(\eta_{30} + \eta_{12})^2 - 3(\eta_{21} + \eta_{03})^2] + (3\eta_{21} - \eta_{03})(\eta_{21} + \eta_{03})[3(\eta_{30} + \eta_{12})^2 - (\eta_{21} + \eta_{03})^2] \\
I_6 &= (\eta_{20} - \eta_{02})[(\eta_{30} + \eta_{12})^2 - (\eta_{21} + \eta_{03})^2] + 4\eta_{11}(\eta_{30} + \eta_{12})(\eta_{21} + \eta_{03}) \\
I_7 &= (3\eta_{21} - \eta_{03})(\eta_{30} + \eta_{12})[(\eta_{30} + \eta_{12})^2 - 3(\eta_{21} + \eta_{03})^2] - (\eta_{30} - 3\eta_{12})(\eta_{21} + \eta_{03})[3(\eta_{30} + \eta_{12})^2 - (\eta_{21} + \eta_{03})^2] \\
I_8 &= \eta_{11}[(\eta_{30} + \eta_{12})^2 - (\eta_{21} + \eta_{03})^2] - (\eta_{20} - \eta_{02})(\eta_{30} + \eta_{12})(\eta_{03} + \eta_{21}) \tag{1}
\end{aligned}$$

- 21 Chebyshev discrete orthogonal moments up to 5th order (Mukundan et al., 2000; Mukundan, 2004). Chebyshev orthogonal moment of order $(p+q)$ for an image $N \times N$ is defined as (Eq. 2):

$$T_{pq} = \sum_{x=0}^{N-1} \sum_{y=0}^{N-1} \hat{t}_p(x) \hat{t}_q(y) f(x, y), \tag{2}$$

$$\begin{aligned}
\hat{t}_0(x) &= \frac{1}{\sqrt{N}}, \quad \hat{t}_1(x) = 2x + 1 - N \sqrt{\frac{3}{N(N^2 - 1)}} \\
\hat{t}_p(x) &= (\alpha_1 x + \alpha_2) \hat{t}_{p-1}(x) - \alpha_3 \hat{t}_{p-2}(x)
\end{aligned}$$

where

$$\begin{aligned}
\alpha_1 &= \frac{2}{N} \sqrt{\frac{4p^2 - 1}{N^2 - p^2}}, \quad \alpha_2 = \frac{1 - N}{p} \sqrt{\frac{4p^2 - 1}{N^2 - p^2}}, \\
\alpha_3 &= \frac{p - 1}{p} \sqrt{\frac{2p + 1}{2p - 3}} \sqrt{\frac{N^2 - (p - 1)^2}{N^2 - p^2}}
\end{aligned}$$

Beside to Chebyshev moments there are also Legendre moments (Teague 1980) and also Zernike complex moments (Khotanzad & Hong 1990) used for classification tasks. The Legendre moments are defined on unit square $[-1, +1] \times [-1, +1]$ and Zernike complex moments are defined on unit circle, where Zernike polynomials form a complete orthogonal set.

CHARACTER CLASSIFICATION

The goal of classification is to assign the tested sample on the input, represented by the feature vector, into one of the 36 output classes. One output class represents one alphabet character – one letter (A–Z) or a digit (0–9) that can be found in the VRP. For the task of classifying VRP characters, we have created a set of training sample patterns that represented individual characters in VRP. At the beginning, the set contained just one training sample for one class. We further incrementally expanded this set with additional training samples for misclassified characters, and in the case of supervised classifiers we repeated the learning process.

Nearest Neighbour Classification

This classifier computes the Euclidean distance between the vector describing the examined object and the vector describing the class (sample from the sample set). The tested sample is classified into a class for which the Euclidean distance is minimal (Eq. 3):

$$d(V_o, V_j) = \min_{j \in 1..n} \left\{ \sqrt{\sum_i (V_o(i) - V_j(i))^2} \right\} \quad (3)$$

Where V_o is feature vector describing tested sample and V_j is feature vector of j-th sample in the sample set.

Artificial Neural Network - Multilayer Perceptron

The artificial neural networks (ANNs) are computing systems inspired by the biological neural networks that constitute an animal brains. Although biological neurons are extremely complicated cells, their essential computational nature in terms of inputs and outputs is relatively straightforward. Each neuron has multiple dendrites and a single axon. The neuron receives its inputs from its dendrites and transmits its output through its axon.

We have used a basic type of feed-forward neural network - Multilayer Perceptron. The input layer neurons were fully-connected with the hidden layer neurons, which were again fully-connected with the output layer neurons. The number of the input neurons corresponded to the number of elements in the feature vector. The number of the output neurons corresponded to the number of classes, i.e. number of letters and numbers in alphabet. In the hidden layer, we have used between 20 and 80 neurons according to the size of the input feature vector, and as a activation function of the neurons we have used a sigmoid function (in one case the hyperbolic tangent).

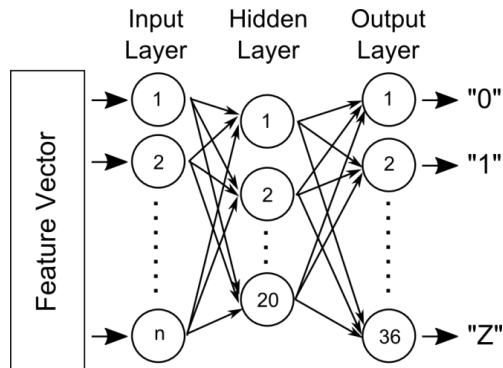


Fig. 4 Scheme of 2-layer fully connected neural network with forward propagation
Obr. 4 Schéma 2-vrstvovej plne prepojenej neurónovej siete s dopredným šírením

Basic computational function of an artificial neuron (Fig. 5) lies in following:

- Every input (x_i) received by synapses is multiplied by weights (w_{ij}),

- Then all of the weighted inputs are summarized (Σ),
- Finally the output of the activation function is computed (commonly used are non-linear activation functions: hyperbolic tangent or sigmoid)

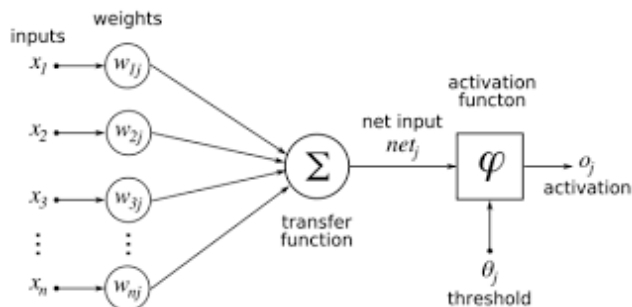


Fig. 5 Scheme of an artificial neuron
Obr. 5 Schéma umelého neurónu

Table 2 Common activation functions of an artificial neuron
Tabuľka 2 Bežne používané aktivačné funkcie umelého neurónu

Linear	Step	Sign	Sigmoid	Hyperbolic tangent
$y = x$	$y = \begin{cases} 0, & \text{if } x < 0 \\ 1, & \text{if } x \geq 0 \end{cases}$	$y = \begin{cases} -1, & \text{if } x < 0 \\ +1, & \text{if } x \geq 0 \end{cases}$	$y = \frac{1}{1+e^{-x}}$	$y = \frac{2}{1+e^{-x}} - 1$

Probabilistic Neural Network

The feed-forward neural network with 4 layers (input layer, pattern layer, summation layer and output layer) is used for classification tasks. The number of neurons in the input layer corresponds to the number of features in feature vector. The input layer is fully connected with the hidden layer.

The neurons of first hidden layer (pattern layer) are organized into groups where one group represents one class (the number of all neurons in pattern layer corresponds to the number of all training samples). The first hidden layer computes the distance between the tested input vector and the input vectors from the training set, and its output is a vector that expresses as close is the tested input to the inputs from the training set.

The neurons of one group (class) are connected to just one neuron of the second hidden layer (summation layer).

The number of neurons in the second hidden layer (summation layer) corresponds to the number of classes. One neuron of this layer represents one class. Neurons sum contributions from the previous layer individually for each class.

The output of the layer is a probability vector. Finally, the highest probability class is selected.

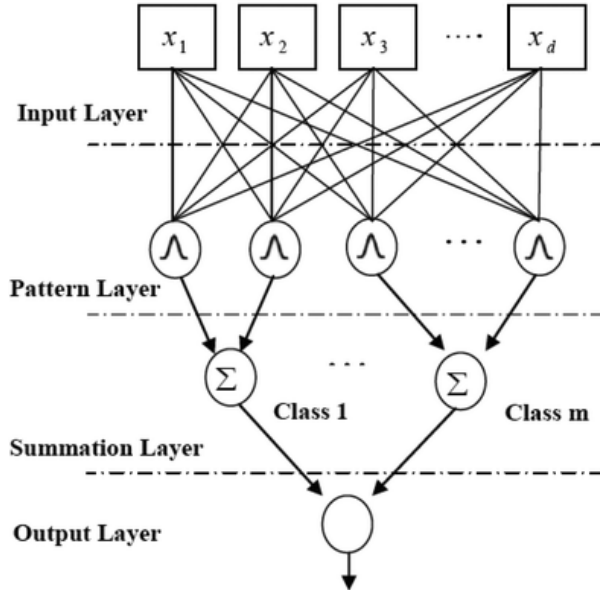


Fig. 6 Scheme of a probabilistic neural network
 Obr. 6 Schéma pravdepodobnostnej neurónovej siete

Naive Bayes Classifier

The Naive Bayes Classifier is based on Bayes' conditional probability and assumes the independence of all elements of the feature vector, i.e. that the impact of individual elements on assignment into a given class is not affected by the values of other elements (therefore "naive").

For n-dimensional feature vector $X=(x_1, \dots, x_n)$, m-classes $C=(c_1, \dots, c_m)$, we maximize probability, that observed feature vector X belongs to the class C_i :

$$P(C_i | X) = \frac{P(X | C_i)P(C_i)}{P(X)} \quad (4)$$

Where, $P(X)$ is constant for all classes C_i (so we can ignore it because we are looking for the class with the highest probability, and we do not need to know exactly the probability value) and $P(C)$ represents the probability that a randomly selected sample belongs to the class C_i .

Because we assume independence of $x_1 \dots x_n$:

$$P(X | C_i) = P(x_1, \dots, x_n | C_i) \approx P(x_1 | C_i) \times P(x_2 | C_i) \times P(x_n | C_i) = \prod_{k=1}^n P(x_k | C_i) \quad (5)$$

$$P(x_k | C_i) = \frac{s_{ki}}{s_i} \quad (6)$$

Where, s_{ki} is the number of samples of the i -th class, which have k -th attribute equal x_k .

RESULTS

We tested these character recognition methods on 60 VRP photos that contained together 420 letters and numbers. Each number and letter of the alphabet occurred at least 3 times (except letters Q and W). We worked with two sets of training samples in one set were samples of size 7×10 (width \times height) and in second set were samples of size 12×17 . At the beginning, each set contained just one sample for one of 36 characters (0–9, A–Z). After each test cycle, we added 10 new samples, which were not correctly recognized, into the training set and we have repeated the tests. When we were gradually expanding the training set, recognition rate had been increasing (Tab. 3). The table 3 shows the number of successfully recognized characters for the training set 7×10 (with 4 VRP localization errors, there has been 56 VRP successfully localized, that means 392 characters).

Table 3 Comparison of tested feature vectors and classifiers

Tabuľka 3 Porovnanie testovaných príznakových vektorov a klasifikátorov

Feature vector	Classifier	Number of training samples				
		36	46	56	66	76
Bitmap	Nearest Neighbour	346	353	362	374	388
	Multilayer Perceptron	321	327	345	362	382
	Probabilistic NN	346	355	351	363	381
	Naive Bayes	346	302	338	331	357
Shape features	Nearest Neighbour	347	348	356	363	364
	Multilayer Perceptron	338	342	345	354	354
	Probabilistic NN	347	348	355	359	361
	Naive Bayes	342	275	290	316	321
Run-Length Encoding	Nearest Neighbour	346	346	335	359	361
	Multilayer Perceptron	341	341	354	357	365
	Probabilistic NN	346	353	349	351	359
	Naive Bayes	346	298	312	352	362
Chebyshev Moments (*)	Nearest Neighbour	339	343	351	370	379
	Multilayer Perceptron	278	297	303	335	347
	Probabilistic NN	339	342	351	370	377
	Naive Bayes	339	237	157	190	209

(*) During the testing, we found that Hu moments are not an appropriate descriptor, so we did not include them in the results.

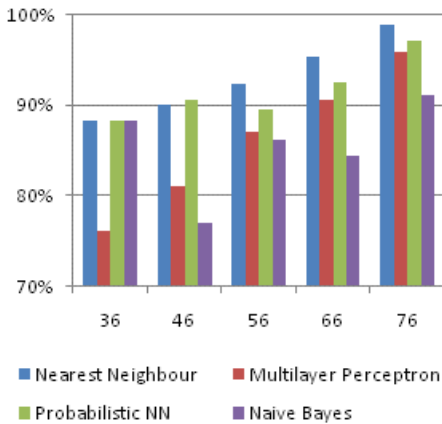


Fig. 7 Bitmap
Obr. 7 Bitmapa

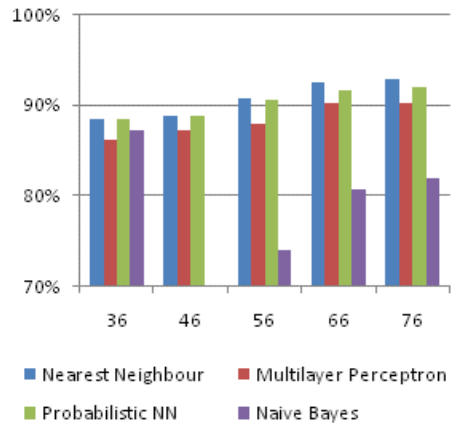


Fig. 8 Shape features
Obr. 8 Príznyaky tvaru

In Fig. 7-10, the individual classifiers for the given feature vectors and their recognition rate (on y-axis) for an increasing number of training samples (on x-axis) are compared.

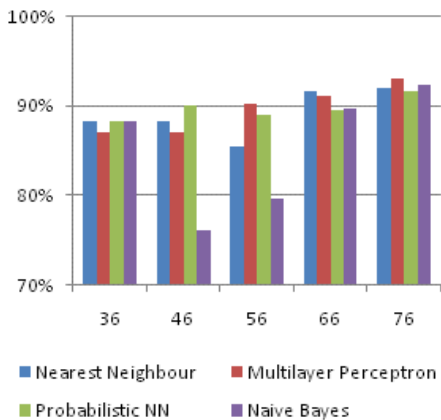


Fig. 9 RLE
Obr. 9 RLE

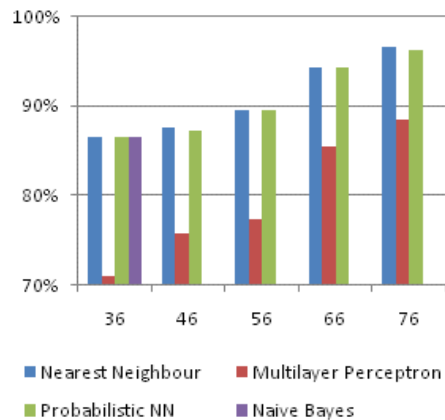


Fig. 10 Chebyshev Moments
Obr. 10 Čebyševove momenty

In Fig. 11–12, the individual feature vectors for the given classifiers and their recognition rate for an increasing number of training samples are compared.

In the case of Multilayer Perceptron, we have used a configuration with hidden layer with 20 neurons and also with 40 neurons (in the case of Shape features), respectively 60 neurons (in the case of Bitmap). We found that the configuration with a higher number of neurons in the hidden layer had slightly better results, as shown in the result table (Tab. 2). For the Moments feature vector, we have used the hyperbolic tangent as activation function (instead of the sigmoid).

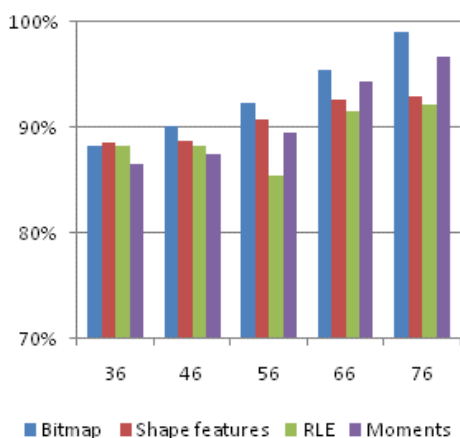


Fig. 11 Nearest Neighbour
Obr. 11 Najbližší sused

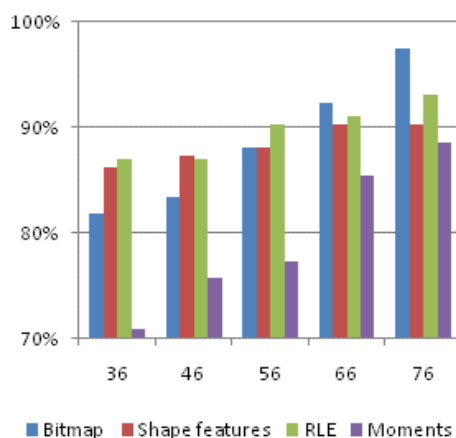


Fig. 12 Multilayer Perceptron
Obr. 12 Viacvrstvový perceptrón

The results show that the Nearest Neighbour classifier followed by the Probabilistic Neural Network using a bitmap, as a feature vector, has achieved best recognition rate. On the other hand, the Naive Bayes classifier proved as not suitable.

In Table 4 we list the mostly misclassified characters for individual feature vectors.

Table 4 The most common errors in character recognition
Tabuľka 4 Najbežnejšie chyby v rozpoznávaní znakov

Size of training samples	Feature vector	Mostly misclassified characters
7×10	Bitmap	D-O, 0-O
	Shape features	1-Y, 0-O, D-O
	Run-Length Encoding	8-B, 0-O, D-O
	Chebyshev Moments	1-X, 0-O, D-O
12×17	Bitmap	8-B, D-O
	Shape features	8-B, D-O, K-R
	Run-Length Encoding	8-B, 7-T, 0-O
	Chebyshev Moments	8-B, 0-G, 6-8

DISCUSSION

When recognizing the VRP characters, we assumed the horizontal position of the VRP, where all the characters are in the vertical position. Our opinion is that this is not a limiting factor for most applications, like parking and security systems, where car must stop at certain place (before the gate) and the camera has a fixed position.

The worse results of the Multilayer Perceptron are partly due to the fact that we required for the successful classification besides the highest score an output of at least 0.2, while for other classifiers we were satisfied with only the highest score.

The bad results of the Naive Bayes classifier were due to a small number of training samples in each class and by their uneven distribution in classes. If some of the continuous attributes of a feature vector in a given class have the same values for various samples, then we cannot correctly determine the dispersion needed to calculate the conditional probability of the continuous random variable.

For the “Shape features” feature vector, there occurred interchange of characters, with similar characteristics (8–B, 0–O, K–R), so it will be necessary to add such attributes to the feature vector, which will distinguish these characters.

For training set with samples of size 10×10 for 100 % recognition of all 392 characters, were needed altogether 83 samples, while for the training set of size 12×17 for 100 % recognition was sufficient 62 samples. Moreover, the 0 (“zero”) and O (“ou”) characters when resized to 10×10 can have very similar patterns (Fig. 13), which suggests that it is preferable to use a training set of larger samples to distinguish them.

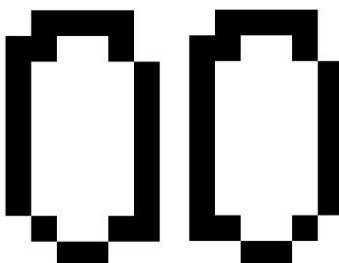


Fig. 13 Left „0“ and right „O“ samples is difficult to distinguish
Obr. 13 Vľavo vzorku „0“ a vpravo vzorku „O“ je ťažké rozlíšiť

CONCLUSION

In the article, we compared the various methods of recognizing the characters extracted from the VRP. From a classical pattern matching approach, that uses a pixel-by-pixel comparison of training and test patterns to various methods that compare specific extracted features – representative properties of characters. The feature vector has primary effect on the recognition accuracy, whereas the classifier itself, when correctly trained, has a secondary effect. Our comparative experiments showed that training samples of size 12×17 are more suitable than smaller samples of size 10×10 . The methods of image processing and text recognition could be adopted for various purposes from above mentioned traffic security to commercial use in parking systems.

Automated text recognition and object identification in the image could be also used for recognition of traffic signs, recognition of objects in robotics systems, identification of components and their identification numbers in production or in equipment for visually impaired persons.

REFERENCES

- ABOLGHAEMI, V., AHMADYFARD, A. 2009. An edge-based color-aided method for license plate detection. *Image and Vision Computing*, 27. pp. 1134-1142.
- BRADLEY, D., ROTH, G. 2007. Adaptive thresholding using the integral image. *Journal of Graphics Tools*.
- BRÉDOVÁ, L., KOVÁČOVÁ, A. 2012. Naivný Bayesovský klasifikátor. [online]. [cit. 2018-06-09]. Available in: <http://oz.koncz.sk/attachments/article/173/oz_zadanie_bredova_kovacova.pdf>
- FLUSSER, J., SUK, T., ZITOVA, B. 2017. 2D and 3D Image Analysis by Moments.
- HU, M., 1962. Visual Pattern Recognition by Moment Invariants. *IRE Transactions on Information Theory*. [online]. [cit. 2018-11-01]. Available in: <<https://ieeexplore.ieee.org/document/1057692>>
- KARRACH, L., PIVARČIOVÁ, E. 2017. Data matrix code location marked with laser on surface of metal tools. *Acta Facultatis Technicae XXII*, 2017 (2): 29–38, ISSN 1336-4472.
- KARRACH, L., PIVARČIOVÁ, E. 2019. Location of vehicle registration plates in real scene images. *Acta Facultatis Technicae XXIV*, 2019 (1): 63–70.
- KHAN, A. M., SHARIF, M., JAVED, M. Y., AKRAM, T., YASMIN, M., SABA, T. 2017. License number plate recognition system using entropy-based features selection approach with SVM. *IET Image Processing*, Volume 12, Issue 2, p. 200–209
- KHOTANZAD, A., HONG, Y. H. 1990. Invariant image recognition by Zernike moments. *IEEE Transactions on Pattern Analysis and Machine Intelligence*, vol. 12, no. 5, pp. 489-497, 1990.
- KOLEDA, P., HRČKOVÁ, M. 2018. Global and local thresholding techniques for sawdust analysis. *Acta Facultatis Technicae*, XXIII, 2018(1), pp. 33–42.
- KOLEDA, P., NAŠČÁK, Ľ. 2011. Skeletization algorithms. *Acta Facultatis Technicae*, Zvolen: Technická univerzita vo Zvolene, XVI 2/2011, s. 73–82, ISSN 1336–4472.
- KUNTE, RS., SAMUEL-SADHANA, RDS. 2007. A simple and efficient optical character recognition system for basic symbols in printed Kannada text. *Sadhana*.
- LOONEY, CG., . Probabilistic Neural Network Tutorial. [online]. [cit 2018-11-28]. Available in: <<https://www.cse.unr.edu/~looney/cs773b/PNNtutorial.pdf>>
- MAHINI, H., KASAEI, S., DORRI, F., DORRI, F. 2006. An Efficient Features - Based License Plate Localization Method. 2. 841-844. 10.1109/ICPR.2006.239.
- MUKUNDAN, R., ONG S.H., LEE P.A. 2000. Discrete Orthogonal Moment Features Using Chebyshev Polynomials.
- MUKUNDAN, R. 2004. Some Computational Aspects of Discrete Orthonormal Moments. *IEEE Transactions on image processing*, Vol. 13, No. 8.
- OUJAOURA, M., AYACHI, EL R., MINAOUI, B., FAKIR, M., BOUIKHALENE, B., BENCHAREF O. 2013. Invariant Descriptors and Classifiers Combination for Recognition of Isolated Printed Tifnagh Characters. *International Journal of Advanced Computer Science & Applications*.
- PAWLAK, M., 2006. Image Analysis by Moments: Reconstruction and Computational Aspects.
- PIVARČIOVÁ, E., 2016. Identification of image objects and its application in the manufacturing technology. *Acta Facultatis Technicae*, Zvolen: Technická univerzita vo Zvolene, XXI 1/2016, s. 91–98, ISSN 1336–4472
- RAO, P. B., PRASAD D.V., KUMAR CH.P. 2013. Feature Extraction Using Zernike Moments. *International Journal of Latest Trends in Engineering and Technology*, Vol. 2 Issue 2, 2013.
- ROSENFELD, A., PFALTZ, J. 1966. Sequential operations in digital image processing. [online]. [cit 2017-07-11]. Available in: <<http://www.cse.msu.edu/~stockman/Book/2002/Chapters/ch3.pdf>>.

- SPECHT, DF., 1990. Probabilistic Neural Networks. *Neural Networks*, Vol. 3. pp. 109-118, 1990.
- ŠIKUDOVÁ, E., ČERNEKOVÁ, Z., BENEŠOVÁ, W., HALADOVÁ, Z., KUČEROVÁ, J. 2013. Počítačové videnie Detekcia a rozpoznávanie objektov. [online]. [cit 2017-07-11] Available in: <<http://vgg.fiit.stuba.sk/kniha/>>.
- TEAGUE, M. R. 1980. Image analysis via the general theory of moments. *Journal of the Optical Society of America*, Vol. 70, Issue 8, 1980, pp. 920-930.
- TRKAL, O., 2016. Rozpoznávaní EČV. [online]. [cit. 2018-04-22]. Available in: < https://www.vutbr.cz/www_base/zav_prace_soubor_verejne.php?file_id=124167>.
- ZHAI, X., BENSSALI, F., RAMALINGAM, S. 2010. License Plate Localisation based on Morphological Operations. *Control Automation Robotics & Vision (ICARCV)*, 2010 11th International Conference: 7 - 10 Dec. 2010.

Corresponding author:

doc. Mgr. Elena Pivarčiová, PhD., 045 5206 477, pivarciova@tuzvo.sk

METHOD FOR WOOD COLOUR DETERMINING IN DIGITAL IMAGE

METÓDA URČOVANIA FARBY DREVA V DIGITÁLNO M OBRAZE

Pavol Koleda

Department of Manufacturing and Automation Technology, Faculty of Technology, Technical University in Zvolen, T. G. Masaryka 24, 960 01, Zvolen, Slovakia, e-mail: pavol.koleda@tuzvo.sk

ABSTRACT: This paper deals with a colour analysis method using image analysis in Matlab. Colour belongs to the basic characteristics of all entities and objects. Its determination allows as detailed characterization of the objects, as their changes or responses to some stimuli. The paper describes the application design, which determines the colour in the determined area in the digital image. Using proposed application is to compare the colour of natural birch timber and its three thermal modifications.

Key words: image analysis, colour, Matlab, programming.

ABSTRAKT: Článok sa zaoberá metódou určovania farby pomocou obrazovej analýzy v Matlabe. Farba patrí k základným charakteristikám všetkých telies a objektov. Jej určenie umožňuje špecifikáciu určitých vlastností objektov, ako sú ich zmeny alebo reakcie na niektoré podnety. Článok popisuje návrh aplikácie, ktorá umožňuje zistenie farby v určenej oblasti digitálneho obrazu. Navrhnutou aplikáciou je porovnaná farba dreva brezy po jej tepelnej úprave pri troch rôznych teplotách.

Kľúčové slová: analýza obrazu, farba, Matlab, programovanie.

INTRODUCTION

Wood is an important natural renewable material, which colour is one of the most important macroscopic features differentiating the appearance of individual wood species. Wood colouring is caused, besides basic chemical components: cellulose, hemicelluloses, and lignin, by accessory substances such as dye, tanning agent, resins located in cell walls and lumens. Wood, as a natural material, is a compound predominantly of organic substances (Dzurenda, 2019). Mainly it is composed of organic macromolecular substances: cellulose (35% to 50%), hemicelluloses (20% to 35%), and lignin (15% to 35%) (Geffert 2013). These basic structures of wood differently absorb and reflect light, and pigments absorb certain wavelengths of light. Part of the light that is not absorbed into the cell walls disperses and rejects, and partially passes through the wood substance. Unabsorbed light is recognized as the wood colour, and by nature of wavelength changes, we

sense specific wood colour of some wood species. The natural wood colour is specific for each species, and the total number of more than 30000 wood species is the largest source of variability of the wood colours. Growth conditions can also affect the colour variation within the same wood species; growth rate, soil nutrition and the brightness affects the wood colour (Chen, 2012; Sinković, 2014).

At present, colour and shade are measured by colorimetry, which is based on the standards and technical requirements stated and issued by the International Commission on Illumination (Commission Internationale de l'Éclairage) (Hrčka, 2008). The colour space CIE $L^*a^*b^*$ (fig. 1) is the closest to the human perception. Its construction is based on the theory of opposite colours. The colour space CIE $L^*a^*b^*$ is characterized by three parameters: L^* , a^* , and b^* (Babiak, 2004; Brischke, 2007; Šuriansky, 2010; Dzurenda 2019).

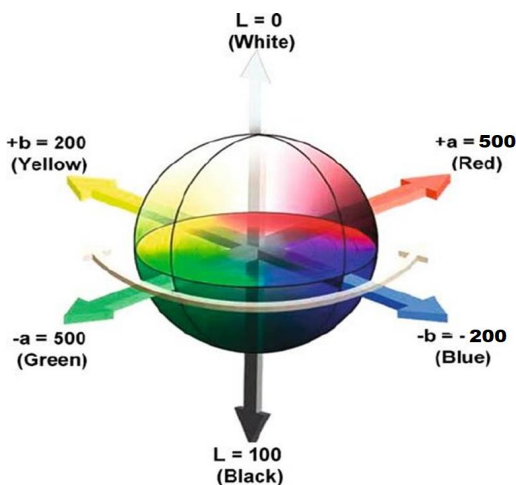


Fig. 1 Colour space CIE $L^* a^* b^*$ (Singh, 2009)
 Obr. 1 Farebný priestor CIE $L^* a^* b^*$ (Singh, 2009)

MATERIAL AND METHODS

For experiment were Birch (*Betula pendula*) samples scanned (Fig. 2). The samples of the Birch wood in the form of lumber of thickness $h = 40$ mm and moisture content $W_p = 56.8 \pm 5.3\%$. For the measurement were natural timber and three thermally modified timber used. Modified samples was thermally treated with saturated water steam in the pressure autoclave: APDZ 240 (Himmasch AD, Haskovo, Bulgaria) in the company Sundermann Ltd. Banská Štiavnica, Slovakia. The first modified sample was heated to temperature 105 ± 2.5 °C, second to temperature 125 ± 2.5 °C and third to temperature 135 ± 2.5 °C (Dzurenda 2019).

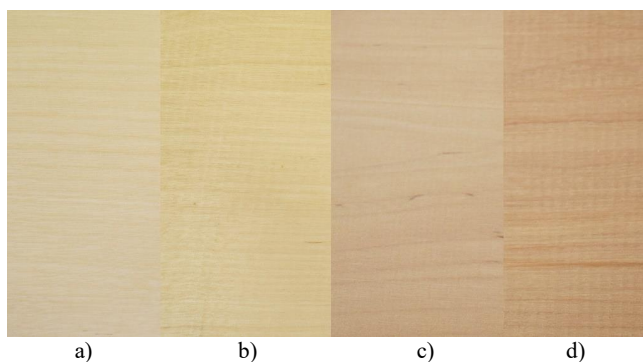


Fig. 2 Birch samples: a) natural, b) c) d) thermally modified
 Obr. 2 Vzorky brezy: a) prírodná, b) c) d) tepelne modifikované

The process of thermal treatment of birch timber with saturated water vapor is shown in the Fig. 3 (Dzurenda, 2019) and the technical parameters of each mode are given in Table 1 (Dzurenda, 2019).

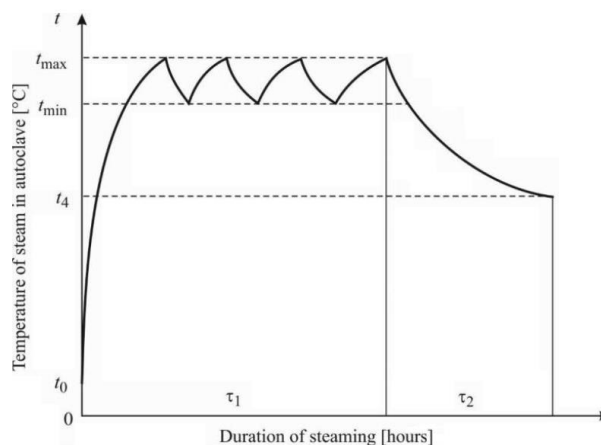


Fig. 3 Procedure of thermal treatment of birch timber with saturated water vapour steam
 Obr. 3 Postup termickej úpravy brezového reziva pomocou sýtenej vodnej pary

Table 1 Procedures of thermal treatment of birch timber with saturated water vapour steam
 Tabuľka 1 Postupy termickej úpravy brezového reziva pomocou sýtenej vodnej pary

Modes	Temperature of the saturated water steam, °C			Duration technological process of thermal treatment of wood τ , h		
	t_{\min}	t_{\max}	t_4	τ_1 -stage I	τ_2 -stage II	Total $\tau_1 + \tau_2$
Mode I.	102.5	107.5	100	6.0	1.5	7.5
Mode II.	122.5	127.5	100			
Mode III.	132.5	137.5	100			

These wood samples were scanned using camera Nikon D3200. It is a single-lens reflex that is equipped with a 4.2 mega pixel sensor complementary metal-oxide-semiconductor (CMOS) and an effective image processor EXPEED 3. The images were produced in full high definition quality; the overall number of pixels was 24.7 million. For wood colour, analysis was created application in software Matlab. It allows you to find out the colour of the selected part in the digital image. The reference standard with the precise colour value of the sample in CIE XYZ ($Y = 83.7$) was aligned with the assessed sample to eliminate the mistakes caused by the change in colour conditions during the production of the photographs. The photographs were processed using Matlab 2010b (Fig. 4) (Kučerka and Očkajová 2014; Hrkčková et al. 2018; Očkajová 2019).

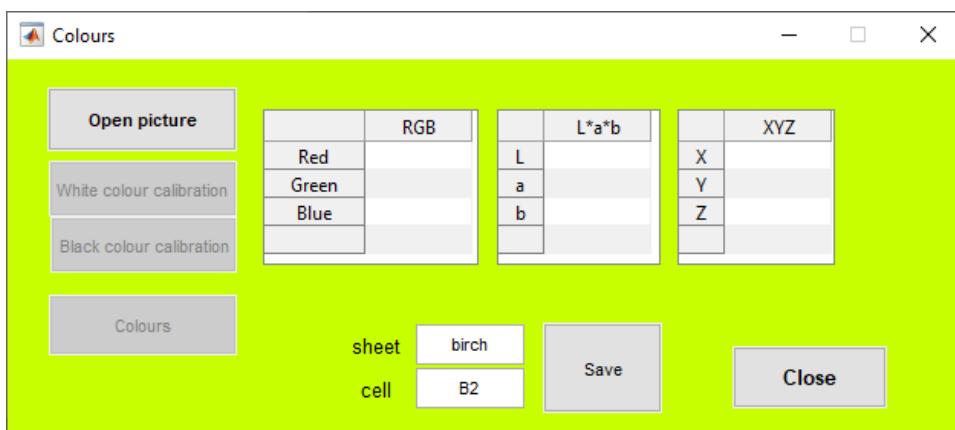


Fig. 4 Proposed application
Obr. 4 Navrhnutá aplikácia

For measurement, the image, in which is the image of the sample to be measured, is read using the application button “Open image” in the application. In order to capture measured objects under different lighting conditions, the image must contain an object with a reference colour. In the application, it is possible to use white or black as a reference. In the experiment, it was used a white reference sample. The reference colour area in the image is selected using “White colour calibration” button. The difference between the detected value of this colour and the actual value is converted into coefficients that adjust the colour of the whole image.

After this adjustment, the colour can be detected in the selected area. The selection of the measuring area is entered using the button “Colours” followed by two clicks into the image that enter the rectangular measurement area. Subsequently, the colour coordinates of all points in the marked area were processed. The results express the colour coordinates in the colour model of RGB. These values can then be recalculated into the colour space of CIE $L^*a^*b^*$ and CIE XYZ. Calculated values can be saved to software MS Excel 2016 using button “Save”.

RESULTS

The results of the measured wood colour values are shown in Fig. 5.

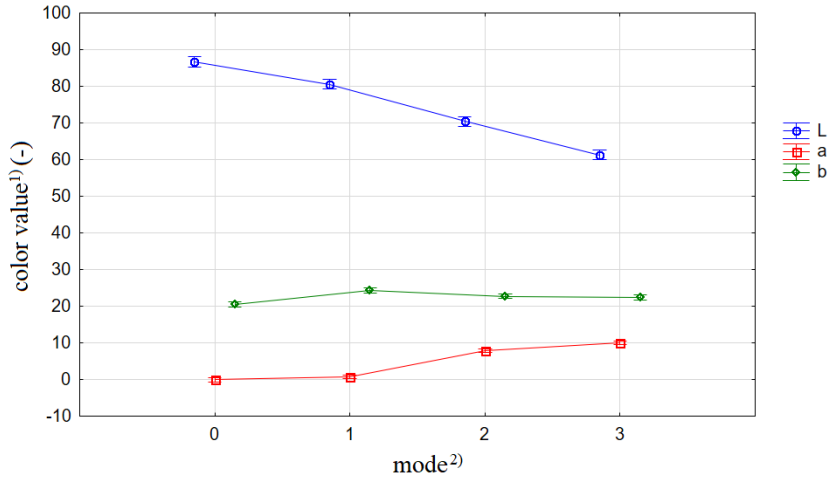


Fig. 5 Measured birch colour values
Obr. 5 Namerané hodnoty farby brezy

¹⁾Hodnota farby, ²⁾Mód

From the previous figure it can be seen, when wood is modified, its lightness decreases (parameter L^*). At higher temperatures during modification, the lightness of the wood decreases. Changes as in each coordinate as the overall colour change ΔE are shown in Fig. 6.

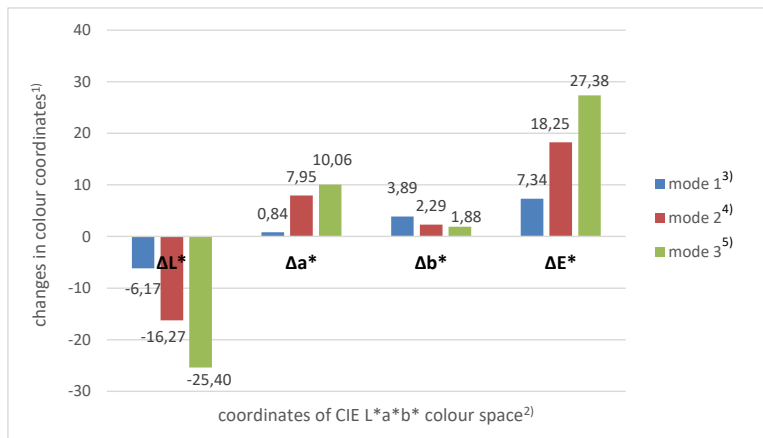


Fig. 6 Changes in colour of thermally modified birch wood
Obr. 6 Zmeny farby termicky modifikovaného brezového dreva

¹⁾zmeny v súradniciach farby, ²⁾súradnice farebného priestoru CIE $L^*a^*b^*$, ³⁾mód 1, ⁴⁾mód 2, ⁵⁾mód 3

As shown the figure 5, if the temperature of the saturated water vapor rises, the decrease in the luminosity coefficient ΔL^* increases. Statistical evaluation of measured data is shown in Table 2.

Table 2 Statistical evaluation of colour values
Tabuľka 2 Štatistické vyhodnotenie hodnôt farby

	mode ¹⁾	0	1	2	3
L	average ²⁾	86,69	80,52	70,42	61,29
	standard deviation ³⁾	2,34	4,40	3,32	3,06
	standard error ⁴⁾	0,47	0,88	0,66	0,61
	confidence interval -95 % ⁵⁾	85,73	78,71	69,05	60,03
	confidence interval +95 % ⁶⁾	87,66	82,34	71,79	62,55
a	average ²⁾	-0,07	0,77	7,88	9,99
	standard deviation ³⁾	1,32	1,43	1,38	1,21
	standard error ⁴⁾	0,26	0,29	0,28	0,24
	confidence interval -95 % ⁵⁾	-0,62	0,18	7,31	9,49
	confidence interval +95 % ⁶⁾	0,47	1,36	8,45	10,49
b	average ²⁾	20,46	24,35	22,75	22,34
	standard deviation ³⁾	1,99	2,14	1,40	1,47
	standard error ⁴⁾	0,40	0,43	0,28	0,29
	confidence interval -95 % ⁵⁾	19,63	23,47	22,17	21,73
	confidence interval +95 % ⁶⁾	21,28	25,23	23,33	22,95

¹⁾mód, ²⁾priemer, ³⁾smerodatná odchýlka, ⁴⁾chyba smerodatnej odchýlky, ⁵⁾interval spoľahlivosti -95%, ⁶⁾interval spoľahlivosti +95%

DISCUSSION

The measurement revealed that as the temperature of the thermal treatment of the wood increases, its lightness decreases. Similarly writes Dzurenda, 2018, by increasing the temperature of the saturated water vapour in the thermal treatment process and by prolonging the heat treatment time, the birch wood loses its brightness (darkening) and by decreasing values on the red colour coordinate a^* and on the yellow colour coordinate b^* in the colour space CIE-L* a^* b^* new brown shades are achieved.

The darkening of birch wood might be due to degradation of lignin and other non-cellulosic polysaccharides (Hon and Chang, 1985, Grelier et al., 2000, Petric et al., 2004). As wood is heated, acetic acid is formed from acetylated hemicelluloses by hydrolysis (Forsman 2008). The released acid serves as catalyst in the hydrolysis of hemicelluloses to the soluble sugars. The heat caramelizes the sugar to a brown colour, which affects the colour of wood. As the degradation of hemicelluloses accelerates with temperature, the

colour will become darker with increased treatment temperature (Forsman 2008; Tuong, 2010; Chen, 2012).

CONCLUSION

The proposed software allows you to determine the colour of any object in digital image. It is interpreted in the three most commonly used colour spaces, RGB, CIE XYZ and CIE L* a* b*. Using this application, for example, it is possible to detect the colour change of the wood during its thermal modifications or temperature fields in holographic interferometry analysed. The software allows saving the measured data in an .xls file for further processing.

ACKNOWLEDGMENT

This work was co-funded by the funding of the project VEGA 1/0315/2017: “The Research of the Relevant Properties of Thermally Modified Wood in the Contact Processes of Machining Addressing the Optimal Surface Achievement”, KEGA 005TU Z-4/2018 “Building a progressive CNC machining workplace for the innovation of teaching forms in study programs at the Faculty of Environmental and Manufacturing Technology” and project of Internal Project Agency No. 2/2019 and the “Impact of selected technological, tool and material factors on the surface finish quality and energetic intensity at plane milling of thermally modified spruce wood.”.

REFERENCES

- BABIÁK, M., KUBOVSKÝ, I., MAMOŇOVÁ, M. 2004. Colour space of the selected domestic species. In *Interaction of Wood with Various Forms of Energy*, Technical University of Zvolen, Zvolen, Slovakia, pp. 113–117.
- BRISCHKE, C., WELZBACHER, C., BRANDT, K., RAPP, A. 2007. Quality control of thermally modified timber: Interrelationship between heat treatment intensities and CIE L*a*b* colour data on homogenized wood samples. In *Holzforschung*, vol 61, no. 1, pp. 19–22.
- Dzurenda, L. 2019. Technical-technological characteristics of the thermal process of color modification of birch wood with saturated water steam. In *Acta facultatis technicae: scientific journal of Faculty of Technology*. 2019. no. 2, p. 61-73. ISSN 1336-4472.
- FORSMAN, S. 2008. Heat-treated wood. M.Sc. Thesis, Lulea University of Technology, Lulea, Sweden, 107 pp.
- GEFFERT, A., GEFFERTOVÁ, J. 2013. Chemical processing of wood. 1. vyd. Zvolen: Technical University in Zvolen, 2013. p. 90. ISBN 978-80-228-2492-7.
- GRELIER, S., CASTELLAN, A., KAMDEM, D.P. 2000. Photo-protection of copper amine treated wood. In *Wood and Fiber Science*. 32(2): 196-202.
- HON, D.N.S., CHANG, S. T. 1985. Photo protection of wood surfaces by wood-ion complexes. In *Wood and Fiber Science*. 17(1): 92-100.
- HRČKA, R. 2008. Identification of discoloration of beech wood in CieLab space. In *Wood Res-Slovakia*, vol. 53, no. 1, pp. 119–124.
- HRČKOVÁ et al. 2018. Color change of selected wood species affected by thermal treatment and sanding. In *BioResources*, vol. 13, no. 4, pp. 8956–8975. DOI: 10.15376/biores.13.4.8956-8975.

- CHEN, Y.; GAO, J.; FAN, Y.; TSHABALALA, M. A.; STARK, N. M. 2012. Heat-induced Chemical and Color Changes of Extractive-free Black Locust (*Robinia pseudoacacia*) Wood. In *Bioresources*, Volume: 7, Issue: 2, Pages: 2236-2248.
- KART, S., BAYSAL, E., TURKOGLU, T., KUCUKTUVEK, M., PEKER, H., ALTAY, C., GUNDUZ, A., TOKER, H. 2018, The effect of natural weathering on change in the color of heat treated and varnished scops pine and oriental beech woods. In *Wood Research*, vol. 63 (5): 2018. pp. 771-782. ISSN 1336-4561.
- KOLEDA, P., BARCÍK, Š., NOCIAROVÁ, A. 2018. Effect of technological parameters of machining on energy efficiency in face milling of heat-treated oak wood. In *BioResources*, no. 3, pp. 6133-6146.
- KUČERKA, M., OČKAJOVÁ, A. 2014. Particle size analysis of sawdust rising in the process of sawn dry spruce and oak wood. In IX. International scientific conference Chip and chipless woodworking processes, vol. 9, no. 1, pp. 105-110.
- MIKLEČIĆ, J., JIROUŠ-RAJKOVIĆ, V., ANTONOVIĆ, A., ŠPANIĆ, N. 2011. Discolouration of thermally modified wood during simulated indoor sunlight exposure. In *Bioresources*, Volume: 6, Issue: 1, Pages: 434-446.
- OČKAJOVÁ, A., BARCÍK, Š., KUČERKA, M., KOLEDA, P., KORČOK, M., VYHNÁLIKOVÁ, Z. 2019. Wood dust granular analysis in the sanding process of thermally modified wood versus its density. In *BioResources*. 2019. no. 4, pp. 8559-8572. ISSN 1930-2126
- PETRIC, M., KRICEJ, B., HUMAR, H., PAVLIC, M., TOMAZIC, M. 2004. Patination of cherry wood and spruce wood with ethanolamine and surface finishes. In *Surface Coatings International Part B: Coatings Transactions*. 87(B3): 95-201.
- SINGH, B., PARWATE, D. V., SHUKLA, S. K. 2009. Radiosterilization of fluoroquinolones and cephalosporins: Assessment of radiation damage on antibiotics by changes in optical property and colorimetric parameters. In *AAPS PharmSciTech*, vol. 10, no. 1, pp. 34–43. DOI: 10.1208/s12249-008-9177-y.
- SINKOVIĆ, T., GOVORČIN, S., RAJKOVIĆ, V. J., SEDLAR, T., MIKLEČIĆ, J., MAROŠAN, M. 2014. Defining of Wood Colour. In *Proceedings of the 57th International Convention of Society of Wood Science and Technology*. June 23-27, 2014, Technical University in Zvolen, Slovakia. Pp. 847-855. ISBN 978-0-9817876-4-0.
- ŠURIANSKY, J., HRČKOVÁ, M. 2010. Influence of light source spectre on digital image of wood texture. In *Acta facultatis technicae*, vol. 15, no. 1, pp. 113-122.
- TUONG, V. M., LI, J. 2010. Effect of heat treatment on the change in color and dimensional stability of *Acacia* hybrid wood. In *BioResources*, vol. 5, no. 2, pp. 1257–1267. DOI: 10.15376/biores.5.2.1257-1267.

Corresponding author:

Ing. Pavol Koleda PhD., tel. +421 45 520 6570, e-mail: pavol.koleda@tuzvo.sk

CONSTRUCTION OF THE LOADED HANDLING PART OF A PNEUMATIC MANIPULATOR

KONŠTRUKCIA ZAŤAŽENEJ MANIPULAČNEJ ČASTI PODTLAKOVÉHO MANIPULÁTORA

Mária Vargovská¹, Martin Mokryš², Ľubomír Javorek³, Ján Svorenň⁴

¹KVAT, FEVT, TU vo Zvolene, T. G. Masaryka, 2117/24, 960 01, Zvolen, SR, vargovska@tuzvo.sk

²GEVORKYAN, s.r.o., Zvolenská cesta 14, 974 03 Banská Bystrica, SR, mokryš@gevorkyan.sk

³KVAT, FEVT, TU vo Zvolene, T. G. Masaryka, 2117/24, 960 01, Zvolen, SR, lubomir.javorek@tuzvo.sk

⁴KVAT, FEVT, TU vo Zvolene, T. G. Masaryka, 2117/24, 960 01, Zvolen, SR, jan.svoren@tuzvo.sk

ABSTRACT: The contribution is intended as an educational material for a pneumatic manipulator design within the KEGA project. When designing the pneumatic manipulator, it is very important to properly design a framework. A manipulator handling part and its solution is a part of the framework. The contribution focuses on the methodical procedure of a bending moment course determination, on the basis of which the pneumatic manipulator framework is designed. An essential part of the construction design is to calculate the additional parts of the pneumatic manipulator, which are an important part of the input conditions for a static load determination. A result of the constructional design of the handling part of the pneumatic manipulator was the aim of the methodology on the basis of the initial conditions and computational methods.

Key words: pneumatic; construction; manipulation; transport

ABSTRAKT: Predkladaný príspevok je určený ako edukačný materiál pre návrhy konštrukcie pneumatických manipulátorov v rámci projektu KEGA. Pri návrhu pneumatického manipulátora, je veľmi dôležité správne navrhnuť jeho nosnú konštrukciu. Súčasťou takejto nosnej konštrukcie je aj manipulačná časť manipulátora a jej riešenie. Príspevok sa zameriava na metodický postup riešenia určenia priebehu ohybových momentov na základe ktorého je navrhnutá nosná konštrukcia pneumatického manipulátora. Nevyhnutnou súčasťou návrhu konštrukcie je výpočet prídavných častí pneumatického manipulátora, ktoré sú dôležitou súčasťou vstupných podmienok pre určovanie statického zaťaženia. Výsledok konštrukčného návrhu manipulačnej časti pneumatického manipulátora bolo hlavným cieľom tvorby metodiky v závislosti od vstupných podmienok a výpočtových metód.

Kľúčové slová: pneumatika; konštrukcia; manipulácia; doprava

INTRODUCTION

Manipulation is an important part of current production. Nowadays, a manipulation improvement together with a robot use affects the velocity and quality of manipulating part in the production. This fact is reflected on the company economics. When manipulating with a large-scaled material, the pneumatic manipulators are irreplaceable in modern service. This issue, presented in this contribution, is being solved within the KEGA project

“Progress and Application of Educational Methods in the Mechanics of Solids. All tasks and solutions are adapted to the project character. Because the robot and manipulator use affects a material flow velocity, quality and economy, it is necessary to develop individual parts and control, analyze and simplify all aspects.

From the design point of view, the static loading of a handling part of the pneumatic manipulator is an important factor. When using the mechanics for various kinds of problems, the finite element method which is based on the numerical solutions using mathematic algorithms is very useful (Kotšmíd et al. 2015). The only used criteria it is the demand of the minimum quantity of the consumed energy (Bodnár and Minárik 2015). The aim of this contribution is to make the approach of a construction design closer to the students with a manipulation and transport major. The first and also main assumption of a correct solution is knowledge of the initial conditions (Oswald 1982). Both mathematical and graphic methods are used in the educational process as a support of the solution.

MATERIAL AND METHODS

Design of the handling part of pneumatic manipulator is performed on the basis of working conditions, initial parameters and computed values. (Beňo 2001).The gripping force depends on:

- safety factors,
- kind of manipulation,
- friction coefficient between a suction cup and object,
- accelerations obtained during a manipulation (mainly in automation).

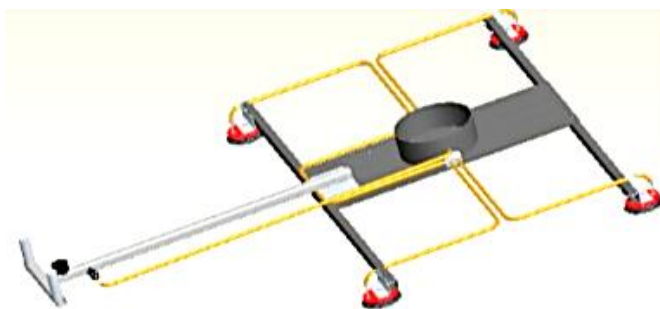


Fig. 1 The model of the handling part of pneumatic manipulator
Obr. 1 Model manipulačnej časti pneumatického manipulátora

Table 1 The friction coefficients between the suction cup and object
Tabuľka 1 Koeficienty trenia medzi prísavkou a objektom

Surface	Friction coefficient μ
Fet	0,1
Humid-wet	0,2–0,3
Wood, glass, metal	0,5
Thickness surfaces	0,6

The scheme of the forces acting in a process of a material manipulation is shown in Fig. 2.

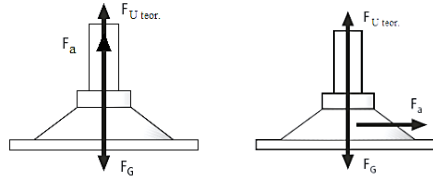


Fig. 2 The forces acting in the handling process
Obr. 2 Sily pôsobiace pri manipulácii

If the movement in lateral direction appears during the lifting an object (perpendicularly to the suction cup), the theoretical gripping force $F_{U\ teor}$ can be computed as follows:

$$F_{U\ teor} = (F_G + F_a) \cdot n = m \cdot \left(g + \frac{a}{\mu}\right) \cdot s \quad [\text{N}] \quad (1)$$

where: μ – the friction coefficient between the suction cup and object surface [–],
 a – distance [mm],
 m – weight [kg],
 g – gravitational acceleration [9,81 m. s⁻²],

Because the maximum acceleration cannot be determined, an additional load can be substituted by a safety factor increase ($s = 2.5$).

$$F_{U\ teor} = m \cdot g \cdot s = 150 \cdot 9,81 \cdot 2,5 = 3\,679 \text{ N} \quad (2)$$

In the next step, a suction cup number in longitudinal and lateral direction is required to specify.

In longitudinal direction, the stability and dimension of a moved object is the base. Therefore, it is necessary to take into account the maximum allowed overhang p regarding the minimum thickness h , maximum length l , and width b . For the material thickness $h > 12$ mm, it is necessary to take into account the maximum allowed overhang $p = 1500$ mm. According to practice, at least four suction cups (depends on a plate dimension) are needed for a manipulation with the large-scaled plates. The suction cups are distributed in the H shape.

Required suction cup number in longitudinal direction n_l :

$$n_l = \frac{l}{2 \cdot p} = \frac{2800}{2 \cdot 1500} = 0,9 \text{ pc} \quad (3)$$

In longitudinal direction, one suction cup was chosen on the basis of the computation. Required suction cup number in lateral direction n_b :

$$n_b = \frac{l}{2 \cdot p} = \frac{2070}{2 \cdot 1500} = 0,7 \text{ pc} \quad (4)$$

In lateral direction, one suction cup was chosen on the basis of the computation.

Total suction cup number n :

$$n = n_l \cdot n_b = 0,9 \cdot 0,7 = 0,63 \text{ pc} \quad (5)$$

On the basis of information from practice and depending on the total load for one suction cup, four suction cups in the H shape were chosen.

The total force for one suction cup is determined from the maximum theoretical gripping force and suction cup number as follows:

$$F_p = \frac{F_{U \text{ teor}}}{n} \quad [\] \quad (6)$$

$$F_p = \frac{3679}{4} = 920 \text{ N}$$

Required force in an active suction cup F_p depends on a suction pressure and active surface. The value is the same as the computed force for one suction cup, therefore:

$$F_p = \frac{\Delta p \cdot S}{10^3} \quad [\] \quad (7)$$

where: S – the active surface of a suction cup [mm],

Δp – the suction pressure between a suction cup and material surface [kPa]

(60% of the vacuum level is recommended by a producer = – 60 kPa).

At oval and rectangle suction cups, the active surface is determined by the length l_p and width b .

$$S = \frac{10^3 \cdot F_p}{\Delta p} = l_p \cdot b \text{ [mm}^2\text{]} \quad (8)$$

The suction cup diameter for a circular shape is determined by a simplified formula from noticed parameters as follows:

$$d = 113 \cdot \sqrt{\frac{m \cdot s}{\Delta p \cdot n}} \quad [mm] \quad (9)$$

$$d = 113 \cdot \sqrt{\frac{150 \cdot 2,5}{60 \cdot 4}} = 154,7 \text{ mm} \rightarrow 155 \text{ mm}$$

On the basis of the computed values and gotten knowledge of catalogues, the suction cup diameter was changed on $d = 150$ mm. The suction cup F 150 was selected from the PIAB company catalogue. The specification is shown in Tab. 2.

Table 2 The characteristics of the suction cup F150
 Tabuľka 2 Charakteristika prísavky F150

Type	The Normal Force in [N]			Min. radius of the handling object	Max. active pull-up of the suction cup	Weight
	-20 KPa	-60 kPa	-90kPa			
F150	300	850	1100	[mm]	[mm]	[g]

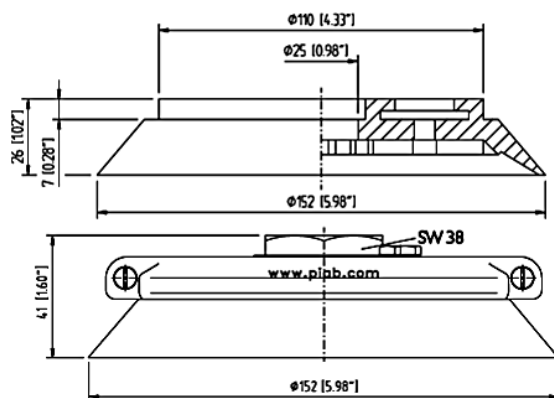


Fig. 3 The suction cup F150
 Obr. 3 Prísavka F150

The suction cup framework design (traverse):

The framework loading in a place of the lateral plate join is substituted by a point load on the plate edge. A construction balance is performed by the plate set in a traverse center. Considering this design, the force for a manipulation, a mass of the suction cups and their mounts are taken into account. The force acting on the traverse is computed as follows:

$$G_{trav} = (m_{object} + m_{cup} + m_{holder}) \cdot g \text{ [N]} \quad (10)$$

where: G_{traver} – traverse gravity [N],
 m_{object} – object mass per one suction cup [kg],
 $m_{object} = 37,5$ kg,
 m_{cup} – suction cup mass [kg],
 $m_{cup} = 0,2$ kg (provided by a producer),
 m_{holder} – mount mass [kg],
 $m_{holder} = 2$ kg,
 g – gravitational acceleration [$m \cdot s^{-2}$],
 $g = 9,81$.

After substitution, we get:

$$G_{trav} = (37,5 + 0,2 + 2) \cdot 9,81 \text{ [N]}$$

$$G_{trav} = 390 \text{ N}$$

Reaction forces are computed as follows:

$$R_1, R_2 = \frac{G_{trav} + G_{trav}}{2} \text{ [N]} \tag{11}$$

$$R_1, R_2 = \frac{390 + 390}{2} \text{ [N]}$$

$$R_1, R_2 = 390 \text{ N}$$

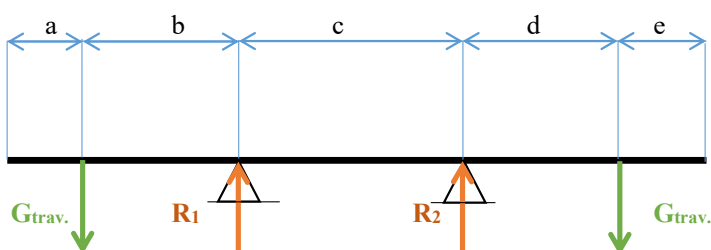


Fig. 4 Diagram of the forces acting on the traverse
Obr. 4 Schéma pôsobiacich síl na traverze

$a = e = 0,2 \text{ m};$
 $b = d = 0,5 \text{ m};$
 $c = 0,4 \text{ m}$

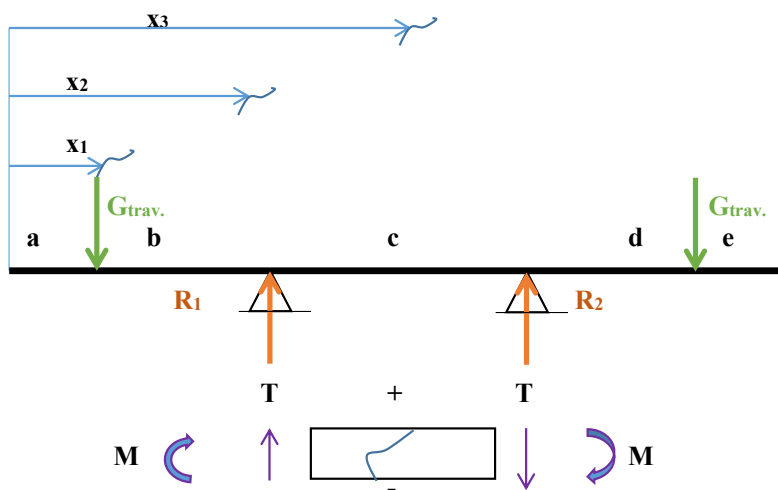


Fig. 5 Diagram of the forces acting on the traverse (sectional view)
Obr. 5 Schéma síl pôsobiacich na traverze (čiasťončný pohľad)

$$0 \leq x_1 \leq a \quad (12)$$

$$T_1 = 0 \text{ N } M_1 = 0 \text{ Nm}$$

$$a \leq x_2 \leq a + b$$

$$T_2 = -G_{trav} = -390 \text{ N}$$

$$M_2 = -G_{trav} \cdot (x_2 - a) \rightarrow M_2 = -390 \cdot 0 = 0 \text{ Nm}, M_2 = -390 \cdot 0,5 = -195 \text{ Nm}$$

$$a + b \leq x_3 \leq a + b + c$$

$$T_3 = -G_{trav} + R_1 = -390 + 390 = 0 \text{ N}$$

$$M_3 = G_{trav} \cdot (x_3 - a) \rightarrow M_3 = -390 \cdot 0,5 = -195 \text{ Nm}$$

$$M_3 = G_{trav} \cdot (x_3 - a) + R_1 \cdot (x_3 - a - b) \rightarrow M_3 = -390 \cdot (0,5 + 0,4) + 390 \cdot 0,4 = -195 \text{ Nm}$$

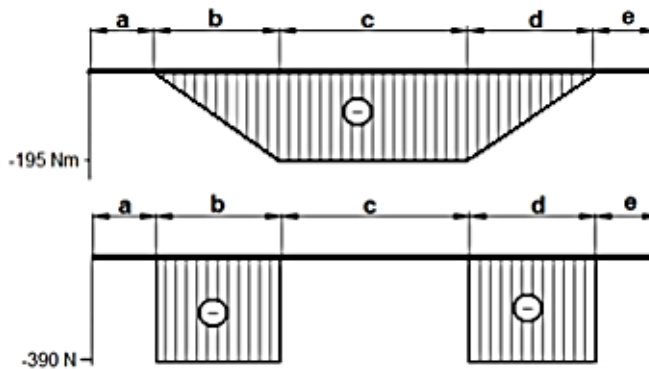


Fig. 6 The course of the forces and bending moments
Obr. 6 Priebeh síl a ohybových momentov

The traverse span of the pneumatic manipulator is shown in Fig. 6. The forces have distances a, b, c among each other.

On the basis of previous computations, a traverse profile design is required to be performed. Thin-walled profile TR 40 x 20 x 2 – STN 42 6936 -11 320 is the most suitable one from the constructional point of view. Based on the elastic section modulus W_o , the profile dimensions were determined.

$$W_o \geq [m^3] \quad (13)$$

$$W_o \geq 1,3 \cdot 10^{-6} m^3 = 1,3 \cdot 10^3 mm^3$$

where: M_{max} – maximum bending moment [$N.m^{-1}$],
 $M_{max} = M2 = 195 N.m^{-1}$,
 σ_{dov} – allowable stress [MPa],
for 11 320 material $\sigma_{dov} = 150 \cdot 10^6$ MPa.

Because the static state was a base for the traverse design, it is necessary to take into account the dynamic load (appeared during acceleration and deceleration of the manipulator moving parts). Thin-walled profile TR 40 x 35 x 3 –STN 42 6936 -11 320 with the length of $l = 1\ 800$ mm was chosen as a beam for the suction cup mount.

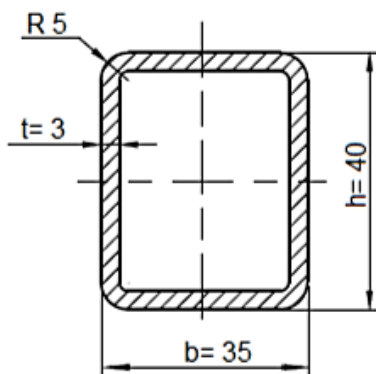


Fig. 7 The Cross section of the selected beam
Obr. 7 Prierez vybraného nosníka

Both traverses are joined by the lateral plate. It has a robust construction owing to the framework for a manipulator hook; it has a shrinking hose and control handle. When designing the plate, the total mass of the lifting object and a mass of the suction cups, mounts and traverses are taken into account.

$$G_{plate} = 2 \cdot G_{trav} + (m_{prof} \cdot g) \quad [N] \quad (14)$$

$$G_{plate} = 2 \cdot 390 + (5,85 \cdot 9,81) \quad [N]$$

$$G_{plate} = 838 \text{ N}$$

$$R = 2 \cdot G_{plate} = 1\ 676 \text{ N} \quad (15)$$

where: G_{traver} – traverse gravity [N]
 m_{prof} – traverse mass [kg] (2 pieces),
 $m_{prof} = 5,85$ kg– 1 pc,
 g – gravitational acceleration [$m.s^{-2}$],
 $g = 9,81 m.s^{-2}$.

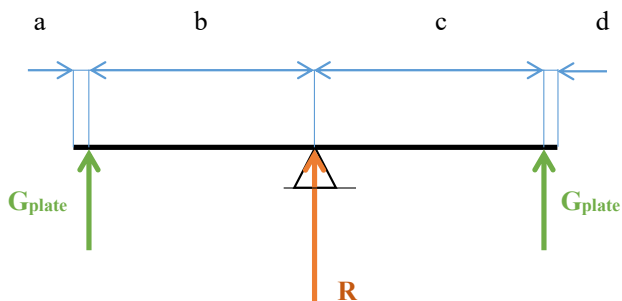


Fig. 8 Diagram of the forces acting on the plate
Obr. 8 Schéma síl pôsobiacich na dosku

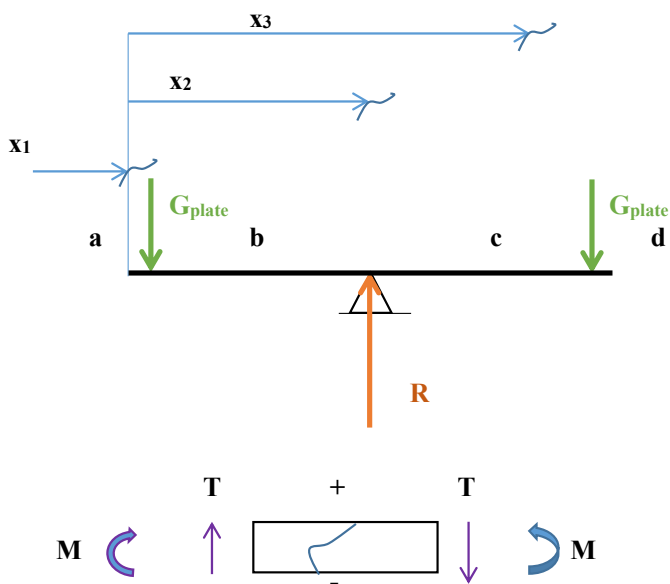


Fig. 9 Diagram of the forces acting on the plate (sectional view)
Obr. 9 Schéma síl pôsobiacich na dosku (čiastočný pohľad)

$$0 \leq x_1 \leq a \quad (16)$$

$$T_1 = 0 \text{ N } M_1 = 0 \text{ Nm}$$

$$a \leq x_2 \leq a + b$$

$$T_2 = -G_{\text{plate}} = -838 \text{ N}$$

$$M_2 = -G_{\text{plate}} \cdot (x_2 - a) \rightarrow M_2 = -838 \cdot 0 = 0 \text{ Nm}, M_2 = -838 \cdot 0,48 = -402,25 \text{ Nm}$$

$$a + b \leq x_3 \leq a + b + c$$

$$T_3 = -G_{\text{plate}} + R_1 = -838 + 1\,676 = 838 \text{ N}$$

$$M_3 = -G_{\text{plate}} \cdot (x_3 - a) \rightarrow M_3 = -838 \cdot 0,48 = -402,25 \text{ Nm}$$

$$M_3 = -G_{\text{plate}} \cdot (x_3 - a) + R_1 \cdot (x_3 - a - b) \rightarrow M_3 = -838 \cdot (0,48 + 0,48) + 1\,676 \cdot 0,48 = 0 \text{ Nm}$$

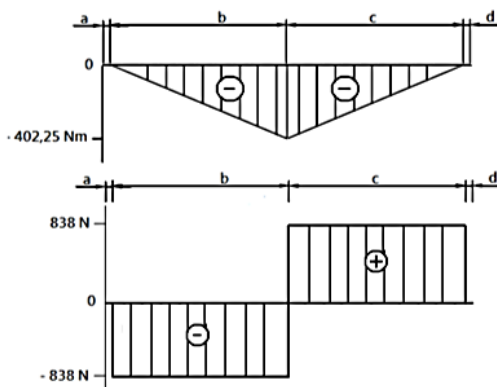


Fig. 10 The course of the forces and moments acting on the plate
Obr. 10 Priebeh síl a momentov pôsobiacich na dosku

RESULTS

A constructional design of the handling part of the pneumatic manipulator was the aim of the methodology on the basis of the initial conditions and computational methods. The engineers decide on the basis of computations as well as experience and economical parameters that affect the final solution (Dogheri 2000). Price, safety and device lifetime are the key factors choosing the constructional and technical solution. These factors affect the final design. The computation methodology and verification of the solution possibilities by several methods such as mathematical, graphical, and simulations are an essential part of a complex design (Toogood 2015).

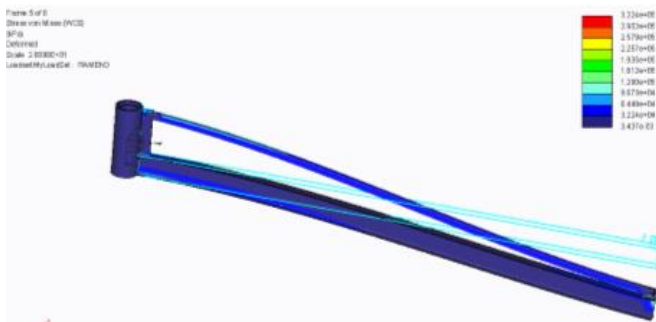


Fig. 11 The stress distribution acting on the manipulator arm carrying the handling part
Obr. 11 Rozloženie napätí pôsobiacich na rameno manipulátora nesúceho manipulačnú časť

DISCUSSION

The contribution, describing the constructional design of the handling part of pneumatic manipulator, brings the most effective approach. The design and methodology can be used for both educational and practice use. At the example solution of the handling part of pneumatic manipulator and mainly at the framework, the solution approach is explained in case of the initial parameters knowledge (Shigley et al. 2004) Experience, approaches, knowledge and initial parameters are the key factors choosing and dimensioning the framework of pneumatic manipulator.

CONCLUSION

Drafting this contribution, one of partial goals of the KEGA project (for educational purposes) has been taken into account. Its results meet all requirements. A comparison of the solutions by several methods has proved the correctness of chosen approach as well as the solution results. The main aim was to provide the methodology for solving the static load of the handling part of pneumatic manipulator construction. Nowadays, when the finite element method is world-wide used, classic analytic methods retreated. For the educational purposes, several classic methods were used and verified with the progressive approaches on the basis of the results.

ACKNOWLEDGEMENT

The contribution has been written on the basis of the grants projects “Progress and Application of Educational Methods in the Mechanics of Solids” no. 015TU Z-4/2019 and 005TU Z-4/2018 Building a progressive CNC machining workplace for the innovation of teaching forms in study programs at the Faculty of Environmental and Manufacturing Technology.

REFERENCES

- BEŇO, P.: 2001. Časti a mechanizmy strojov. Zvolen: Vyd. Technická Univerzita vo Zvolene, 200.390s ISBN 80-228-0985-3.
- BODNÁR F., MINÁRIK M.: 2015. *Coniform-shape tool for splitting of wooden logs*. Res. Agr. Eng., 61: 29-34.
- DOGHRI, I.: 2000. *Mechanics of deformable solids linear, nonlinear, analytical and computational aspects*. Berlin: Springer-Verlag Berlin Heidelberg, 2000, 579 s. ISBN 978-3-642-08629-8.
- KOTŠMÍD, S., MINÁRIK M., BEŇO P.: 2015. *Comparison of the Experimental and Theoretical Critical Buckling Force at the Rod of a Defined Shape*, Technics Technologies Education Management 10(2):139 - 143
- OSWALD, J.: 1982. *Manipulácia s materiálom*, Zvolen: vyd. Vysoká škola lesnícka a drevárska vo Zvolene 134s.
- TOOGOOD R. , 2015. *Creo Parametric 3.0 Tutorial*. SDC Publications, 2015. ISBN 978-15-850-3948-7
- SHIGLEY, J. E., MISCHKE, Ch. R., BUDYNAS, R. G.: 2004. *Mechanical engineering design*. New York: The McGraw-Hill Companies, Inc., 2004, 1030 s. ISBN 978-0-072-52036-1.

Corresponding author:

Ing. Mária Vargovská PhD., e-mail: vargovska@tuzvo.sk

EFFECT OF FEED SPEED AND TYPE OF ROUTING TO TOTAL FORCE

EFEKT POSUVNEJ RÝCHLOSTI A SPÔSOBU FRÉZOVANIA NA CELKOVÚ SILU

Lubomír Javorek

*KVAT, FEVT, TU vo Zvolene, T. G. Masaryka, 2117/24, 960 01, Zvolen, SR,
lubomir.javorek@tuzvo.sk*

ABSTRACT: The material machining with using of routers is very frequent for modern CNC routers. If the values of forces, moments respectively that stress machined piece or cutting tool, than the suitable strategy of routing permits machining of thin-walled pieces without losing of accuracy (dimensions and shapes). In this contribution are mentioned values of final force like functionality of various feed speed (3.2 m/min., 3.6 m/min.), depth of cut (1mm, 2 mm, 3 mm, 4 mm), for up and down cutting. Tool revolutions were constant – 16000/min. Tool rotational frequency was 16000 min⁻¹.

Key words: routing, router bit, cutting forces, medium density fibreboard (MDF).

ABSTRAKT: Obrábanie materiálov stopkovými frézami je rozšírené predovšetkým na moderných frézovacích číslicovo riadených strojoch. Vhodná stratégia frézovania umožňuje obrábať aj tenkostenné prvky bez straty rozmerovej a tvarovej presnosti, ak sú známe hodnoty síl, resp. momentov, ktoré obrobok, resp. nástroj namáhajú. Príspevok uvádza hodnoty výslednej sily pri obrábaní konštantnými otáčkami, pri dvoch rôznych posuvoch a hĺbkach rezu od 1 mm do 4 mm.

Kľúčové slová: frézovanie, stopková fréza, rezné sily, drevovláknitá doska (MDF).

INTRODUCTION

The routing is one from the most frequent technology wood machining. The importance of this technology accrete together with more and more extensive using router machines. The routers are used in furniture production let us say in production its parts, or for technologies like moulding, profiling, trimming, grooving etc. Machining of medium density fibreboards like very perspective nowadays was in the centre of (Davim, P.J., Clemente, V.C., Silva, S. 2009) research. In this research was used cemented carbide end router with two cutting enges, revolutions were in range from 3000/min. till 18000/ min. and feed speed was changed from 0.5 m/min. to 5 m/min. The authors measured surface roughness and received the influence for example feed speed to dimensional precision (IT), or feed speed to arithmetic surface roughness (Ra), or mean/maximum peak to valley heights for various spindle speeds. In contribution (Huang, Y.S. et all. 2003.) are present results from

measure of horizontal force that increase with increasing of depth of cut and decreased with rake angle increase. The vertical cutting force increased with an increase of cutting depth. The critical value of cutting force (Ispas et al. 2006) or some its component (Javorek et al. 2001), (Javorek and Hric 2005), torque moment (Marthy and Cismaru 2009) or some other parameter (amplitude, temperature, noise etc.) are used in CNC machines (Ohuchi and Murase 2005) for automatic scanning of correct working cycle. The influence of rake angle, chip thickness and upward/downward milling were independent factors for analyse of two components of total force. The force sensor ATI Gamma with sampling frequency 7000 Hz was used for sawing of data from cutting process (Palmquist 2003). They received value of depends variable, that depends very strictly from input parameters.

By (Palmquist et all 2005), which examined the cutting forces when up-milling in beech wood feed force varied from 40 N/cm to 86 N/cm and passive force in range from 14 N/cm to 51 N/cm.

MATERIAL AND METHODS

Samples

The MDF (Medium Density Fibreboard) samples with dimensions 190 mm x 125 mm and thickness 18 mm and 50 mm were used for routing. MDF is material with very high homogeneity in whole cross cut.

Tool

Samples of wood were machined by router bit (producer Karned Dečín, Czech rep.) with exchange inserts. Parameters of router are follows:

- Diameter of cutting circle (mm): 19;
- Number of inserts (-): 2;
- Geometry – back, wedge, rake angles ($^{\circ}$): $\alpha_o=35^{\circ}$, $\beta_o=36^{\circ}$, $\gamma_o=19^{\circ}$.



Fig. 1. Router with inserts and collet
Obr. 1. Fréza s platničkami a upínačom

Technological conditions and methodology of machining

The experimental measurements were realized on CNC machine, type Homag Venture 13M.



Fig. 2. General view to CNC machine
Obr. 2. Celkový pohľad na CNC frézovačku

- Tool rotational frequency (1/min.): 16 000;
- Depth of cut (mm): 1; 2; 3; 4;
- Feed speed (m/min.): 3,2; 3,6;
- Type of milling (–): up milling, down milling.

The total path of routing was divided to two stages; up and down cutting and every stage was divided to two substages – with interrupting in half of length and join with changing of feed speed.

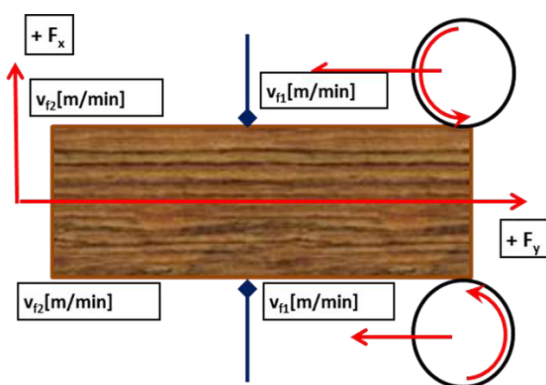


Fig. 3. Machining methodology
Obr. 3. Metodika obrábania

Measuring system

The experimental measuring system consists from Quartz 3-Component Dynamometer Type 9257B, multichannel Charge Amplifier for Multi-Component Force Measurement Type 5070A, A/D convertor Kistler 5657A and software DynoWare 2825A.

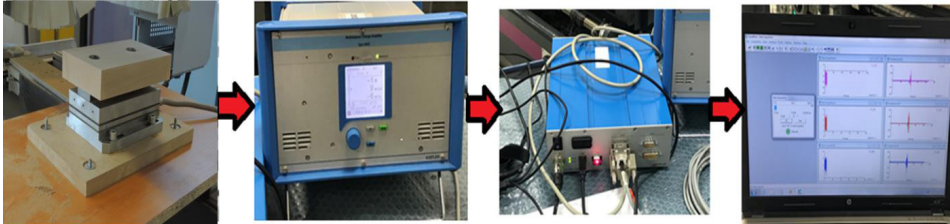


Fig. 4. Experimental measuring system
Obr. 4. Experimentálny merací systém

Procedure

Due to the methodology of experiment, one full cycle consists from four particular records interrupted by three idling runs for change of feed speed and tools position, i.e. changing of up milling to down milling, except idling run before and after cutting. The whole cycle, with comments is displayed in Fig. 5

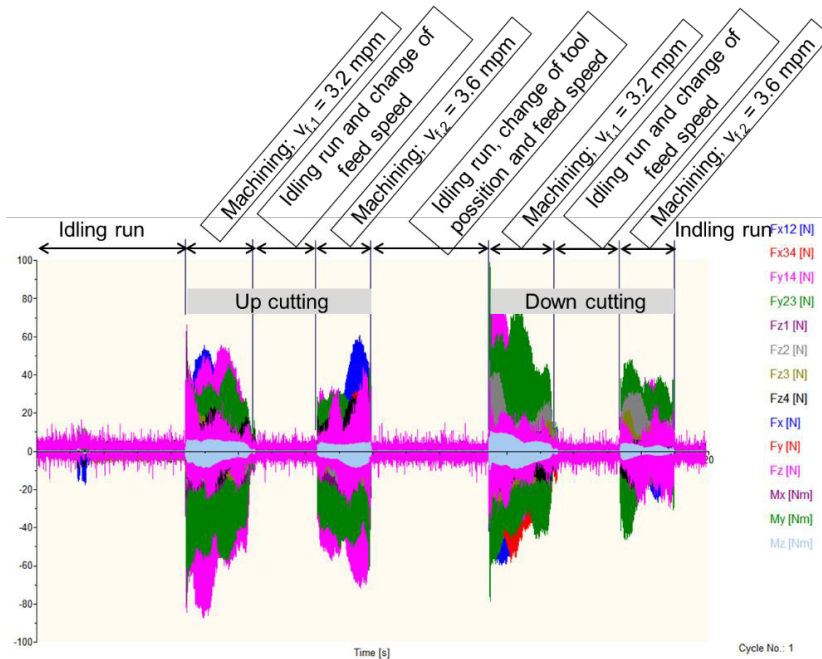


Fig. 5. The original records of signals and phases of process
Obr. 5. Zdrojový záznam signálov a časti procesu

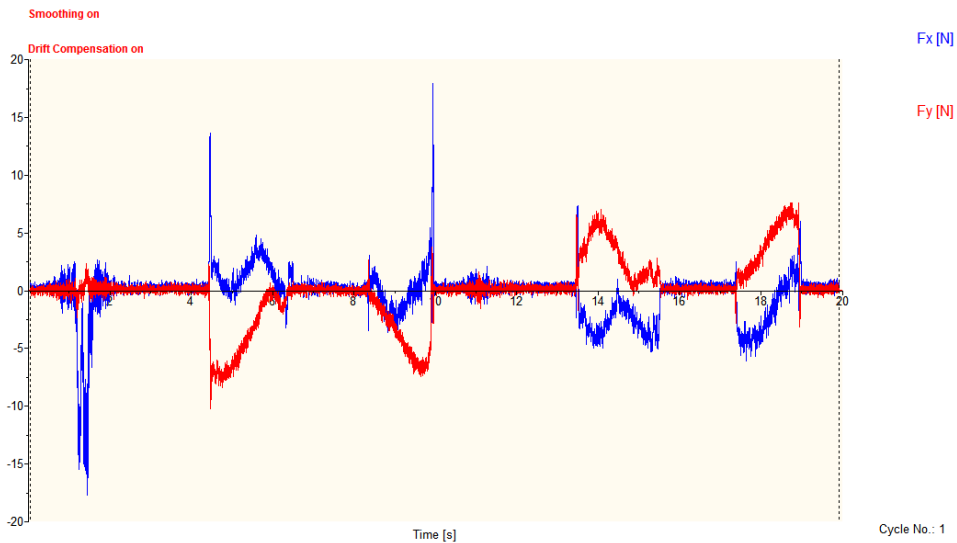


Fig. 6. The signals after filtering
Obr. 6. Filtrované signály

RESULTS

The values displayed in table 1 are average values received from original records using of available filter. Original record of every part contended cca 2500 values, idling runs were eliminated before computing, including of drift compensation. Moving mean with windows size 200 was used like smoothing method and from values which were received after this manner the average value was estimated.

Table 1. The total force F
Tabuľka 1. Celková sila F

Type of milling	Feed speed [m/min.]	Depth of cut [mm]			
		1	2	3	4
		Total force [N]			
Up milling	3.2	5.5	8.8	11.4	15.6
	3.6	4.4	7.7	14.1	16.5
Down milling	3.2	4.6	8.4	11.4	13.9
	3.6	5.4	9.1	11.3	15.8

$$F = \sqrt{F_x^2 + F_y^2 + F_z^2} \quad (1)$$

where F_y is force perpendicular to feed direction [N],

F_x is force in feed direction [N],

F_z is thrust force (axial) [N] ($F_z=0$)

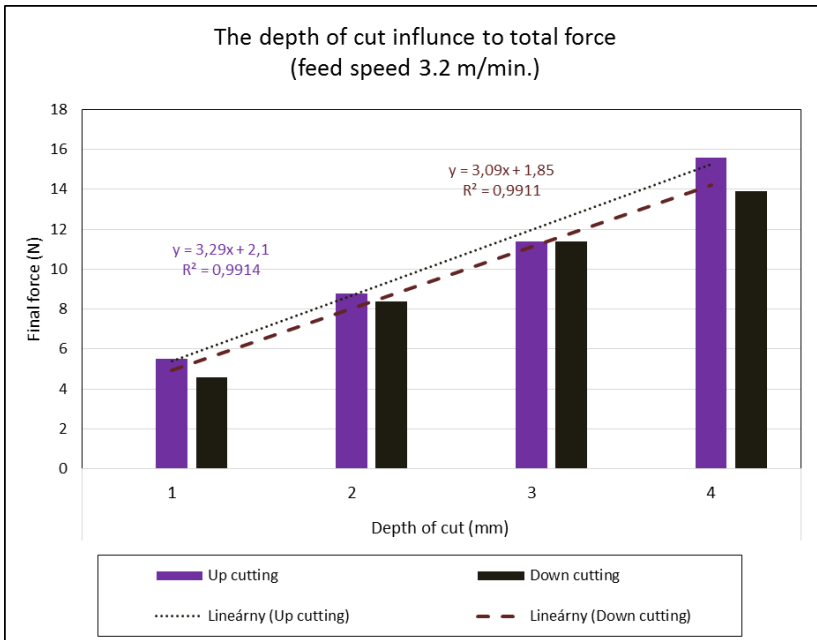


Fig. 7. Influence of depth of cut and feed speed to total force ($v_f = 3.2$ m/min)
Obr. 7. Vplyv hĺbky rezu a rýchlosti posuvu na celkovú silu ($v_f = 3.2$ m/min)

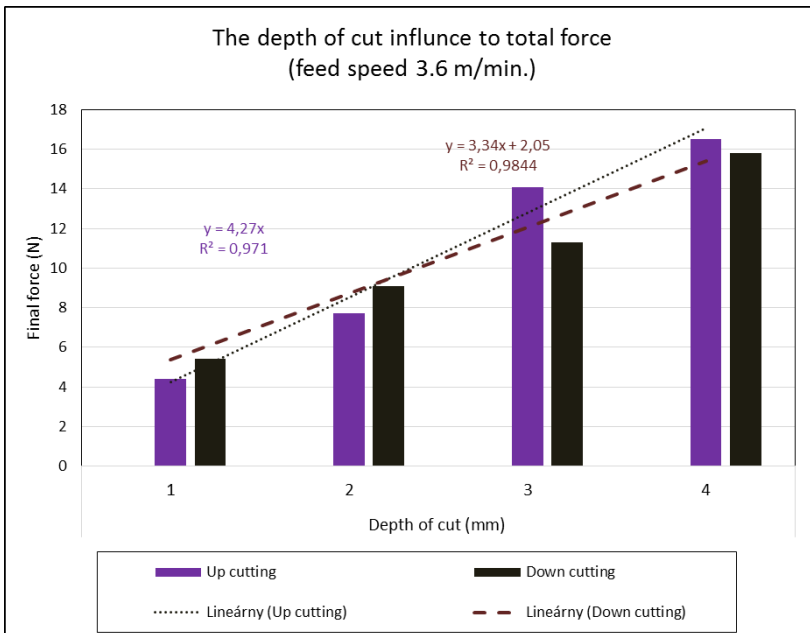


Fig. 8. Influence of depth of cut and feed speed to total force ($v_f = 3.6$ m/min)
Obr. 8. Vplyv hĺbky rezu a rýchlosti posuvu na celkovú silu ($v_f = 3.6$ m/min)

On the graphs (Fig. 7 and Fig. 8) is clearly visible that the change of depth of cut from 1 mm to 4 mm, i.e. cca 3 times for feed speed 3.2 m/min and 4 times for feed speed 3.6 m/min has significant influence to total force. The influence of depth of cut for up cutting, respectively down cut is so so linear, with slope of a straight line 3.29 resp. 3.09 for feed speed 3.2 mm/s, 4.27 resp. 3.34, for feed speed 3.6 mm/s with R-square 0.971, resp. 0.984 for feed speed 3.6 mm/s. So that, for this model of cutting, the influence of that of cut to final force is as near as proportioned (Notice: all results valid in the range of this experiment and it is impossible to apply its for another conditions).

CONCLUSION

The paper describes experiment of routing and process of the final force computing. The mathematical model for final force calculation is known from the Cartesian system of tool and workpiece positioning. Values for computing were obtain from experimental measuring.

Generally may by conclude that:

1. The depth of cut has proportionable influence to final force; slope of a straight line (angular coefficient) depends from type of machining.
2. The type of machining had very small influence to final force in this case, i.e. during machining of MDF. Hardness of MDF is a several times smaller than hardness of some another samples for example from hard wood.

ACKNOWLEDGMENT

Acknowledgement: This work was supported by the Slovak Research and Development Agency under the contract No. APVV-16-0177 and by the Scientific Grant Agency of the Ministry of Education SR and the Slovak Academy of Sciences Grant No. 1/0822/17.

LITERATURE

- HUANG, Y.S. et al. 2003. Peripheral milling properties of compressed wood manufactured from planted China-fir. *Holz als Roh- und Werkstoff* 61 201-205. DOI 10.1007/s00107-003-0376-7
- DAVIM, P.J., CLEMENTE, V.C., SILVA, S. 2009. Surface roughness aspects in milling MDF. *Int J Adv Manuf Technol* 40 pp.49-55. DOI:10.1007/s00170-007-1318-z
- ISPAS, M. et al. 2006. Experimental researches on the workability of some wood-based composites by routing with diamonded tools. *PRO LIGNO Journal* 2 (4). (2006).ISSN 1841-4737. pp. 27-34.
- JAVOREK, L., OSWALD, J., SCHELCHER, CH. 2001. Feed force during milling. *Wood Research* 46 (2). (2001). ISSN 0012-6136. pp. 29-36
- JAVOREK, L., HRIC, J. 2005. Konštrukcia nástroja a výkon potrebný na rezanie. *Acta Facultatis Technicae. Technická univerzita vo Zvolene*. VIII (1). (2005). ISBN 80-228-1517-9. pp. 107-116.
- MARTHY, M., CISMARU, I. 2009. Experimental study concerning the power consumption at the milling of pear. *PRO LIGNO Journal* 5 (3). (2009). ISSN 1841-4737. pp. 47-53.
- OHUCHI, T., MURASE, Y. 2005. Milling of wood and wood-based materials with a computerized numerically controlled router IV: development of automatic measurement system for cutting

- edge profile of throw-away type straight bit. *The Japan Wood Research Society* 51. (2005). pp. 278-281
- PALMQVIST, J. 2003. Parallel and normal cutting forces in peripheral milling of wood. *Holz als Roh- und Werkstoff* 61 409-415. DOI 10.1007/s00107-003-0427-0
- PALMQVIST, J. et al. 2005. Cutting-forces when up milling in beech. *Wood Sci Technol* 39: 674-684. DOI 10.1007/s00226-005-0010-4
- PATWARI, U., FARIS, W. 2008. Response surface methodological approach for the prediction of tangential cutting forces in milling of steel. *Journal of engineering*. ISSN-1584-2673 pp.171-178.
- Y. LI., S. Y. LIANG. 1999. Cutting force analysis in transient state milling processes. The *International Journal of Advanced Manufacturing Technology* 15, pp.785–790.

Corresponding author:

doc. Ing. Lubomír Javorek, CSc., e-mail: lubomir.javorek@tuzvo.sk

APPLICATION OF SELECTED REVERSE ENGINEERING TECHNIQUES IN THE CREATION OF CAD MODEL OF A PART WITH A COMPLEX SHAPE

APLIKÁCIA VYBRANÝCH POSTUPOV REVERZNÉHO INŽINIERSTVA PRI TVORBE CAD MODELU TVAROVO ZLOŽITEJ SÚČIASTKY

Mária Hrková¹, Pavol Koleda¹, Marek Kassai²

¹ KVAT, FT, TU Zvolen, Študentská 26, 960 01 Zvolen, Slovakia, hrckova@tuzvo.sk

² FT, TU Zvolen, Študentská 26, 960 01 Zvolen, Slovakia

ABSTRACT: In the paper we described the process of reverse engineering in the reconstruction of a part with a complex shape. We focused on a 3D scanning of the part and its reconstruction in a 3D model. When scanning, we used a combination of scanning by measurement and a laser scanning to compensate for the imperfections of either of the methods. The result was a 3D scan of the part. Furthermore, we made a 3D scan correction to minimize the scanning errors. After the necessary modifications, we continued with the reconstruction of the 3D scan into a 3D model. The reconstruction was done using two methods: the Auto Surface method and a method of re-modelling the 3D scan. We compared the created models with the 3D scan and evaluated the size of the created deviations.

Key words: reverse engineering, scanning, reconstruction, 3D model

ABSTRAKT: V článku sme popísali realizovaný proces reverzného inžinierstva pri rekonštrukcii tvarovo zložitej súčiastky. Zamerali sme sa na 3D skenovanie danej súčiastky a jej rekonštrukciu. Pri skenovaní sme využili kombináciu dotykového a laserového skenovania, aby sme kompenzovali nedokonalosti jednej metódy skenovaním pomocou druhej metódy. Výsledkom bol 3D sken súčiastky. Ďalej sme realizovali korekciu 3D skenu tak, aby sme zminimalizovali chyby skenovania. Po nevyhnutných úpravách sme pristúpili k rekonštrukcii 3D skenu na 3D model. Rekonštrukciu sme urobili dvomi metódami: metódou s využitím funkcie Auto Surface a metódou premodelovania 3D skenu. Vytvorené modely sme porovnali s 3D skenom a vyhodnotili veľkosť vzniknutých odchýlok.

Kľúčové slová: reverzné inžinierstvo, skenovanie, rekonštrukcia, 3D model

INTRODUCTION

In order to avoid industry stagnation, it is essential to introduce more and more cutting edge solutions that will enable businesses to be more flexible, faster and more efficient. One of them is reverse engineering. Reverse engineering technology is a powerful tool

in integrated engineering that enables optimization of product design and performance, flexible production with minimal cost, accelerated design of new products and high quality (Tut et al. 2010).

Reverse engineering is a rapidly evolving methodology that can be applied in various industries. The primary use of reverse engineering is to manufacture again any object or reconstruct it (Kumar et al. 2013). Reverse engineering uses an existing object (Paulic et al. 2014). The aim is to create a digitized CAD model that is identical to original object (Li et al. 2002) and thus to obtain information about it. Reverse engineering can be defined as an object analysis process in order to: determine its operation, shape and dimensions, convert it into a digital form without access to the original technical documentation or CAD model, to produce the same object to replace the original, or improve its required features (Anwer & Mathieu 2016). Reverse engineering can be used in a variety of cases. If no original drawings or documentation are available, if we want to try different modifications or analyses on existing objects, which would lead to improvement or comparison with another object, in design modification, in making individual adjustments and so on. (Varades et al. 1997).

Equipment for digitizing components is used for the reverse engineering process. They are used to transfer physical shapes and dimensions to a digital version in the form of a CAD model. This conversion of a real component into a digital version is called 3D digitization (Slota et al. 2010). The scanning devices work on different principles. The most common are contact scanning devices that work on the principle of direct contact with the part. Their disadvantage is that they are more time consuming and thus have lower productivity and limited scanning of hard-to-reach places of small parts with complicated shapes. There are also contactless sensing devices that do not require physical contact with the object surface. They are fast and capable of capturing surface details. However, their accuracy is lower.

Reverse engineering has many advantages. With this method, companies can create a product in a significantly shorter time than would be possible using conventional production methods. From a physical model already created in this way, it is possible to quickly and efficiently create a digital CAD model and then start production according to it or adapt the digital model to requirements without the need for costly and time consuming production of the physical model. In some situations, this is the only possible alternative for manufacturing the desired component or system. (Raja & Fernandes 2008). The disadvantages include, in particular, the economic requirement of the technical means necessary to carry out reverse engineering procedures. Nevertheless, reverse engineering has a significant place in contemporary technology (Wang 2010).

The aim of our experiment was to get acquainted with the issues of reverse engineering of complicated parts, to test the suitability of various object scanning techniques and to compare the processing of scanned data in different ways.

MATERIAL AND METHODS

1. Object selection

Applying reverse engineering to simple objects does not require a combination of different approaches. The aim of our experiment was to use various techniques of scanning and reconstruction of objects into 3D models. Therefore, when we were selecting an ob-

ject suitable for the analysis of individual stages of reverse engineering, we focused on objects that have a complex shape. For these reasons, we used a part – carburettor, for which no drawing documentation was available.



Figure 1 Scanned part – carburettor
Obrázok 1 Skenovaná súčiastka – karburátor

When scanning with a light beam, it is important to adjust the surface of the scanned object. If the surface is shiny or dirty, the scanning process may be inaccurate or the scanned surface may not be detected (Hrčková et al. 2017). Our component has been contaminated, which could have reduced the quality of the scan. For accurate and relevant results, we cleaned and degreased the carburettor prior to 3D scanning.

2. Scanning equipment

3D scanning was performed in CEIT, a.s. Zilina. The company is engaged in research, development and application of progressive technologies and their implementation into practice. The scanning process itself took place in a special laboratory, which is adapted to perform measurements by scanning. The laboratory is air conditioned and maintains constant temperature and constant humidity.

We used the Faro Edge ScanArm® HD for the scanning process (Figure 2). It is a 7-axis articulated measuring device that combines contact measurement using a touch sensor and contactless measurement using a laser scanning head. The device has an arm length of 1.8 m.



Figure 2 Scanning device Faro Edge ScanArm® HD
Obrázok 2 Skenovacie zariadenie Faro Edge ScanArm® HD

Table1. Scanning equipment technical specifications

Tabuľka 1. Technické špecifikácie skenovacieho zariadenia

Touch sensor	
Volumetric accuracy	±0.034 mm
One point repeatability	0.024 mm
Weight	10.7 kg
Laser head	
Accuracy	±25 μm
Repeatability	25 μm, 2σ
Stand-off	115 mm

Focal length	115 mm
Effective scanning width	for a short distance 80 mm, over a greater distance 150 mm
The number of points on the laser line	2 000 points/line
Minimum distance between points	40 μm
Scan speed	280 frames/s, 280 fps x 2,000 points/line = 560,000 points/s
Laser	Class 2M

For touch measurement, the device uses a touch measuring sensor that uses a replaceable small ball of different diameters. The choice of small ball diameter depends on the character of the measured area and the dimensions of the measured element. The coordinate of the measured point in the given coordinate system is generated based on signals from individual joints. When scanning with a laser beam, the position of the laser beam source is recorded. Based on the known position of the laser beam source and triangulation relative to the scanned object, a 3D model of the scanned object is created.

3. Scan

The first step was to calibrate the 3D scanner. An essential prerequisite for the calibration and the entire scanning process is the fixation of the scanning device on the desk. The device cannot change its position during measurement. The calibration itself is carried out using special equipment supplied by the manufacturer. We first calibrated the touch sensor (small ball) and then synchronized the touch sensor with the laser head.

We fixed the scanned part to the table into a clamping device. Because of the way it was secured, the part had to be scanned twice to capture all of its sides. Before the measurement we defined the coordinate system by the method of determination of plane, point and vector. By determining the coordinate system, we determined the position of the 3D scan relative to the central coordinate system of the polyWorks software, and at the same time we have secured a starting point for aligning the model scans obtained. Scanning took place in two phases. In the first phase we measured the basic planar surfaces and circular parts with the touch sensor, in the second phase we used laser beam scanning. The entire scanning process and scanned parts could be viewed directly on the computer. When scanning a complicated shape, it was necessary to scan rugged surfaces from multiple angles. In this way, we achieved higher accuracy of details on the part.

RESULTS AND DISCUSSION

1. Modify 3D scan

By scanning the part at two different fixations, we obtained two 3D scans of the part. We unified these scans on the basis of three selected points in three different axes. The result was a unified 3D model. Scanning was performed in software InnovMetric PolyWorks. The 3D scan obtained can be seen in Figure 3.

The yellow areas in Figure 3 represent the model, the tables contain basic data (XYZ coordinates, circle diameters, etc.) and the blue areas represent problematic areas (dark corners, deep holes, etc.). In the case of a more complex shape of the part, it is necessary

to remove imperfections in the form of holes and open areas before reconstruction. This results in a closed component that does not contain any openings and holes, even those that actually exist. Their dimensions and position are unambiguously defined and will be recreated when the scan is reconstructed. With closure we will eliminate most imperfections and greatly simplify the process of editing the 3D scan and reduce editing time. We modified the 3D scan in program Geomagic Wrap from company 3D Systems.



Figure 3 Scan result – 3D model
Obrázok 3 Výsledok skenovania – 3D model

4. Reconstruction of the 3D scan

The extent and method of reconstruction depends on the purpose for which 3D scanning is performed. If we want high-quality and complete technical documentation, a complex reconstruction is a must. The reconstruction process can be performed in CARE (Computer Aided Reverse Engineering) type programs. These are CAD systems that support reverse engineering. E.g. CATIA, CREO, SolidWorks. The second alternative is programs that are primarily aimed at reverse engineering, such as: Geomagic Design X from 3D Systems. This program provides us with a wider range of options when choosing a reconstruction process. We made two of them to compare them.

Auto surface

Based on the surface of the scan, the tool creates a mesh of points - surface patches that are evenly distributed over the surface. The points are interconnected and create a closed mesh that copies the contours and shapes of the starting surface. This creates a 3D free-form surface body (surface model) of the scanned part. Subsequently, we can modify the model, add or remove material according to the template or according to our own requirements. In some cases, the model created in this way is insufficient and it is necessary to reconstruct the 3D scan using conventional modelling methods.

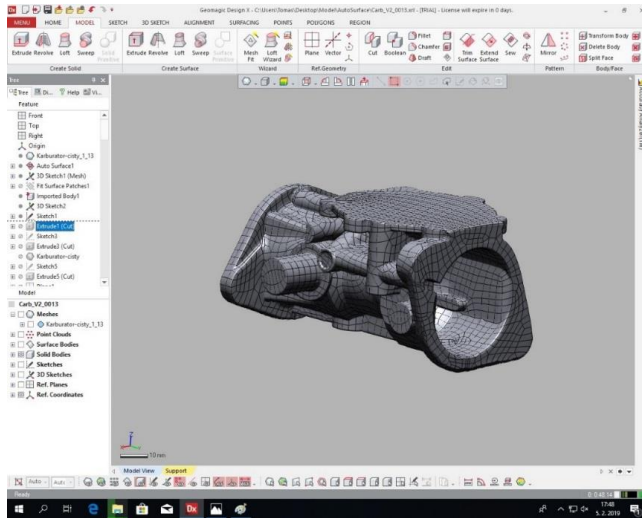


Figure 4 Model created with Auto Surface
 Obrázok 4 Model vytvorený pomocou funkcie Auto Surface

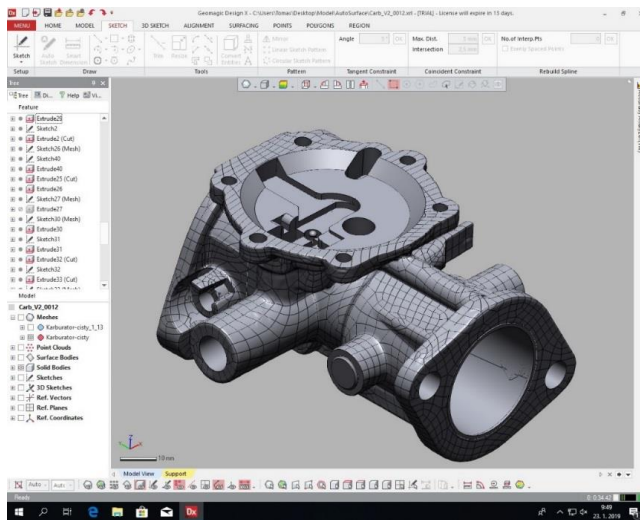


Figure 5 Modified model created with Auto Surface
 Obrázok 5 Upravený model vytvorený pomocou funkcie Auto Surface

Re-modelling

The aim of this method of reconstruction is to create a CAD model of the scanned part using conventional modelling techniques based on an existing 3D scan. Once again, we used Geomagic Design X. software When importing a scan in STL format, we checked the mesh errors (non cohesive polygon elements, overhanging polygon elements, etc.) and corrected them. Subsequently, we divided the mesh into segments - a grouping of polygons. Based on these groupings, we have identified the geometric shapes (planar surface, rotation surface, freeform surface, etc.) that constitute the individual areas of the model.

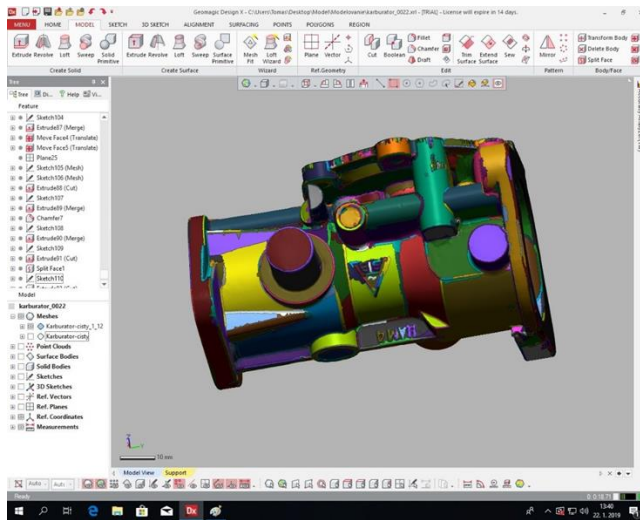


Figure 6 Created segments on model
 Obrázok 6 Vytvorené segmenty na modeli

The resulting reference geometric shapes were used in direct modelling. Their use depends on the shape complexity of the reconstructed part. We can also use creating of the section of 3D scan for direct modelling. By combining these features and common 3D modelling methods, we create a CAD model of the scanned part.

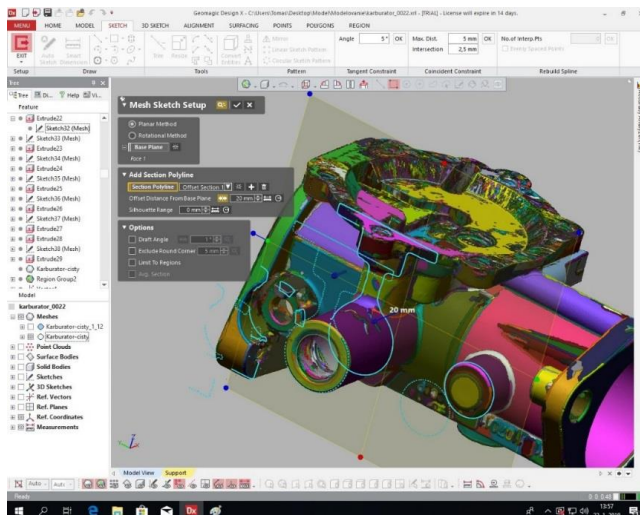


Figure 7 Utilization of model cut during reconstruction
 Obrázok 7 Využitie rezu modelom pri rekonštrukcii

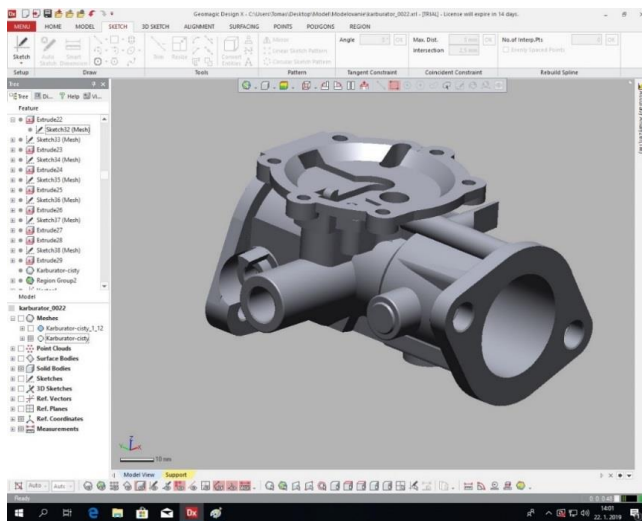


Figure 8 CAD model created by re-modelling
 Obrázok 8 CAD model vytvorený premodelovaním

5. Comparison

It is possible to compare the deviations between the 3D scan of the part and its reconstructed solid model at each step of reverse engineering realization. Deviations are shown in the form of a colour map where the values with the difference of +1 mm are red, with the difference of -1 mm are blue and the values with zero difference are green. One comparison was made for each reconstruction method.

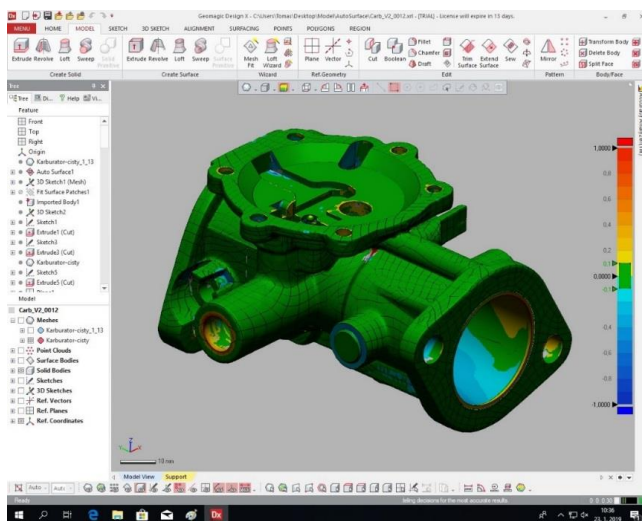


Figure 9 Model comparison – AutoSurface procedure
 Obrázok 9 Porovnanie modelu – postup AutoSurface

The Auto Surface function procedure uses the contours of the original 3D scan, so there are minimal differences. Significant differences arise in regions additionally modified, such as e.g. holes that have been created based on the data obtained by the touch sensor measurement. These are mainly the edges of the holes. This condition is due to the fact that the scanned part has already been used and is therefore partially worn out.

The comparison of the original scan and the model created by the re-modelling method is shown in Figure 10. The deviations are bigger than in the previous comparison, on average 0.2 mm. There are also areas where deviations are greater. These are the edges of the component. This is because it is difficult to capture sharp edges when scanning. Other places where deviations are more pronounced are shown in Figure 11. In area 1, this is a deviation of 1 mm. This deviation is due to the scanned component showing marked wear in area 1. In area 2 and area 3, this difference is smaller, gaining a value of 0.4 mm, and, as in area 1, it is assumed that it is due to wear of the component. The significant deviation in area 4, represented by the blue colour, is due to the fact that the 3D scan has no part data in area 4 because the laser beam could not scan the hole to the required depth.

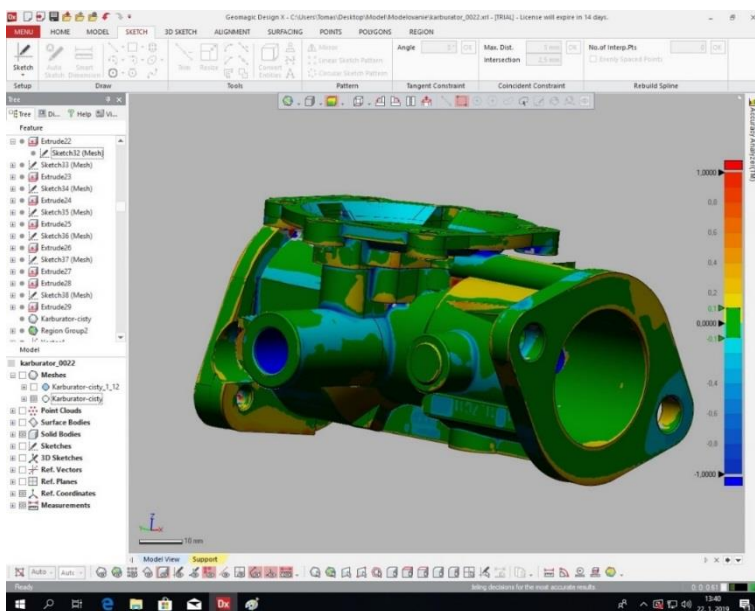


Figure 10 Model comparison – re-modelling
Obrázok 10 Porovnanie modelu – postup premodelovanie

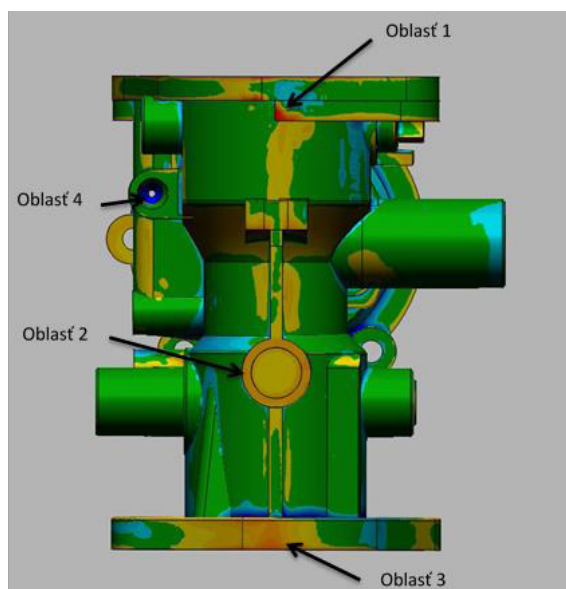


Figure 11 Areas of big deviations
 Obrázok 11 Oblasti veľkých odchýlok

CONCLUSION

By performing reverse engineering procedures on a shape-complicated part, we can conclude that the entire process is significantly more complex than for simple parts. Already when selecting a scanning device, it is necessary to take into account the complexity of the part and combine several scanning methods. As we have seen, the deep holes on our part could not be scanned by conventional methods. It would be necessary to physically divide the part into more parts, or add another method - X-ray scanning. When choosing a method for 3D scan reconstruction it is necessary to consider further use of the finished model. If the model is designed for 3D printing or rapid prototyping, the demands are slightly lower than when using the finished model to produce detailed drawings for production. An important factor is the requirements for the time of reconstruction and the quality of the resulting model.

BIBLIOGRAPHY

- ANWER, N.; MATHIEU, L. (2016) From reverse engineering to shape engineering in mechanical design, *CIRP Annals - Manufacturing Technology*, Volume 65, Issue 1, 2016, s. 165-168, ISSN 0007-8506, <http://dx.doi.org/10.1016/j.cirp.2016.04.052>.
- FAROARM [online] [cit. 2019-07-17]. Dostupné na: <https://www.faro.com/en-gb/products/factory-metrology/faroarm/>.
- HRČKOVÁ, M.; KOLEDA, P.; KASSAI, M. (2017) Reverzné inžinierstvo a jeho aplikácia pri analýze pracovného nástroja. *Acta Facultatis Technicae*, XXII, 2017 (2), s. 17-28 ISSN 1336-4472.

- KUMAR, A.; JAIN, P. K.; PATHAK, P. M. (2013) Reverse Engineering in Product Manufacturing: An Overview. DAAAM International Scientific Book, s. 665-679.
- LI, L.; SCHEMENAUER, X.; PENG, Y.; GU, P. (2002) A reverse engineering system for rapid manufacturing of complex objects, Robotics and Computer-Integrated Manufacturing, Volume 18, Issue 1, 2002, s. 53-67, ISSN 0736-5845, [http://dx.doi.org/10.1016/S0736-5845\(01\)00026-6](http://dx.doi.org/10.1016/S0736-5845(01)00026-6).
- PAULIC, M.; IRGOLIC, T.; BALIC, J.; CUS, F.; CUPAR, A.; BRAJLIH, T.; DRSTVENSEK, I.; (2014) Reverse Engineering of Parts with Optical Scanning and Additive Manufacturing, Procedia Engineering, Volume 69, 2014, s. 795-803, ISSN 1877-7058, <http://dx.doi.org/10.1016/j.proeng.2014.03.056>.
- RAJA, V.; FERNANDES, K. (2008) Reverse Engineering: An Industrial Perspective. Springer-Verlag London 2008. 242 s. ISBN 978-1-84628-855-5.
- SLOTA, J.; MANTIČ, M.; GAJDOŠ, I. (2010) Rapid Prototyping a Reverse Engineering v strojárstve. TU Košice, 2010. 207 s. ISBN 978-80-533-0548-6.
- TUT, V.; TULCAN, A.; COSMA, C.; SERBAN, I. (2010) Application of CAD/CAM/FEA Reverse Engineering and Rapid Prototyping in Manufacturing Industry, International Journal of Mechanics, Volume 4, Issue 4, 2010, s. 79-86, ISSN 1998-4448.
- VÁRADY, T.; MARTIN, R. R.; COX, J. (1997), Reverse engineering of geometric models-an introduction, Computer-Aided Design, Volume 29, Issue 4, 1997, s. 255-268, ISSN 0010-4485, [http://dx.doi.org/10.1016/S0010-4485\(96\)00054-1](http://dx.doi.org/10.1016/S0010-4485(96)00054-1).
- WANG, W. (2010) Reverse Engineering Technology of Reinvention. CRC Press Taylor & Francis Group, an Informa business Boca Raton 2010. 357 s. ISBN 978-1-4398-0630-2. <https://doi.org/10.1201/EBK1439806302>.

The paper was written and research conducted under the funding of the project KEGA MŠVVaŠ SR 005TU Z-4/2018: Building a progressive CNC machining workplace for the innovation of teaching forms in study programs at the Faculty of Environmental and Manufacturing Technology.

Corresponding author:

Ing. Mária Hrčková, PhD., phone: +421 45 5206 565, e-mail: hrckova@tuzvo.sk

ELIMINATING THE MALFUNCTION OF THE VEHICLE COOLING SYSTEM BY USING THERMO DIAGNOSTICS METHODS

ODSTRÁNENIE PORUCHY CHLADIACEHO SYSTÉMU VOZIDLA POMOCOU TERMODIAGNOSTICKÝCH METÓD

Pavol Harvánek, Ján Kováč, Ján Melicherčík

Katedra environmentálnej a lesníckej techniky, Fakulta techniky, Technická univerzita vo Zvolene, T.G.Masaryka 24, 960 01 Zvolen, E- mail: xharvanek@tuzvo.sk, jan.kovac@tuzvo.sk, xmelicher-cikj@tuzvo.sk

ABSTRACT: The main task of the article is to diagnose a failure of the cooling system of a motor vehicle and thus prevent the failure of the whole engine due to a damaged cooling system. The article is focused on diagnostics of motor vehicle cooling system failure by thermal imager. The diagnostic was carried out on a Audi A4 model B6 vehicle with a 2.5-liter diesel six-cylinder engine with a power of 132 kW year of manufacture of the vehicle is 2002 (model 2003). The problem was that the dashboard coolant temperature indicator could not exceed 70 ° C, and either the temperature sensor or the thermostat was suspected to be unable to close the large cooling circuit through the engine cooler and the vehicle could not warm up to working temperature . The vehicle includes two cooling circuits and one resistance temperature sensor that sends coolant temperature information to the engine control unit as well as to the dashboard coolant temperature gauge. The result of the thermovision measurement was the detection of the failure of the coolant temperature sensor, its subsequent replacement with a new one of the same type, and at the same time the elimination of the failure as evidenced by the measured results in the cell.

Key words: Thermodiagnosics, engine cooling system, engine temperature, temperature sensor.

ABSTRAKT: Hlavnou úlohou tohto článku je diagnostikovať poruchu chladiaceho systému motorového vozidla a tak zabrániť poruche celého motora v dôsledku poškodeného chladiaceho systému. Článok je zameraný na diagnostiku poruchy chladiaceho systému motorového vozidla pomocou termokamery. Diagnostika prebiehala na vozidle značky Audi A4 model B6 so vznetovým vidlicovým šesťvalcom 2,5 tdi s výkonom 132kw rok výroby vozidla je 2002 (model 2003). Problém spočíval v tom, že ukazovateľ teploty chladiacej kvapaliny na palubnej doske nedokázal presiahnuť teplotu 70°C, a teda bolo podozrenie buď na poškodený snímač teploty alebo poškodený termostat, ktorý nedokázal uzatvoriť veľký chladiaci okruh cez chladič motora a vozidlo sa nedokázalo zahriať na pracovnú teplotu. Vozidlo obsahuje dva chladiace okruhy a jeden odporový snímač teploty ktorý posiela informácie o teplote chladiacej kvapaliny do riadiacej jednotky motora a zároveň aj do ukazovateľa teploty chladiacej kvapaliny na palubnej doske. Výsledkom termovízneho merania bolo zistenie poruchy snímača teploty chladiacej kvapaliny jeho následná výmena za nový rovnakého typu a zároveň aj odstránenie poruchy čo dokazujú namerané výsledky v článku.

Ключові слова: Термодіагностика, хлiдiацi систем мотора, тeплотa мотора, снiмач тeплоты.

INTRODUCTION

In order to prevent thermal overload, i.e. burning of the lubricating oil (on the piston sliding paths), components that are around the hot combustion chamber (cylinder wall, cylinder head, valves, piston) need to be intensively cooled (Krilek et al. 2014). Heat must be dissipated in such a way that the optimum engine temperature is reached quickly and maintained at all operating conditions (Pošta et al. 2010). The basic diagram of the cooling system is shown in Figure 1. Piston rings and cylinders are worn excessively at low temperatures. The wear of the piston rings at a coolant temperature of 30 °C is eight times faster than at a temperature of 80 °C (Pošta et al. 2008, Šterba et al. 2011). In our case, the working temperature of the engine according to the temperature indicator was max. 70 °C despite trying to warm the engine by aggressive driving or long driving at high speed on the highway. However, measurements using a thermal imager showed that the temperature of the engine around the temperature sensor is in the range of 85-95 °C, even though the dashboard temperature indicator showed a maximum temperature of 70 °C, resulting in increased vehicle consumption. Since the only way to check the cooling system while driving is checking the observing the value of the temperature indicator it was necessarily to find and repair the error as soon as possible.

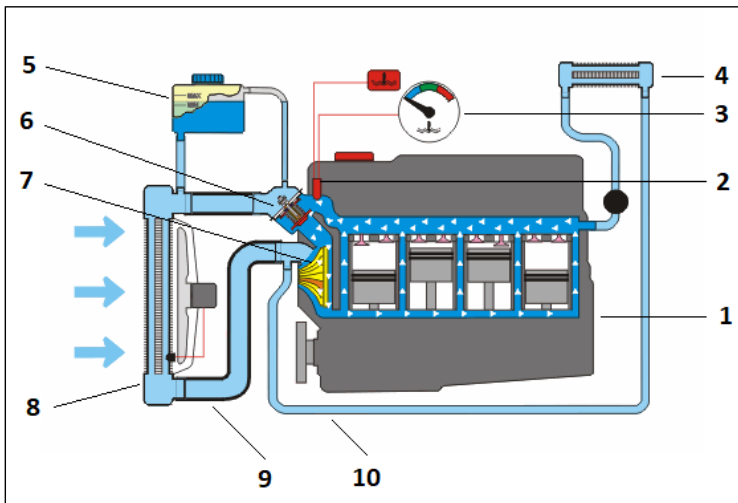


Fig. 1 Diagram of the vehicle cooling system. 1 – internal combustion engine, 2 – resistance temperature sensor, 3 – coolant temperature indicator, 4 – heater radiator, 5 – coolant expansion vessel, 6 – thermostat, 7, pump, 8 – cooler, 9 – large cooling circuit, 10 – small cooling circuit.

(www.aaautoskola.sk)

Obr. 1 Schéma chladiacej sústavy vozidla. 1 – spaľovací motor, 2 – odporový snímač teploty, 3 – ukazovateľ teploty chladiacej kvapaliny, 4 – radiátor kúrenia, 5 – vyrovnávací nádobka chladiacej kvapaliny, 6 – termostat, 7, čerpadlo, 8 – chladič, 9 – veľký okruh chladenia, 10 – malý okruh chladenia. (www.aaautoskola.sk)

Temperature sensors are according to physical principle divided into resistive, thermoelectric, semiconductor, optical, radiation, chemical, noise, etc. According to the contact with the measured environment we know contact and contactless. According to the signal

transformation, the sensors are divided into active and passive. (Kučera et al. 2017, Jan et al. 2009). In our case, it is a sensor resistive, touch and passive, because it needs to operate from an external source. The design of the resistance coolant temperature sensor in the Audi A4 consists of two independent thermistors that measure the temperature at one point. Both thermistors are supplied with 5V input voltage. The output voltage from the first thermistor is used to power the coolant temperature indicator on the dashboard of the vehicle, the second thermistor is used to inform the engine control unit about the engine temperature value. Based on this value, the fuel injection dose to the engine is adjusted. The wiring diagram is shown in Fig 2.

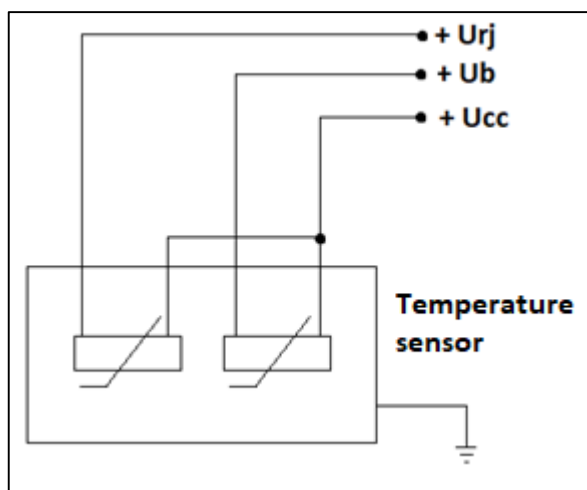


Fig. 2 Wiring diagram of resistive temperature sensor. U_{cc} – supply voltage + 5V, U_b – supply voltage of the dashboard temperature indicator, U_{rj} – voltage supplied to the engine control unit for information and value of the engine temperature. (Author)

Obr. 2 Schéma zapojenia odporového snímača teploty. U_{cc} – napájacie napätie +5V, U_b – napájacie napätie ukazovateľa teploty na palubnej doske, U_{rj} – napätie privádzane do riadiacej jednotky motora kvôli informácii a hodnote teploty motora. (Autor)



Fig. 3 Resistance coolant temperature sensor. (www.skoda-diely.sk)

Obr. 3 Odporový snímač teploty chladiacej kvapaliny. (www.skoda-diely.sk)

The principle of resistance contact thermometers is derived from the temperature resistance of the thermometer element. (Kučera et al. 2017, Kučera et al. 2018). Thermistors, semiconductor or metal resistance sensors are most commonly used for temperature control. Thermistors are electronic elements whose resistance varies with temperature (Pošta et al. 2010). Basically, it is a change in the resistance value of the sensor based on a change in the temperature of the coolant, the higher the temperature, the lower the resistance and the output voltage from the sensor is higher.

MATERIAL AND METHODS

Thermodiagnostic measurement and diagnostics is a non-destructive method based on displaying and evaluating the temperature field (thermograph) of the test object surface. The physical basis of non-contact thermodiagnosics is the measurement of the surface temperature of the bodies by a tomographic camera (thermovision) based on the infrared spectrum of the electromagnetic spectrum radiated by the body surface (Kreidl et al., 2006). Passive thermodiagnosics is the imaging of thermal fields of surfaces of electrical or mechanical objects. The evaluation variables are temperature differences in selected places of the object surface (Kreidl et al. 2006).

Each mechanical and electrical device in its function inevitably generates a certain amount of heat. The operating temperature may vary within an acceptable range. The advantage of thermodiagnosics is the unambiguous location of the fault source. Thermodiagnosics do not require an analytical apparatus for the detection and localization of disorders (Valenčík et al. 2015).

Temperature diagnostic using FLIR E40 was used to diagnostic the problem. As the faculty had this type of thermal imaging camera, the diagnostic was described as the most advantageous and cheapest by this method. Exx series FLIR thermal imagers models FLIR E40, FLIR E50 and FLIR E60 are designed for industry, ie. for diagnostics of electrical switchboards, production machines, motors, photovoltaic cables etc. (www.termokamera-flir.sk)



Fig. 4 Thermal imager FLIR E40 (www.meraciepristroje.sk)
Obr. 4 Termokamera FLIR E40 (www.meraciepristroje.sk)

Table 1 Technical parameters of FLIR E40 thermal imager (www.termokamery-flir.sk)
 Tabuľka 1 Technické parametre termokamery FLIR E40 (www.termokamery-flir.sk)

IR resolution	Temperature range	Field of view	Display	Digital Zoom	Camera	File format
160 x 120 px	-20°C...+650°C	25° x 19°	3.5" LCD	2x	3.1Mpx	JPG
Focus	Bluetooth	WiFi	Software	Operating time	Weight	Dimensions
Manual	Yes	Yes	Flir Tool	4 hours	880g	246 x 97 x 184 mm

For correct function and correct measurement result it was necessary to adjust the emissivity of the surface of the material to be measured. When measuring temperature with an infrared thermometer or thermocamera, we measure the amount of energy that emits (or reflects!) The measured object to the measuring instrument. In this measurement, the emissivity of the material we are measuring is important. Emissivity is a dimensionless quantity that determines how much heat a given material emits (emits) to our surroundings (www.else.sk). The temperature was monitored on a rubber hose just behind the temperature sensor and on the aluminum water cooler in the front of the vehicle.

Table 2 Emissivity value for a different material (www.else.sk).
 Tabuľka 2 Hodnota emissivity pre daný materiál (www.else.sk).

Material	Emissivity
Aluminium	0,25
Rubber hose	0,94

The measurement took place on the Audi A4 B6 2.5 tdi 132kw quattro, manufactured in 2002. The basic vehicle data are shown in the Tab. 3.

Table 3 The basic vehicle data
 Tabuľka 3 Základné technické údaje o vozidle

Engine type	Engine code	Fuel type	Fuel system	Engine alignment	Nr. Of valves
V6	AKE	Diesel	Common Rail	Longitudinal	24
Aspiration	Compression ratio	Maximum power	Maximum torque	Drive wheels	Gearbox
Turbo+ Intercooler	18.5	180 PS	370 Nm	Quattro 4WD	6 speed Manual

The design of the measuring consists of the measuring vehicle, the thermal imager and the PC to evaluate the results. The measurement string diagram is shown graphically in Fig. 5.



Fig 5 Engine temperature measurement. 1-engine 2.5 tdi, 2-thermal imager FLIR E40, 3-PC
 Obr. 5 Merací reťazec merania teploty motora. 1- motor 2,5 tdi, 2- termokamera FLIR E40, 3-PC

RESULTS AND DISCUSSION

In order to identify the origin of the problem, it was necessary to trace by thermodynamics whether there is a faulty thermostat at a low temperature value or only a resistance sensor of the coolant temperature. The method of trouble-shooting by thermodynamics is also discussed by the authors (Wang et al., 2017, Wu et al., 2016). First, it was necessary to find out whether the thermostat was faulty and whether a large cooling circuit was opened by accident even though the engine temperature did not reach operating temperature. Using the thermal imager (Fig. 6) it was found that the water cooler in the front of the vehicle is cold and thus the cooling circuit through the water cooler is closed.

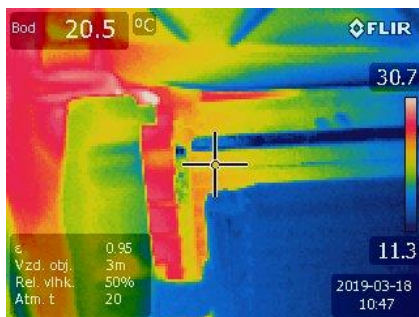


Fig. 6 Cooler outlet temperature
 Obr. 6 Teplota chladiča na výstupe



Fig. 7 Water cooler
 Obr. 7 Chladič vody

As a second step it was necessary to determine whether the temperature of the water around the temperature sensor does not really reach 90° C or the temperature sensor is defective and despite the working temperature has been reached, the sensor shows a bad value (Fig. 8.).

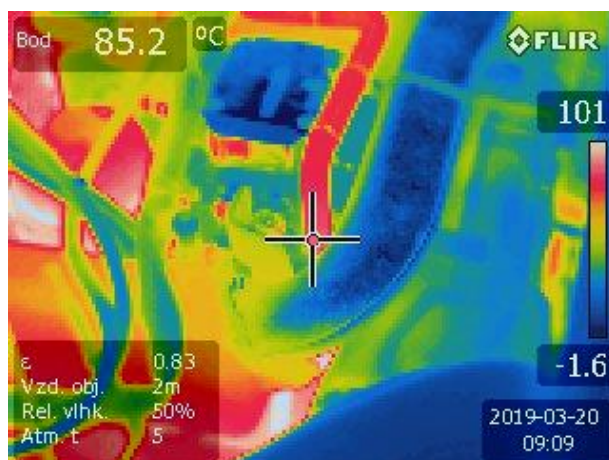


Fig. 8 Temperature of the hose just behind the temperature sensor
 Obr. 8 Teplota hadice tesne za snímačom teploty



Fig. 9 Temperature according to dashboard temperature indicator
 Obr. 9 Teplota podľa ukazovateľa teploty na palubnej doske

The measurements clearly show that the faulty coolant temperature sensor is causing the error and has been replaced. Fig. 10 and Fig. 11. there is apparently damage to the sensor due to leakage resulting in oxidation of the contacts inside the sensor and consequent sensor failure.



Fig. 10 Removal of damaged temperature sensor
Obr. 10 Demontovanie poškodeného snímača teploty



Fig. 11 Damaged contacts inside the sensor
Obr. 11 Poškodené kontakty vo vnútri snímača

After replacing the coolant temperature sensor with a new one (Fig. 12.), the temperature stabilized at 90 ° C according to the dashboard temperature indicator (Fig. 13).



Fig. 12 New Temperature Sensor
Obr. 12 Nový snímač teploty



Fig. 13 Temperature after sensor replacement
Obr. 13 Teplota po výmene snímača

CONCLUSION

Since a malfunctioning engine cooling system can lead to permanent engine damage, it was necessary to diagnose and remedy the fault as soon as possible. Thanks to thermo-diagnostics, it was possible to quickly solve the problem that consisted only of a damaged coolant temperature sensor. The diagnostic technique using thermography was also used by the authors (Huda et al., 2013, Glowacz et al., 2017) who used thermography for preventive maintenance of thermal failure in electrical equipment or for diagnosis of the three-phase induction motor. After the coolant sensor has been replaced, the instrument coolant temperature gauge has stabilized at 90° C. By correcting the fault, the coolant temperature can also be monitored while driving and, in the event of a fault, stop the vehicle at the right time to avoid overheating and possible engine damage.

ACKNOWLEDGMENT

Contribution has been prepared within the solving of scientific grant project VEGA project no. 1/0642/18 "Analysis of the impact of structural parts of forestry mechanisms in the forest environment in terms of energy and ecology".

REFERENCES

- GLOWACZ, A., GLOWACZ, Z. 2017. Diagnosis of the three-phase induction motor using thermal imaging. *Infrared physics & technology*, 81, 7-16.
- HUDA, AN, a TAIB, S. 2013. Application of infrared thermography for predictive/preventive maintenance of thermal defect in electrical equipment. *Applied Thermal Engineering*, 61(2), 220-227.
- JAN, Z., ŽDÁNSKY, B., KUBÁT, J., 2009: Nakladatelství Avid, s.r.o., Brno. *AUTOMOBILY Elektrotechnika motorových vozidiel I*. 2. vyd. ISBN 978-80-87143-13-1. 2009.
- KREIDL, M., ŠMÍD, R., 2006: Nakladatelství BEN – technická literatúra. *Technická diagnostika*. 1 vyd. ISBN 80-7300-158-6. 2006.
- KRILEK, J., KUČERA, M., 2014: Technická univerzita vo Zvolene. *Vysokoškolská učebnica: Cestné a motorové vozidlá*. 1. vyd. ISBN 978-80-228-2694-5. 2014.
- KUČERA, M., KRILEK, J., HELEXA, M., 2017: Technická univerzita vo Zvolene. *Vysokoškolská učebnica: Metrológia pre technikov*. 1. vyd. ISBN 978-80-228-2978-1. 2017.

- KUČERA, M., KRILEK, J., HELEXA, M., 2018: Technická univerzita vo Zvolene. Vysokoškolská učebnica: Metrológia pre technikov. 2. vyd. ISBN 978-80-228-3138-3. 2018.
- POŠTA, J a kol., 2008: Nakladateľství Informatorium, spol. s.r.o.Opravenství a diagnostika II. 2. vyd. ISBN 978-80-7333-066-8. 2008.
- POŠTA, J a kol., 2010: Nakladateľství Informatorium, spol. s.r.o.Opravenství a diagnostika III. 2. vyd. ISBN 978-80-7333-073-6. 2010.
- ŠTĚRBA, P., ČUPERA, J., POLCAR, A., 2011: Nakladateľství Avid, s.r.o., Brno. AUTOMOBILY Diagnostika motorových vozidiel II. 1. vyd. ISBN 978-80-87143-19-3. 2011.
- VALEŇČÍK, Š., STEJSKAL, T., 2015: Technická univerzita v Košiciach. Údržba, diagnostika a opravy strojov. 1. vyd. ISBN 978-80-553-2249-0. 2015.
- WANG H., CAI Y., WANG W., A 2017: dynamic thermal – mechanical model of the spindle – bearing system, Key Laboratory of Vehicle Advanced Manufacturing, Measuring and Control Technology, Ministry of Education, Beijing, 100044, China. ISSN 2191-9151. 2017.
- WU, L., TAN, QC, Thermal characteristic analysis and experimental study of a spindle-bearing system, Entropy 2016, 18, 271;
- Firemná stránka: FLIR, [online], [cit. 22.1.2020]. Dostupné na internete: <http://www.termokamery-flir.sk/>
- Firemná stránka: ELSO, [online], [cit. 22.1.2020]. Dostupné na internete: <http://www.else.sk/>

Corresponding author:

Ján Kováč, tel. +421 45 5206 517, E- mail: jan.kovac@tuzvo.sk

COMPARISON OF CASE STUDIES OF VIBRO, THERMAL AND ACOUSTIC DIAGNOSTICS METHODS

POROVNANIE PRÍPADOVÝCH ŠTÚDII VIBRAČNEJ, TEPELNEJ A AKUSTICKEJ DIAGNOSTIKY

Silvia Kopčanová¹, Marián Kučera²

¹*Department of Mechanics, Mechanical Engineering and Design, Faculty of Technology, Technical University in Zvolen, Študentská 26 960 01 Zvolen, kopcanova15@gmail.com*

²*Department of Mechanics, Mechanical Engineering and Design, Faculty of Technology, Technical University in Zvolen, Študentská 26 960 01 Zvolen, kucera@tuzvo.sk*

ABSTRACT: Orientation in the field of technical diagnostics is decisive for the correct selection of the appropriate diagnostic method, as incorrect selection or assessment of the condition can lead to serious machine failures and this means significant routes for the enterprise. The paper provides a brief overview of some diagnostic methods in the field of vibrodiagnostics and acoustic emission. It compares various diagnostic methods and their applicability in practice. Case studies show, that the most effective way to measure and detect bearing errors from the vibration diagnostic point of view is to use multiparametric diagnostics associated with temperature measurement and evaluation through the PCA analysis statistical method. Furthermore, the paper also describes a new view of bearing diagnostics, namely acoustic measurement, which according to previous research is more accurate for detecting early stages of failure.

Key words: maintenance, acoustic emissions, principal component analysis, temperature, machines

ABSTRAKT: Orientácia v oblasti technickej diagnostiky je kľúčová pre správny výber vhodnej diagnostickej metódy, pretože nesprávny výber alebo posúdenie stavu môže viesť k vážnym poruchám strojov a to znamená významné traty pre podnik. Príspevok prináša krátky prehľad niektorých diagnostických metód v oblasti vibrodiagnostiky a akustickej emisie. Porovnáva rôzne diagnostické metódy a ich využiteľnosť v praxi. Prípadové štúdie dokazujú, že najúčinnjší spôsob merania a detekovania chýb ložísk z pohľadu vibrodiagnostiky je použitie viacparametrickej diagnostiky spojenej s meraním teploty a vyhodnocovaním prostredníctvom štatistickej metódy PCA analýzy. Ďalej však príspevok popisuje aj nový pohľad na diagnostiku ložísk a to meranie akustiky, ktoré podľa doterajších výskumov je presnejšie na detekovanie už ranných štádií porúch.

Kľúčové slová: údržba, akustické emisie, analýza hlavných komponentov, teplota, stroj

INTRODUCTION

Prediction monitoring of machines have an irreplaceable role in production plants, so it is important to monitor their technical condition. Any decommissioning will cause

companies to incur time and financial losses. Therefore, prediction in the area of diagnostics is important. In this way, we can completely prevent standstill failure and minimize maintenance time. The notion of multiparametric diagnostics is currently coming to the forefront. Several authors discuss this method by examining the interaction of two or more interrelated parameters. Each machine has three basic parameters: vibration, temperature and acoustics. In order to correctly evaluate the condition of the machine, it is also necessary to know the problem of lubrication - tribology (Beňo et al. 2016, Marienčík et al. 2016). All these parameters are interrelated, but it is necessary to determine to what extent their interaction and changes have a verifiable value for more thorough and faster machine diagnostics.

Technical diagnostics is a process that is carried out by non-destructive and indelible methods and leads to the determination of the technical condition of the machine or its components. There are two ways to diagnose: Earliest maintenance and Later maintenance. The prediction is a very important element in the entire production process, as it prevents more damage during regular maintenance. It is important to collect information and process it properly throughout the production process. This procedure uses the Condition Based Maintenance (CBM) method of maintenance (Jardine et al., 2006). During the machine tracking process, it is important to create a basic diagnostic chain that senses and evaluates signals from sensors located on the monitored device (Fig. 1) (Hudák, Hoľvová, 2013).

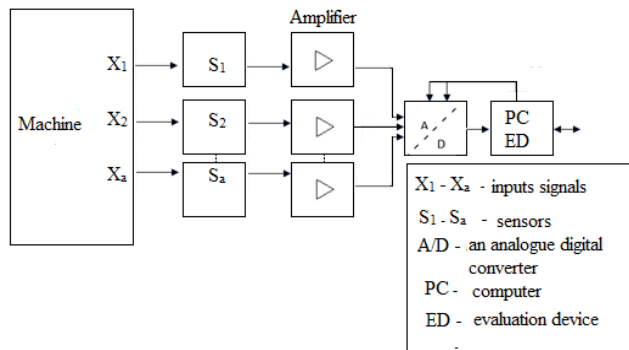


Fig. 1 Scheme of Multiparametric Diagnostics

Obr. 1 Schéma multiparametrickej diagnostiky (Hudák, Hoľvová, 2013)

There are currently studies on the interaction of vibration and temperature, vibration and noise, and the relationship between vibration and machine lubrication (Turis et al., 2012). The following section provides an overview of vibro-thermal diagnostics.

MULTIPARAMETRIC DIAGNOSTICS METHODS

Structural damage causes changes in machine parameters and performance (Xu, Chen, 2010). Damage is also defined as a change in the original material and structural properties that cause undesirable vibrations and stresses. These unwanted changes can be caused by cracks, loose screws, broken welds, corrosion or fatigue of the material (Das et al., 2016).

The fault diagnosis process has the following steps:

1. collecting data on the technical condition of the equipment
2. analysis of data or signals
3. decision on steps to improve maintenance (Doebling et al., 1998).

Rytter (1993) damage classification system (defined by four levels of damage identification, as follows:

- Level 1: Determine structural damage
- Level 2: level 1 and determination of the geometric position of the damage
- Level 3: level 2 plus quantification of the severity of the damage
- Level 4: Level 3 and structural life prediction (Rytter, 1993).

Condition monitoring of machines

Many studies (Doebling et al., 1998; Lipus, 2016; Fugate et al., 2001; Sohn et al., 2000; Alvadi, et al., 2006) seek to bring a new approach to machine monitoring and diagnostic techniques and their components. The maintenance technique - multiparametric diagnostics – is used for greater efficiency. This way of diagnosing diagnostics brings the benefits of faster and more accurate localization and troubleshooting.

The most common parameter for standstill monitoring is vibration. In many cases, fast Fourier transform (FFT) is used for vibration signal analysis. The FFT converts the signal from the time domain to the frequency domain. The disadvantage of this method is that one type of signal may indicate multiple errors. Figure 2 shows that it is not always possible to estimate where the failure is in terms of misalignment or crack, as the spectral analysis of misalignment and crack is similar (El-Thalji, Jantunen, 2015). Therefore, proper diagnostic approaches should be developed. In many published works (Nembhard et al., 2014; Delvecchio et al., 2018; Tandom et al., 1999; Opocenska et al., 2017) it is a combination of vibration with methods of measuring heat, acoustics or lubrication.

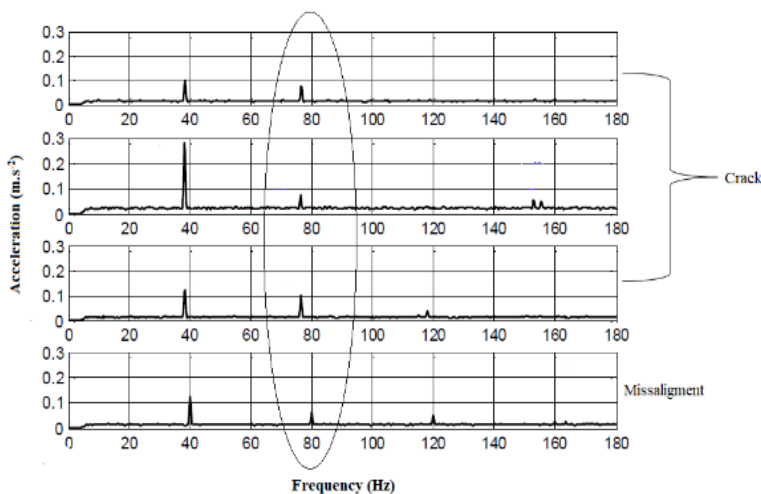


Fig. 2 Spectral analysis of crack and misalignment (Nembhard (2014)

Obr. 2 Spektrálna analýza hriadeľa trhliny a vychýlenia

Principal Component Analysis (PCA) for fault diagnosis

PCA is a method that selects only the most important data from a wide range of data. Figure 3 shows the procedure for the PCA method. In this way, the distribution of the major components that appear to be related is achieved (Lebold et al., 2018; Čuchran, 2012; Ringner, 2008). Using this method, the main components can be represented graphically, which is clearer than a complex data set (Trendafilova et al., 2008; Jolliffe, 2002).

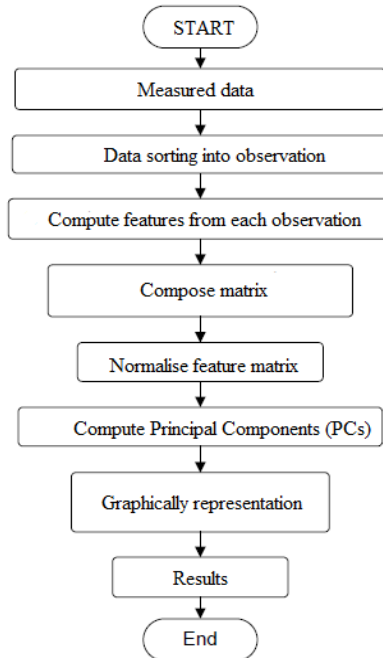


Fig. 3 PCA analysis
Obr. 3 PCA analýza

Case study of vibration and thermal analysis

In recent years, many studies have been published on the combination of vibration and thermal analysis of rotary machines. The researcher Nembhard (2014) presented a multi-parameter method in combination of vibration and temperature in rotary machines with multiple bearing systems. According to the data obtained, which is shown in Fig. 4, found that the combination of these two parameters is more useful than the vibration alone, since in Fig. 4b it is easier to distinguish the deviation from the cracks, whereas in Fig. 4a it is ambiguous.

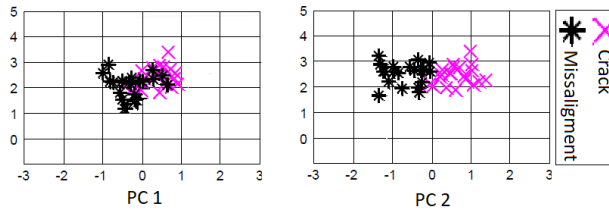


Fig. 4 Comparison of PCA analysis with and without temperature (Nembhard 2014)

Obr. 4 Porovnanie PCA analýzy bez a s teplotou

However, a similar theory is compared by Gabrhel et al. (2013) in her research, where she observed the effect of temperature on vibration in Gabrhel's research. Its results are presented in Fig. 5, where it has been shown that as the temperature rises, the vibration increases directly proportionally, but at a certain temperature and overheating of the machine, the vibration decreases as a result of bearing clearance determination.

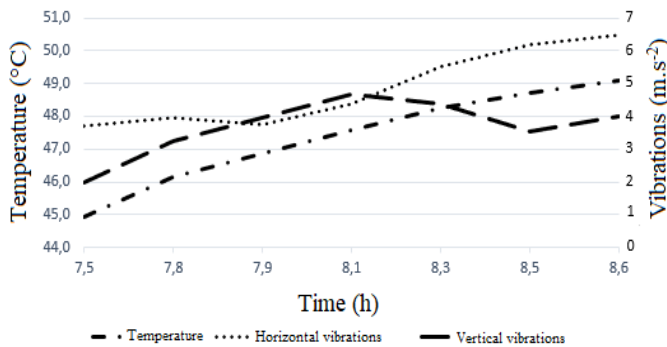


Fig. 5 Vibration and Temperature Changes over Time (Gabrhel et al. (2013)

Obr. 5 Zmeny vibrácií a teploty na čas

Case study of vibration and acoustic measurement methods for bearing diagnostics

This study investigates vibration and acoustic measurement methods for bearing diagnostics.

Bearings are a very important component for all forms of rotary machines and are among their most common elements. Due to their importance and widespread use, bearing failure is one of the most common causes of decay in rotary machines. Increased temperature, vibration, noise, or oil leakage through seals may result from incorrect bearing operation.

Measurement of vibration, temperature, acoustics determines the actual condition of bearings at the time of their operation. These methods of diagnostics are non-destructive and non-removable, so they are the most frequently used and most effectively used in technical practice.

Research on vibration and acoustic measurement techniques to detect rolling element bearing errors shows that the focus is on vibration measurement methods.

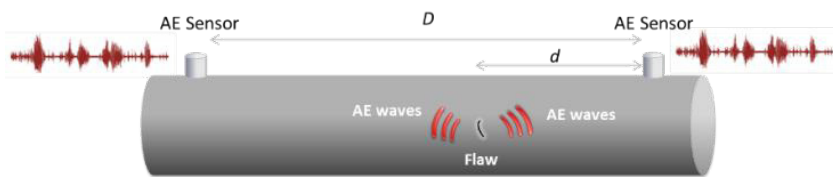
Time-domain vibration can be measured using parameters such as RMS, oscillation factor, probability density and curtose. Of all these variables, curtose is the most effective, but the pulse shock method has also gained wide industrial acceptance.

Measuring vibration in the frequency domain has the advantage of being able to locate the fault. High-frequency resonance technology is the most popular vibration measurement technique and has been successfully researched by several researchers. For this technique, the signal processing procedure is well described as well as the explanation of the resulting demodulated spectrum. The method has the disadvantage that it is difficult to detect advanced damage. In recent years a method of wavelet transformation (Wavelet transformation) has been proposed for the extraction of very weak signals for which the Fourier transform becomes ineffective (Tandon, N., Choudhury, A. 1992).

However, very few studies have been conducted to detect bearing failures through noise measurement. Pressure and sound intensity measurements were used for this purpose. Research results came out better for sound intensity measurement technology than for sound pressure measurement in bearing diagnostics.

Some studies suggest that these measurements are better than vibration measurements and may detect an error before they appear on the surface. (Cabada et al., 2017). To illustrate the operation of acoustic diagnostics, Fig. 6 illustrates a sensor source position calculation based on the detected time difference between the wave influx into the sensors and the known velocity of these waves. Observing figures 7 and 8 can clearly identify the harmonics of the fault frequency for both vibration and acoustic sensors, that the vibration signal provides a cleaner spectrum (Freitas, C., Cuenca1, J., Morais P. 2016).

In recent years, attention has also focused on automated interpretation of bearing diagnostics data. The pattern recognition technique and neural networks were applied to data obtained from time and frequency domain vibration measurements to detect defects in rolling element bearings.



$$d = \frac{1}{2}(D - \Delta T \cdot V)$$

d = distance from first hit sensor

D = distance between sensors

V = wave velocity

Fig. 6 Calculation of Sensors source location based on the detected time difference between wave arrivals to sensors and known wave velocity (Zhou, Jing Zhou, Z. et al., 2017)

Obr. 6 Výpočet umiestnenia zdroja snímačov na základe zisteného časového rozdielu medzi príchodmi vln do snímačov a známou rýchlosťou vln

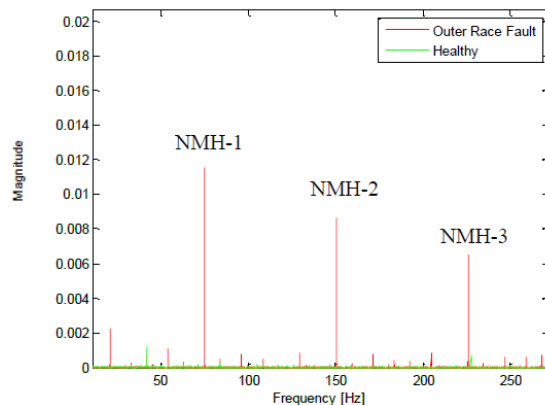


Fig. 7 Spectrum of the autocorrelation of the envelope for the vibration signal (Freitas et al. 2016)

Obr. 7 Spektrum autokorelácie obálky pre vibračný signál

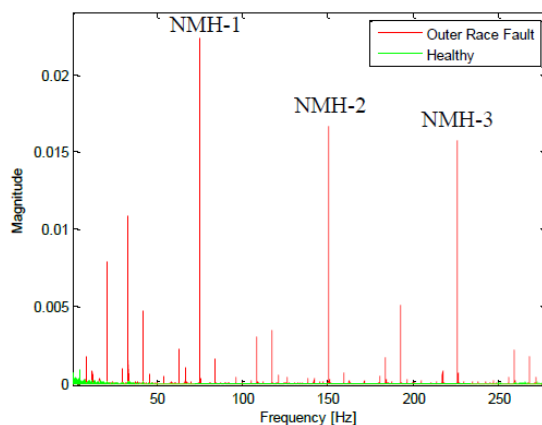


Fig. 8 Spectrum of the autocorrelation of the envelope for the acoustic signal (Freitas et al. 2016).

Obr. 8 Spektrum autokorelácie obálky pre akustický signál

DISCUSSION AND CONCLUSION

Although there are many ways to monitor standing conditions, it is important to choose a method that is more efficient and easier to apply in practice. This simplification is provided by multiparametric diagnostics.

The paper was divided into several parts, where the individual diagnostic procedures were described.

The defect detection section described the requirement to develop a better method for vibrodiagnostics, as there is a lack of accuracy in estimating the origin of the error, thereby extending the overall diagnostic time.

The next part describes the approach of multiparametric diagnostics in combination of vibration diagnostics and thermal analysis. According to the results of Nembhard et al. (2014) the combination of vibration and temperature significantly improves condition monitoring in the diagnosis of disorders. This method provides a more accurate determination of the occurrence of a bearing error because some errors are manifested by a similar frequency spectrum. PCA analysis seems to be a good statistical tool for accurate error identification. To compare this theory, Gabrhel et al. (2013) research where the interaction between vibration and temperature was evaluated. Therefore, follow-up research in this area is needed.

The last part of the paper describes the combination of failure diagnostics with vibration and acoustic measurements. Pressure and sound intensity measurements were used in case studies. Sound intensity measurement seems to be a more effective method for measuring bearing failures. This measurement show, that vibration analysis is more effective, but akustic measurement is more sensitive to a defect at an earlier stage of development.

At present, the industry is focusing on the correct and efficient diagnosis of machines, because an incorrect approach to this issue can cause significant financial losses for the company, such as shutting down the machine for a long time or shutting it down completely. If you want to perform effective diagnostics, you must choose the right diagnostic approach. This is offered by multiparametric diagnostics, in which several parameters are combined. Further research is needed to achieve better approaches to these issues in order to find the most appropriate diagnostic method applicable in practice.

ACKNOWLEDGMENT

The authors are grateful for the support of the Scientific Grant Agency of the Ministry of Education, Science, Research, and Sport of the Slovak Republic, Project VEGA no. 1/0609/2020 „Research of the cutting tools at the dendromass processing in agricultural and forestry production.

REFERENCES

- ALVADI A., CREMONA C., 2006. Assessment of vibration-based damage identification techniques. *Journal of Sound and Vibration* 292 (2006) 179-202, ISSN 0022-460X
- BEŇO, P., MARIENČÍK, J., TURIS, J., KOZAK, D., KONJATIĆ, P. 2016. Friction factor dependence on the load and revolutions in sliding bearings without relubrication. *Tehnički vjesnik*. 2016. no. 4 , pp. 997-1001, ISSN 1330-3651
- CABADA C., Q. LECLERE, J. ANTONI, N. HAMZAOU, 2017. Fault detection in rotating machines with beamforming: Spatial visualization of diagnosis features, *Mechanical Systems and Signal Processing*, Vol. 97 (2017), pp. 33-43. ISSN: 0888-3270
- ČUCHRAN, J. 2012. Určenie najvhodnejších metód pre diagnostiku olejových náplní mobilných strojov: doktorandská práca. Zvolen: Technická univerzita vo Zvolene. 2012.173 s
- DAS, S., SAHA, P., PATRO, S.K. 2016 Vibration-based damage detection techniques used for health monitoring of structures: A review. *J. Civ. Struct. Health Monit.* 2016, 6, ISSN 477–507
- DELVECCHIO S., BONFIGLIO P., POMPOLI F., 2018. Vibro-acoustic condition monitoring of Internal Combustion Engines: A critical review of existing techniques. *Mechanical Systems and Signal Processing*. Volume 99(15). 2018. pp 661-683, ISSN 0888-3270

- DOEBLING, S. W., FARRAR, C. R., AND PRIME, M. B., 1998. "A Summary Review of Vibration-based Damage Identification Methods," *Shock and Vibration Digest*, Vol. 30, No. 2, 91–105
- EL-THALJI N, I., JANTUNEN E., 2015. A summary of fault modelling and predictive health monitoring of rolling element bearings. *Mechanical Systems and Signal Processing* 60-61(2015) 252–272, ISSN 0888-3270
- FREITAS, C., CUENCA1, J. MORAIS P. 2016. Comparison of vibration and acoustic measurements for detection of bearing defects. *Proceedings of Isma2016 Including Usd2016*. ISBN: 978-1-5108-3591-7
- FUGATE, M., SOHN, H., FARRAR, CH. 2001. Vibration-based damage detection using statistical process control. *Mechanical Systems and Signal Processing* (2001) 15(4). 707-721. 2001 Academic Press, ISSN 0888-3270
- GABRHELOVÁ, L., HUDCZEK, M., BRYCHCY, J. 2013. Souvislosti medzi teplotou a vibraciami v diagnostice rotačných strojů. *Transfer inovácií* 25/2013. ISSN 1337-7094
- HUDÁK, R., HOLVOVÁ, P. 2013. Možnosti využitia viacparametrickej diagnostiky v technickej praxi. *Transfer inovácií* 25/2013, ISSN 1337 - 7094
- JARDINE A., LIN D., BANJEVIC D. 2006. A review on machinery diagnostics and prognostics implementing condition-based maintenance. *Mechanical Systems and Signal Processing*, Volume 20. Issue 7. 2006. pp 1483-1510, ISSN 0888-3270
- JOLLIFFE, I. 2002. *Principal Component Analysis*. Springer. New York. 2002, ISBN 978-0-387-22440-4
- LEBOLD, M., MCCLINTIC, K., CAMPBELL, R., BYINGTON, C., MAYNARD, K. 2013. Review of Vibration Analysis Methods for Gearbox Diagnostics and Prognostics. *Proceedings of the 54th Meeting of the Society for Machinery Failure Prevention Technology*. p. 623-634. Available in: <http://www.aapb.org/i4a/pages/index.cfm?pageid=3336> [cit 2018-04-20] *Technicae XVII* 2012 (3): 33-42. ISSN 1336-4472
- LIPUS J., JANKOVYCH R., HAMMER M., LIPUS T. 2016. Vibration and related diagnostics of motors and generators. *MM Science journal* 2016, ISSN 1803-1269
- MARIENČÍK, J., TURIS, J., BEŇO, P., DROBA, A. 2014 A friction characteristics comparison at the contact layer of the sliding fit. *Acta Facultatis Technicae XIX* 2014 (1): 105-111, ISSN 1336-4472
- NEMBHARD A., SINHA J., PINKERTON A., ELBHBAH K. 2014. Combined Vibration and Thermal Analysis for the Condition Monitoring of Rotating Machinery. *Structural Health Monitoring*, vol. 13. 3: pp. 281-295. First Published February 26. 2014. ISSN 1475-9217
- OPOCENSKA, H., NAHODIL, P., HAMMER, M. 2017. Use of Multiparametric Diagnostics in Predictive Maintenance. *MM Science Journal*, ISSN 1803-1269
- RINGNER M., 2008. What is principal component analysis? *Nature Biotechnology*. 26, 303–304, ISSN 1546-1696
- RYTTER, A., 1993. "Vibration based inspection of civil engineering structures," Ph. D. Dissertation, Department of Building Technology and Structural Engineering, Aalborg University, Volume R9314. ISSN: 0902-7513
- SOHN, H., CZARNECKI, J., FARRAR, C. 2000. Structural health monitoring using statistical process control. 2000 *Journal of Structural Engineering*. ASCE, ISSN 0733-9445
- TANDO, N., CHOUDHUR, A. 1999. A review of vibration and acoustic measurement methods for the detection of defects in rolling element bearings. *Tribology International*. Volume 32. Issue 8. August 1999. Pages 469-480. ISSN 0301-679X
- TANDON, N, CHOUDHURY, A.1993. A review of vibration and. *Shock and Vibration Digest* 1992;24(3): ISSN: 0583-1024

- TRENDAFILOVA, I., CARTMELLB, M., OSTACHOWICZC, W. 2008. Vibration-based damage detection in an aircraft wing scaled model using principal component analysis and pattern recognition. *Journal of Sound and Vibration*. 313 (2008) 560–566, ISSN 0022-460X
- TURIS, J., BEŇO, P., MARIENČÍK, J., REMPEROVÁ, M. 2012. The prediction of contact phenomena and degradating processes influence in gearing mechanism. *Acta Facultatis* ISSN 1336-4472
- ZHOU, Z. ET AL., 2017. Experimental study on the location of an acoustic emission source considering refraction in different media. In *Natur Research journal*. ISSN 1476-4687
- XU YL, CHEN, B. 2010. Integrated vibration control and health monitoring of building structures: a time-domain approach. *Smart Structure and System*. Volume 6. Issue 7. 2010. pp. 811-833, ISSN 1738-1584

Corresponding author:

Silvia Kopčanová, e-mail: kopcanova15@gmail.com

ANALYSIS OF TECHNICAL PARAMETERS OF HARVESTER HEADS IN FORESTRY

ANALÝZA TECHNIKÝCH PARAMETROV HARVESTEROVÝCH HLAVÍC V LESNÍCTVE

Ján Melicherčík, Jozef Krilek, Pavol Harvánek

ABSTRACT: This article focuses on the analysis of the technical parameters of harvester heads in forestry. The aim of this paper is to select the different types of harvester heads, to describe their principle of activity, to present the main parameters of the device. For each harvester head there are basic parameters in the database file, such as the weight without the rotor, the maximum stroke, the maximum cutting capacity, the maximum deflection diameter. From these parameters, 3D histograms are created, from which it is clear to see the individual dependencies that are important in selecting a suitable head. The aim of this article is to create a database of the individual harvester heads, most commonly used in the Czech Republic and abroad, from the data provided by the manufacturer, thereby speeding up and facilitating the customer selection process.

Key words: Harvester head, wood procesing, delimiting knives, forestry

ABSTRAKT: Tento článok sa zameriava na analýzu technických parametrov harvesterových hlavíc v lesníctve. Cieľom tohto článku je vybrať rôzne typy hlavíc harvesterov, opísať ich princíp činnosti, prezentovať hlavné parametre zariadenia. Pre každú hlavu harvesteru sú v databázovom súbore základné parametre, ako je hmotnosť bez rotátora, maximálny zdvih, maximálna kapacita rezania, maximálny priemer vychýlenia. Z týchto parametrov sa vytvárajú 3D histogramy, z ktorých je zrejmé, že sú vidieť jednotlivé závislosti, ktoré sú dôležité pri výbere vhodnej hlavice. Cieľom tohto článku je vytvoriť databázu jednotlivých zberacích (harvesterových) hlavíc, ktoré sa najčastejšie používajú v Českej republike a v zahraničí, z údajov poskytnutých výrobcom, čím sa urýchli a uľahčí proces výberu pre zákazníka.

Kľúčové slová: Harvesterová hlavica, spracovanie dreva, odvetvovacie nože, lesné hospodárstvo

INTRODUCTION:

The harvester head has an important role in the efficiency and quality of wood procesing. The task of the harvester head is to spin the tree, branch, cut the tree to the specified length and store it at the assembly point (Kováč et. al 2017). Today there is a large number of competing harvester heads on the market. The main differences are mainly in the maximum diameter of the treated wood, which depends on the robustness of the head, the number of knives, the type of feed and the assortment of wood.

On the harvester heads are these working mechanisms:

- Spinning mechanism,
- Delimiting mechanism,
- Feeding mechanism,
- Measuring mechanism,
- Loading and unloading mechanism.

Delimiting mechanism serves to delimiting the tree trunk. In wood processing and transportation machines, the knife is the most common (Kováč et al. 2017). They are essentially hyperbolic shaped knives, mounted in the head or on a telescopic boom. Most harvester heads have one solid and two movable knives. Between these knives, the branched trunk stretches and its branches are cut off. Delimiting knives should be able to best replicate the shape of the stem (Hatton et al., 2015).

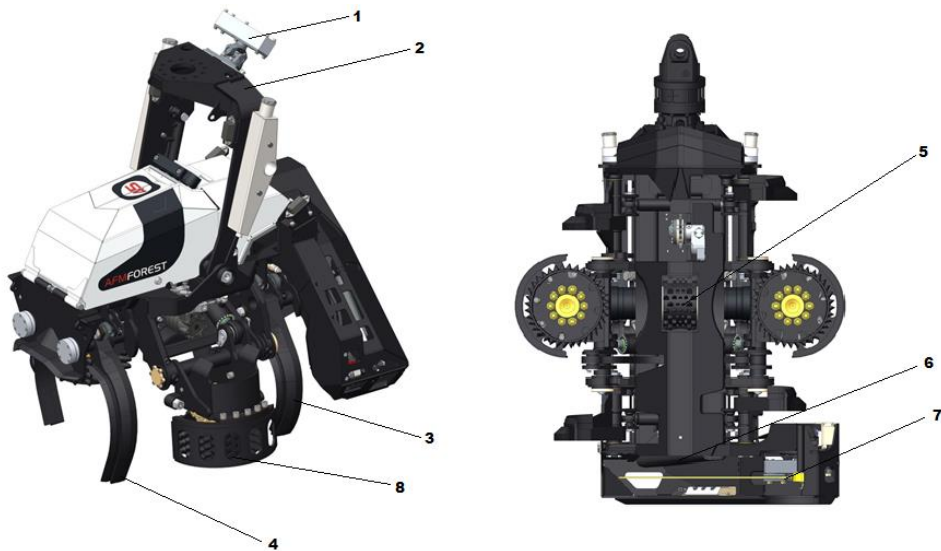


Fig. 1 Delimiting head AFM FOREST 45

Obr.1 Odvetvovacia hlavica ASM FOREST 45

1. Rotator, 2. Fixed head frame, 3. Lower movable knife, 4. Upper movable knife,
 5. Length measuring wheel, 6. Fixed blades, 7. Cutting unit (chain), 8. Feed roller rotators
- (<http://www.afm-forest.com>)

Harvesting – transport equipment must be in the woods to work in very difficult conditions, terrain and climate. There are high demands on reliability, operational capability, productivity, durability and economic efficiency. In operation LH working today Harvesting – Transport Machines various complex and developmental shift from simple machines to machine complex, using a greater range of automation components of computer technology. Harvesting – transport machines can be classified according to different points of view, where one of the main criteria is the number of transactions, whichever are (Mikleš et.al 2004):

a.) single-operation machines – perform one main operation

b.) multi-operation machines – perform at least two major operations

Multi-operation machines include work machines that are equipped with a multi-operation head. Modern multi-operation machines are now harvesters. (Kováč 2004).

In terms of implementation of at least 2 major operations of these machines is their distribution as follows:

Splitting by way of delimiting branch from tree:

- a.) By twisting or blending branches (especially in bulk separators),
- b.) Milling – currently unused
- c.) Cutting off using blades or link chains.

Splitting according to log drive type:

- a.) Spin out a special forest wheeled tractor equipped with a grab or other gripping device (eg winch, rope)
- b.) Linear motion derived from the feeder jaws or the feeder carriage
- c.) Drive link chain – when one chain is used, the chain pressure on the chain is ensured by the pressure of its own blades, which are complemented by a pair of pressing surfaces pressed by linear hydraulic motors.
- d.) Drive rollers – the most used method, drive rollers are part of the head
- e.) Combination of the drive rollers and the drive chain – wherein the drive chain is fixed and the driving tire rollers are movable.

Splitting by operations performed :

- a.) Delimiting machines – perform the separation of branches from the trunk, grip the tree and place the trunk on the landfill
- b.) Processors – are multi-operative machines that process a slashed tree (industry, debarking) and for short distances they transport (carry, approach, load, fold).
- c.) Harvesters – are multi-operative machines that shade the tree and partially (branch, dehumidify) it, or also transport it at a shorter distance (approach, load, fold) (Kováč J., 2004, Dvořák, J., 2008).

The task of the harvester head (Fig.1) is to spin a tree, branch, cut a tree to a specified length and store it in a dump. There are a number of structural variants of the heads (Table 1). The heads are different in particular by the thickness of the treated wood, the shape and number of the blades, the type of the feeding device, the method of measuring the lengths and thicknesses, the arrangement of the cutting part. A typical harvester head (Fig. 1) consists of a chain or knife undercut mechanism. Nowadays, however, the chain is used because it is lighter and does not tear off wood fibers on the cutting surface, it does not cause cracks and pulping in the cutting area. The saw is driven hydraulically. It has a more robust chain and higher performance than any other human-serviceable chain. Furthermore, there are two or more bent venting blades that remove branches around the perimeter of the tree. Since their curvature, the quality of the branching, as well as the two rotating feeders (rollers) that work with the trunk, depends on the trunk in a horizontal position. The feeders may be either belt or wheel type with different types of steel tips. Wheel pins on the sides allow the tree to be clamped with a harvester head. The wheels rotate to force the cut tree through the delimiting knives.

MATERIAL AND METHODS

Currently on the market offered by a large number of harvester heads with different technical parameters due to various kinds of base machines which are applied to the head. Therefore, the basic warhead parameters such as; the weight of the head without the rotor, the maximum stroke force, the maximum cutting capacity and the maximum strain relief. From these parameters, a regression analysis will be performed to examine the linear dependence between the two quantitative variables, making it a specific case of multiple regression. The essence of regression analysis is to find a functional relationship, estimate the parameters of regression function using the least squares method.

$$y_i = \beta_0 + \beta_{1x_i} + \epsilon_i \quad (1)$$

where:

y_i – value of dependent variable Y (criterion) in i-th observation,

x_i – the value of the independent variable X (predictor) in the i-th observation,

β_0 – regresná konštanta (priesečník regresnej priamky s osou x),

β_1 – regression coefficient (regression line directive),

ϵ_i – random error of i-th observation.

The regression coefficient is interpreted according to the type of research. In the case of the experiment (in which the variable X is manipulated), it expresses how much the expected value of the variable Y increases if the value of the variable X increases by 1 unit. In the case of an observation study, the coefficient is interpreted as the expected difference of the values of the variable Y of two observations, whose value of variable X differs by one unit. Assuming that the data represent a random sample from the population, the calculated regression coefficients and the correlation coefficient are the best point estimates of the unknown parameters. In addition, hypotheses can be tested (the null hypothesis that a coefficient is equal to zero that there is no relationship between the variables in the base set) and construct their interval estimates. Hypothesis tests and interval estimates of regression coefficients assume that ϵ_i errors are independent of each other (which implies that y_i is independent), normally divided by a 0 average and the same variance for all X values. the least squares method estimates unknown parameters β_0 and β_1 so that the sum of the squares of the residues is minimal. The residue ϵ_i is the difference between the actual value of the dependent variable y_i and the value calculated from the regression function by substituting the value x_i (Schmidtová et.al 2013):

$$e_i = y_i - x_i \quad (2)$$

where:

y_i – value of dependent variable Y (criterion) in i-th observation,

x_i – the value of the independent variable X (predictor) in the i-th observation,

To create regression analysis it was necessary to create a database file, which is located 37 types of harvester heads used in our country and in the world (Table 1).

Table 1. Database set of harvester heads (source: www.merimex.cz, www.forsttechnik.at, www.forestmeri.cz www.ponsse.com, www.nisulaforest.com, www.kesla.fi)

Tabuľka 1 Databáza harvesterových hlavíc (zdroje: www.merimex.cz, www.forsttechnik.at, www.forestmeri.cz www.ponsse.com, www.nisulaforest.com, www.kesla.fi)

Number	Manufacturer/Harvester head	Weight without rotator (kg)	Max.stroke force (MPa)	Max.cutiing capacity (mm)	Max. relief Ø (mm)
1	Waratah H270 series	1350	28	650	740
2	Waratah H290 series	1970	28	750	800
3	Waratah H215E series	1690	28	550	580
4	Nisula 425C	425	21	425	435
5	Nisula 500 C	650	23	500	500
6	Nisula 555C	840	24	550	500
7	Nisula 325 H	285	19	340	240
8	Nisula 425 H	425	21	425	430
9	Nisula 500 H	640	22	500	500
10	Nisula 555 H	840	24	550	500
11	Kesla 16 RH	430	23	450	420
12	Kesla 18 RH	450	21	450	400
13	Kesla 20 RH	570	24	450	450
14	Kesla 25 RH	790	24	670	580
15	Kesla 28 RH	1280	27	670	700
16	Kesla 30 RH	1400	27	750	700
17	Kesla 20 SH	520	17	450	-
18	Kesla 25 SH	880	19	670	-
19	Ponsse H 10	2600	31	950	900
20	Ponsse H8HD	1450	28	700	740
21	Ponsse H8	1250	28	740	780
22	Ponsse H7HD	1200	28	640	750
23	Ponsse H7	1150	28	640	750
24	Ponsse H7 EUCA	1200	28	630	620
25	Ponsse H77 EUCA	1300	28	600	600
26	Ponsse H6	1050	28	640	650
27	Ponsse H5	900	28	550	600
28	Woody Harvester 50	1090	30	550	500
29	Woody Harvester 60	1350	33	650	600
30	Woody Harvester H61	1220	25	750	650
31	Woody Harvester 70	1720	30	750	700
32	John Deere H412	735	28	470	530
33	John Deere H754	890	28	620	560
34	John Deere H413	940	28	580	560
35	John Deere H414	1100	28	620	640
36	John Deere H480C	1350	28	710	680
37	John Deere H415	1330	28	750	680

RESULTS AND DISCUSSION

Using regression analysis, we statistically evaluated and created 3D histogram graphs where we set the maximum stroke force dependency from the maximum cutting capacity in the first case.

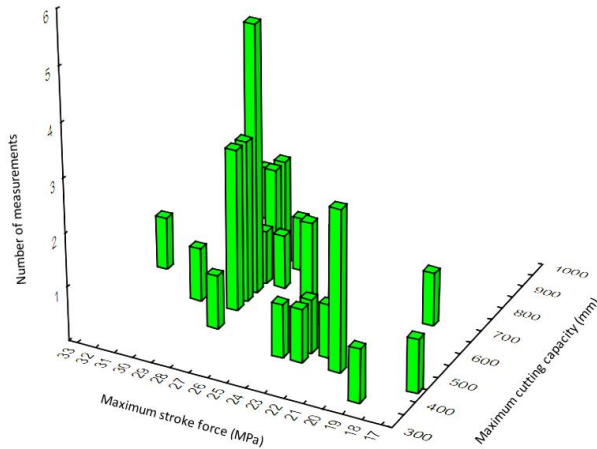


Fig. 2 Histogram of max. lifting force and max. cutting capacity
Obr. 2 Histogram maximálnej zdvíhacej sily a maximálnej reznej capacity

The picture two can clearly see that the manufacturers have mainly focused on the production of the two groups, and especially with a maximum lifting power of 20-28 bar, with a maximum cutting capacity of harvester heads 350-800 mm.

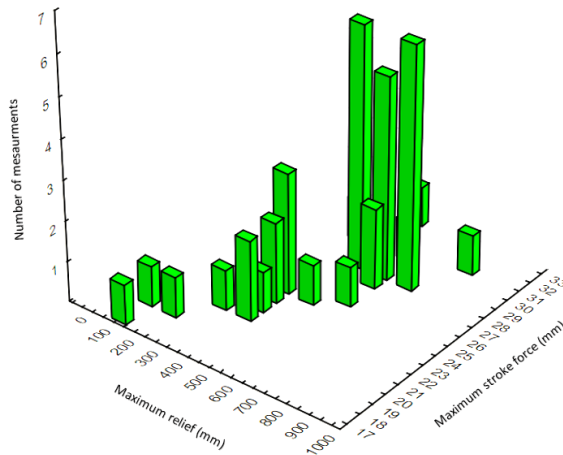


Fig. 3 Histogram of Max Stroke Strength and Max. delimiting branch (mm)
Obr. 3 Histogram maximálnej priemer odvetvovania a maximálnej sily zdvihu

From the picture 3 can see that manufacturers provide optimal maximum lifting force is necessary even with relief wood. Thus, the maximum diameter of the wood relief where it is most common is from 350 to 750 mm at a stroke force of from 20 to 28 MPa.

CONCLUSION

Currently on the market a large amount of equipment offered to facilitate the work in forestry. The effectiveness of individual devices depends on their operating parameters, which each customer should know. Therefore, the goal of this post was to make it easier for customers to select harvester heads from the most famous manufacturers with a description of the basic parameters. There are 37 types of harvester heads in the paper. From the above parameters, the dependencies were created by means of regression analysis, which form groups of the most offered head types, where the maximum stroke force is from 20 to 28 MPa and cutting capacity, that is, the maximum diameter of the fired tree is from 350 to 800mm and the maximum strain diameter is from 350 to 700 mm.

ACKNOWLEDGMENT

The authors are grateful for the support of the Scientific Grant Agency of the Ministry of Education, Science, Research, and Sport of the Slovak Republic, project VEGA no. 1/0609/2020 "Research of the cutting tools in the dendromass processing in agricultural and forestry production"

REFERENCES

- DVOŘÁK, J. 2008. Performance of the Small Tracked Harvesters in Spruce Stands. *Nauka za gorata – Forest Science*, 2008, roč. 44, č. 3, s. 77 – 85. ISSN: 0861-007X.
- HARVÁNEK, P., KOVÁČ, J. 2018. Analýza technických parametrov vertikálnych štiepačiek dreva v lesníctve. In *Kolokvium ku grantovej úlohe č. 1/0826/15: vedecký recenzovaný zborník*. 2018. s. 16--24. ISBN 978-80-228-3128-4. VEGA 1/0642/18.
- HATTON, B., POT, G., BOUZGARROU, B. CH., GAGNOL, V., GOGU, G., 2015. Experimental determination of delimiting forces and deformations in hardwood harvesting, *Croatian journal of forest engineering*. ISSN 1845-5719, 2015,
- KOVAC, J., KRILEK, J., JOBBAGY, J., DVOŘÁK, J. 2017. *Technika a mechanizácia v lesníctve*. 1. vyd. Zvolen: Technická Univerzita vo Zvolene, 2017. 354s. ISBN 978-80-228-3021-8.
- KOVÁČ, J. 2006. Environmental analysis of working aspects in the harvester technologies. – VEGA 1/3534/06. In the *Colloquium on Grant Assignment No. 1/3534/06: Proceedings*. – Zvolen: Technical University in Zvolene, 2006. ISBN 80-228-1692-2. – S. 28-36.
- KOVÁČ, J., KRILEK, J., JOBBÁGY, J., KRIŠTOF, K. 2016. Výskum prevádzkovej spoľahlivosti harvesterových hlavíc, *Technická univerzita vo Zvolene*, 2016. – ISBN 978-80-228-2920-5.
- MIKLEŠ, M., 2009. Studying the geometry of the cutting head knives. *Acta Facultatis Technicae, XIV*, 2009 (2): p. 121 – 129, ISSN 1136 – 4472
- SCHMIDTOVÁ, J., VACEK, V. 2013. *Applied statistics*. Technical University in Zvolene, 2013. 139 p. ISBN 978-80-228-2496-5
- MIKLES, M. HOLIK, J. MIKLES. J. 2004. *Lesné stroje*. 1. vyd. Zvolen: Technická Univerzita vo Zvolene, 2004, 331 p. ISBN 80-228-1403-2.
- WIESIK, J. et.al. 2015. *Urządzenia techniczne w produkcji lesnej*, Wydawnictwo SGGW Warszawa 2015, 591 p., ISBN 978 – 83 – 7583 – 574 – 8

- KOREN. J. 1983. Beztrieskové rezanie dreva. Vedecké a pedagogické aktuality. 1. vyd. Zvolen: Technická Univerzita vo Zvolene, 1983. 105 p. č.6/1983.
- KOVÁČ, J., KRILEK, J., JOBBÁGY, J., AND DVOŘÁK, J. 2017. Technika a mechanizácia v lešnictve [Technique and mechanization in forestry] Technical University in Zvolen, Zvolen, Slovakia. ISBN 978-80-228-3021-8
- FIREMNÁ STRÁNKA Deere a.s, [online], [cit. 20. 02. 2019]. Dostupné na internete:<<http://www.deere.com/>>.
- FIREMNÁ STRÁNKA Waratah a.s, [online], [cit. 21. 02. 2019]. Dostupné na internete:<<http://www.waratah.com/>>.
- FIREMNÁ STRÁNKA Ponsse a.s, [online], [cit. 21. 02. 2019]. Dostupné na internete:<http://ponsse.com/>>.
- FIREMNÁ STRÁNKA Kesla a.s, [online], [cit. 22. 02. 2019]. Dostupné na internete: <<http://kesla.fi/>>.

Corresponding author:

Ing. Melicherčík Ján

tel. č. : +421 908 342 059

e-mail: janmelichercik88@gmail.com

INVESTIGATION ON HEAT TRANSFER AND TEMPERATURE PROFILE OF COUNTERCURRENT AND PARALLEL FLOW ARRANGEMENT IN A PLATE HEAT EXCHANGER

VÝŠETROVANIE PRENOSU TEPLA A TEPLOTNÉHO PROFILU V PROTIPRÚDOVOM A PARALELNOM DOSKOVOM VÝMENNÍKU TEPLA

Mohammad Emal Qazizada¹, Elena Pivarčiová²

1Department of chemical engineering Bagh-e-Bala, Faculty of chemical Technology, Kabul Polytechnic University, Fifth District, Kabul Afghanistan, qazizada198@gmail.com

2Department of Manufacturing and Automation Technology, Faculty of Technology, Technical University in Zvolen, Masarykova 24, 960 01 Zvolen, Slovakia, pivarciova@tuzvo.sk

ABSTRACT: Heat transfer in a plate heat exchanger is important issue in many engineering processes.

The objective of this paper is to determine the heat transfer and the behaviour of temperature across the heat exchanger, comparing the heat exchanger effectiveness with number of transfer units NTU method, the NTU effectiveness method application is calculated with output temperatures in a plate heat exchanger. Firstly, focuses to calculate the heat transfer in counter current and parallel flow, to measure the temperature profile and to determine the (NTU) effectiveness of a plate heat exchanger. The calculated data from the obtained result of the heat flow from the hot fluid $q_h = 1247.8$ [W], from the cold fluid $q_c = 1116.06$ [W], the countercurrent and parallel hot streams configuration of the overall heat transfer coefficient $U_h = 890.68$ [$W m^{-2} K^{-1}$], $U_h = 706.58$ [$W m^{-2} K^{-1}$] are calculated, Furthermore NTU for hot fluid are calculated $NTU_h = 1.09$, $NTU_h = 0.83$ respectively, the capacity coefficient of hot fluid for both countercurrent $CR = 0.64$, and for parallel $CR = 0.62$, and the effectiveness ϵ -NTU of PHE ϵ -NTU = 0.54 are calculated. This plate heat exchanger allows to investigate the heat transfer between hot water flowing through an internal sheets and cold water flowing in the ring area lying between the internal and external sheets, the plate heat exchanger allows measuring hot and cold water temperatures in different points of the heat exchanger and comparing the counter current and parallel flow arrangements,. An addition to calculate the overall heat transfer coefficient using criteria equations, also focused to draw the temperature profile of the heat exchanger for both configurations counter current and parallel flow with temperature on the horizontal axis.

Key words: heat transfer, temperature profile, energy balance, NTU

ABSTRAKT: Prenos tepla v doskovom výmenníku tepla je dôležitou otázkou v mnohých inžinierskych procesoch.

Cieľom článku je určiť prenos tepla a správanie sa teploty v tepelnom výmenníku, porovnaním účinnosti výmenníka tepla s rôznymi prenosovými jednotkami NTU metódou, NTU účinnosť sa počíta

s výstupnými teplotami v doskovom výmenníku tepla. Najskôr sa zameriava na výpočet prenosu tepla v protiprúdovom a paralelnom výmenníku, na meranie teplotného profilu a na stanovenie NTU účinnosti doskového výmenníka tepla. Vypočítané údaje zo získaného výsledku tepelného toku z horúcej kvapaliny $q_h = 1247,8$ [W], zo studenej tekutiny $q_c = 1116,06$ [W], sú vypočítané konfigurácie protiprúdového a paralelného toku horúcich prúdov celkového koeficientu prenosu tepla $U_h = 890,68$ [$W m^{-2} K^{-1}$], $U_c = 706,58$ [$W m^{-2} K^{-1}$]. Ďalej je vypočítané NTU pre horúcu tekutinu $NTU_h = 1,09$, $NTU_c = 0,83$, kapacitný koeficient horúcej tekutiny pre protiprúd $CR = 0,64$ a pre paralelný $CR = 0,62$ a vypočíta sa účinnosť ϵ -NTU PHE ϵ -NTU = 0,54. Tento doskový výmenník tepla umožňuje skúmať prenos tepla medzi horúcou vodou tečúcou cez vnútorné pláty a studenou vodou tečúcou v prstencovej oblasti ležiacej medzi vnútornými a vonkajšími doskami, doskový výmenník tepla umožňuje merať teplotu teplej a studenej vody v rôznych bodoch výmenníka tepla a porovnávať usporiadanie protiprúdového a paralelného prúdenia. Okrem výpočtu celkového koeficientu prenosu tepla pomocou kritériálnych rovníc sa tiež venuje zobrazeniu teplotného profilu výmenníka tepla pre obidve konfigurácie protiprúdového aj paralelného toku s teplotou na horizontálnej osi.

Kľúčové slová: prenos tepla, teplotný profil, energetická bilancia, NTU

INTRODUCTION

Heat exchangers are commonly used in energy conversion and transport processes in which heat transfers from hot fluid to cold fluid.

Nowadays, the use of compact heat exchangers, for example, the plate heat exchangers, has been increasing owing to their advantages of compactness and high heat transfer efficiency (Zhang *et al.* 2018). The behavior of the fluid inside the internal circulation system of a plate heat exchanger is complex due to the influence of many factors. The flow distribution has a significant influence on the performance of fluidic apparatus such as PHE. In this paper, a multi-objective is carried out such as heat transfer in countercurrent and parallel flow, overall heat transfer coefficient and minimization of the total pressure drop of PHE, NTU effectiveness of PHE, The PHE running under a steady state, with negligible heat loss, achieving the temperature profile for both countercurrent and parallel flow configurations. A plate heat exchanger consists of a set of corrugated metal plates confined in a shell. Each metal plate has 4 ports or holes. The plates and the ports are sealed by joints at their edge to allow hot and cold fluids flowing through narrow alternate passages formed between the plates. Heat transfers through the thin plates offering relatively low thermal resistance (Haydary 2013). Plate heat exchangers are typically categorized in three types: shell and plate, frame and plate, and brazed plate heat exchanger. The plate heat exchanger is the forerunner in heat exchanger technology; compact and manufactured to a high standard of quality and offers a durable solution that can stand high pressures and temperatures. Frame-and plate heat exchanger is commonly used for their ease of cleaning, simple adjustment of heat transfer area, compactness and excellent thermal-hydraulic performance (Holger, 2010). The brazed plate heat exchanger, such plates could withstand higher pressure and later on found its increasing application as condenser and evaporator in air-conditioning and refrigeration systems (Jin 2017). Plate heat exchangers are known to be highly efficient with negligible heat loss, achieving the temperature profile for both countercurrent and parallel flow configurations (Solotych 2015). Subsequent researchers have used numerical simulations to investigate plate heat exchangers:

Dvořák and Vít used CFD to illustrate effects of plate pitch, material thickness and material thermal conductivity on flow and heat transfer in a heat exchanger, when non-zero material thickness was considered (Dvořák and Vít 2015). Giurgiu et al. in work used CFD to study the influence of geometric characteristics of the two plates on the intensification process of heat transfer (Giurgiu *et al.*, 2016), (Dvořák and Vít 2017). Jackson and Troupe and Kandlikar used numerical method to analyze the e-NTU relationship in various numbers of plates (Jackson 1966), (Kandlikar 1984), (Jin 2017). Zhen-Xing Li and Li-Zhi Zhang investigated the flow unfavorable distribution and the consequent performance deteriorations in a cross flow and in a counter flow hollow fiber membrane module, they found that the packing fraction affects the flow unfavorable distribution substantially (Li *et al.*, 2014). Najafi and Najafi performed a multi-objective optimization of PHE with pressure drop and heat transfer coefficient of a heat exchanger as objective functions (Najafi 2010), (Bansi 2018). The temperature profiles were determined from the experimentally calculated data of temperature scopes, and local parameters of heat transfer were calculated (Černecký *et al.* 2017). This experimental study is thus intended to investigate the effect of the countercurrent and parallel flow conditions on the heat transfer of the Plate heat exchanger.

METHODOLOGY AND DEVICE DESCRIPTION

This Extended Plate Heat Exchanger allows the study of heat transfer between hot and cold water through alternate channels formed between parallel plates. The PEH consists of a set of stainless-steel plates arranged in parallel. The space between the plates forms a channel through which water flows. Hot and cold-water channels alternate along the plate heat exchanger so that heat is transmitted by the thin plates. The PHE has 10 thermocouples: 5 (ST-1 to ST-5) for measuring hot water temperature (inlet, outlet and interim positions) and 5 (ST-6 to ST-10) for measuring cold water temperature (inlet, outlet and interim positions). These exchangers usually feature baffles to increase the heat transfer as shown in Figure 1.

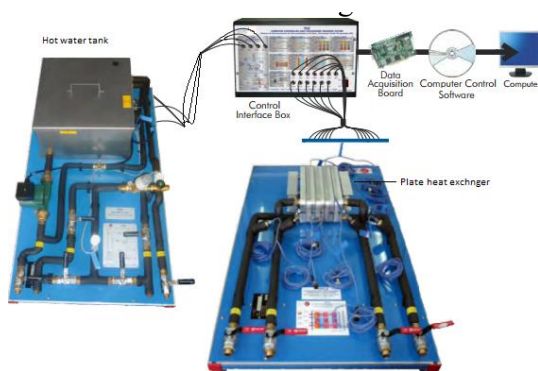


Fig. 1 Unit of plate heat exchanger [TICC, 2014]
 Obr. 1 Jednotka doskového výměníka tepla [TICC, 2014]

Water exits the exchanger and flows to the drainage system. Cold water can enter the exchanger at either end. Depending on the configuration of the valves (AV-2, AV-3, AV-4 and AV-5), parallel or countercurrent flow can be set. This set-up can be experiential in the following scheme of the base unit. The schematics of the experimental apparatus is shown in Figure. 2.

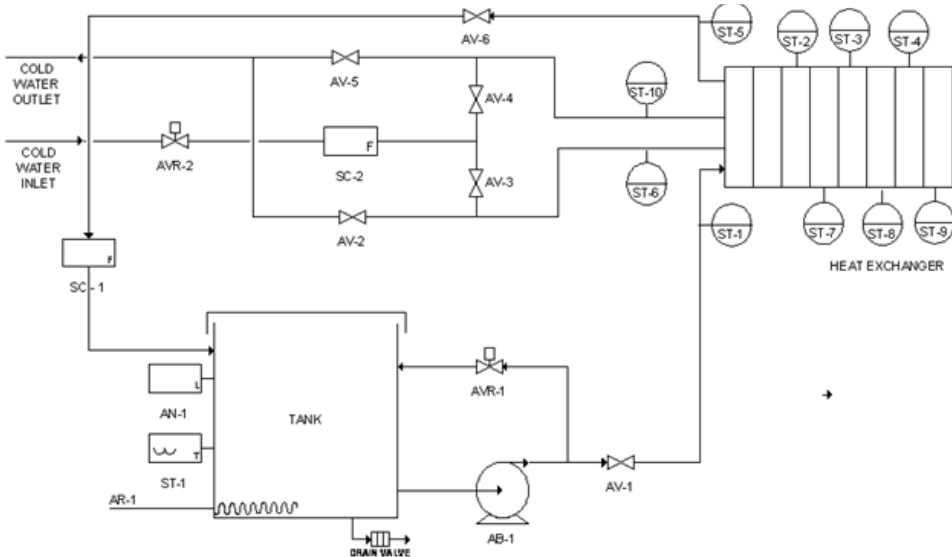


Fig. 2. Scheme of experimental apparatus (TICC, 2014)
 Obr. 2. Schéma experimentálnej aparatúry (TICC, 2014)

This model is feasible only for small flows and it is rarely used. Or the model of global flow in a PHE may be connected flow which flow divides into sub flows that mix before leaving the exchanger. It is used for great volumes of liquid.

- The marking in the scheme of this experiment research apparatus are listed as follows:
- ST-16 Temperature sensor of the water in the tank
 - ST-1 Hot water temperature sensor at the inlet of the exchanger
 - ST-2 Hot water temperature sensor at the intermediate point of the exchanger
 - ST-3 Hot water temperature sensor at the intermediate point of the exchanger
 - ST-4 Hot water temperature sensor at the intermediate point of the exchanger
 - ST-5 Hot water temperature sensor at the outlet of the exchanger
 - ST-6 Cold water temperature sensor at the inlet/outlet of the exchanger
 - ST-7 Cold water temperature sensor at the intermediate point of the exchanger
 - ST-8 Cold water temperature sensor at the intermediate point of the exchanger
 - ST-9 Cold water temperature sensor at the intermediate point of the exchanger
 - ST-10 Cold water temperature sensor at the inlet/outlet of the exchanger
 - SC-1 Hot water flow sensor
 - SC-2 Cold water flow sensor
 - AVR-1 Hot water flow regulation valve

AVR-2 Cold water flow regulation valve
 AN-1 Water tank level switch
 AR-1 Electric resistance
 AB-1 Hot water flow centrifugal pump
 AV-2, AV-3, AV-4, AV-5 Cold water circuit ball valves to set the parallel / counter-current flow
 AV-1, AV-6 Ball valves for pipe draining

ENERGY BALANCE IN A PLATE HEAT EXCHANGER

For energy balance of a PHE, if there are no changes of phases in the heat exchanger, the heat flow from the hot fluid can be calculated by the equation:

$$q_h = m_h c_{ph} (t_{h,in} - t_{h,out}) \quad (1)$$

The heat flow to the cold fluid is:

$$q_c = m_c c_{pc} (t_{c,out} - t_{c,in}) \quad (2)$$

where m_h and m_c are the mass flows ($kg\ s^{-1}$), and c_{ph} and c_{pc} ($J\ kg^{-1}K^{-1}$) are the specific heat capacities of the hot and cold fluids.

Theoretically, q_h should equal q_c , but due to environmental energy losses and also due to instrumental and observational measurement errors, they are not always equal. To represent the global phenomenon of heat transfer between fluids in a plate exchanger, thermal resistances occurring in each medium can be referred to. Heat flow on its way from the hot to the cold fluid has to overcome the resistances of the hot fluid limit layer, the separation wall and the cold fluid limit layer. These three resistances arranged in series constitute the total resistance, R_t :

$$Q = \frac{(t_h - t_c)}{R_t} = \frac{1}{\frac{1}{\alpha_1 A_h} + \frac{\delta}{kA} + \frac{1}{\alpha_2 A_c}} \quad (3)$$

where δ is the thickness of the separation wall. Heat transfer surface area in a plate heat exchanger is $A = a N = L W N$ where N is the number of thermal plates, a is the plate surface area, L is the plate length (m) and W the plate width in (m).

In the differential form, the transferred heat, dq , is proportional to the isothermal surface area perpendicular to the heat transfer direction, dA , the temperature difference in the heat transfer direction, $(t_h - t_c)$ and a proportionality factor, U , called the overall local heat transfer coefficient (Haydary, 2013).

$$dq = U(t_h - t_c)dA \quad (4)$$

When constant values of the overall heat transfer coefficient and of the heat capacities of liquids in the equipment are assumed, integral form of the heat transfer rate equation is:

$$q = UA\Delta t_{lm} \quad (5)$$

where Δt_{lm} is the logarithm mean of the driving force considering its value at the beginning of the heat exchanger, Δt_1 , and at the end of heat exchanger, Δt_2 :

$$(\Delta t)_{lm} = \frac{\Delta t_1 - \Delta t_2}{\ln \frac{\Delta t_1}{\Delta t_2}} \quad (6)$$

While $\Delta t_1 = t_{h,in} - t_{c,in}$ and $\Delta t_2 = t_{h,out} - t_{c,out}$ for parallel flow and $\Delta t_1 = t_{h,in} - t_{c,out}$ and $\Delta t_2 = t_{h,out} - t_{c,in}$ for countercurrent flow. The ε_{NTU} effectiveness method analysis of a plate heat exchanger is defined as the coefficient between the actual heat exchanged and the maximum that can be transferred in an infinite area exchanger in countercurrent flow:

$$\varepsilon_{NTU} = \frac{Q_{real}}{Q_{max}} \quad (7)$$

where $Q_{max} = m_h c_{ph} (t_{h,in} - t_{c,in})$ if $m_h c_{ph} < m_c c_{pc}$ and $Q_{max} = m_c c_{pc} (t_{h,in} - t_{c,in})$ if $m_c c_{pc} < m_h c_{ph}$

Therefore, effectiveness equals to:

$$\varepsilon_{NTU} = \frac{(t_{h,in} - t_{h,out})}{(t_{h,in} - t_{c,in})} \text{ if } m_h c_{ph} < m_c c_{pc} \quad (8)$$

Or to parallel flow connection:

$$\varepsilon_{NTU} = \frac{(t_{c,out} - t_{c,in})}{(t_{h,in} - t_{c,in})} \text{ if } m_c c_{pc} < m_h c_{ph} \quad (9)$$

The number of transfer units (NTU) is a dimensionless parameter defined as:

$$NTU = \frac{UA}{(mc_p)_{min}} \quad (10)$$

Also, the capacity coefficient (C_R) can be defined as:

$$C_R = \frac{(mc_p)_{min}}{(mc_p)_{max}} \quad (11)$$

PROCEDURE OF EXPERIMENT

To evaluate the energy balance, heat losses study and overall heat transfer coefficient the following procedures completed: using the software, the tank temperature is sited to a value between 40–60 [°C], the resistor and the hot water circuit pump are turn on. The hot water flow fixed at about 3 [l min⁻¹]. Via the valves of AV-2, AV-3, AV-4 and AV-5, and choosing of the counter current flow, the cold-water flow set 1.8 [l min⁻¹]. The air should be removed from the shell side of the heat exchanger using. The unit of Q [l min⁻¹] in Table 1 is mention base on the experimental data that obtained, the unit of Q [m³ s⁻¹] in

Table 2 and Table 3 were calculated according to equations which are applied. Whenever the system reaching to stationary operating conditions, we write down the temperatures indicated by all sensors and the flow of hot and cold water, the procedure will repeat until five measurements as shown in Table 1.

Table 1 Recording of measured data during experiment
Tabuľka 1 Namerané údaje počas experimentu

Connections	Countercurrent Flow					Parallel Flow				
Numbers	1	2	3	4	5	1	2	3	4	5
Q_h [l min ⁻¹]	2.8	2.4	2	1.5	1.1	2.9	2.5	2	1.6	1.2
Q_c [l min ⁻¹]	1.8	1.8	1.8	1.8	1.8	1.8	1.8	1.8	1.8	1.8
ST16 [°C]	45	40	40	40	40	40	40	40	40	40
ST 1 [°C]	36.3	36.4	36.3	36.2	36.1	36.3	37.1	37.2	37.3	37.3
ST2 [°C]	35.1	35	34.6	34.2	33.1	31.2	31.4	31	30.6	29.5
ST3 [°C]	34.5	34.2	33.4	32.5	33.8	31.1	31.3	30.9	30.4	29.3
ST4 [°C]	32.2	31.7	30.5	29	27.1	30.6	30.8	30.4	29.7	28.8
ST5 [°C]	29.9	28.1	27	25.2	23.5	30.2	30.5	30.2	29.7	28.9
ST6 [°C]	35.5	35.6	35.3	34.9	34.2	21	20.1	20.2	20.3	20.5
ST7 [°C]	34.2	34	33.2	32.2	30.5	29	29.1	28.7	28	27.1
ST8 [°C]	32.7	32.2	31.1	29.7	27.7	30.2	30.4	30	29.2	28.2
ST9 [°C]	28.7	28	26.9	25.6	24	30.3	30.6	30.2	29.5	28.7
ST10 [°C]	19.8	19.6	19.5	19.3	19.3	30	30.5	30.1	29.5	27.5

RESULTS

In a countercurrent flow the outlet temperature of the cold fluid can exceed then the outlet temperature of the hot fluid but this cannot happen in a parallel flow system as shown Figure 4 and Figure 6. In fact, the hot and cold-water temperatures change continuously along the length of the heat exchanger too, as shown Figure 4 and Figure 6. Measuring hot and cold-water temperatures in countercurrent and parallel flow at different points in five steps along the length of heat exchanger are shown in Table 1. The calculated results for a total energy balance, the overall heat transfer coefficient heat transfer in countercurrent and parallel flow, overall heat transfer coefficient, (NTU) effectiveness of PHE, the effective of average temperature difference between the two heat transfer fluids over the length of the heat exchanger and though derived for countercurrent and parallel flow, are presented in Table 2 and Table 3. The calculation of mentioned objectives are as follows: from the work documentation, we write all necessary information on the dimensions of the heat exchanger in top part of Table 2, and Table 3, such as the average temperature, density, dynamic viscosity, specific heat capacity and thermal conductivity of hot and cold water. For each column of countercurrent flow from Table 1, calculated the heat flow from the hot fluid $q_h = 1247.8$ [W], from the cold fluid $q_c = 1116.06$ [W] and for parallel connection configuration the heat flow from the hot and cold fluid $q_h = 1231.81$

[W], $q_c = 815.1$ [W] using Equation (1) and Equation (2), individually. The estimation of the heat losses for both countercurrent and parallel connection streams are calculated in Table 2 and Table 3 individually. As well for countercurrent and parallel connection streams calculated the hot logarithmic mean of the driving force $\Delta t_{lm,h} = 5.83$ [°C], $\Delta t_{lm,h} = 7.26$ [°C] using Equation (6) one-by-one. The value of the heat transfer surface area, $A = 0.32$ [m²], is available in the laboratory work documentation. To countercurrent and parallel hot streams configuration calculated the theoretical values of the overall heat transfer coefficient $U_h = 890.68$ [W m⁻² K⁻¹], $U_h = 706.58$ [W m⁻² K⁻¹], using criteria equations equation (5). Furthermore the number of transfer units NTU for hot fluid in countercurrent and parallel flow are calculated $NTU_h = 1.09$, $NTU_h = 0,83$ respectively, the number of transfer units for cold fluid $NTU_c = 1.01$, $NTU_c = 0,72$ available in Table 2 and Table 3 using Equation (10). The capacity coefficient of hot fluid for both countercurrent $C_R = 0.64$, and for parallel $C_R = 0.62$ calculated using Equation (11). The effectiveness ε_{NTU} of PHE in an infinite area exchanger in countercurrent flow $\varepsilon_{NTU} = 0.54$ and in parallel $\varepsilon_{NTU} = 0.42$ accessible in Table 2 and Table 3 using Equations (8, 9). For countercurrent flow the calculation processing experiment data are shown in Table 2.

Table 2 Measured data processing for counter current connection configuration
Tabuľka 2 Namerané údaje pre konfiguráciu protiprúdového pripojenia

$t_{av,h} = 41.15$ [°C] $t_{av,c} = 23.95$ [°C] $A = 0.32$ [m ²]					
$Cp_h = 4179$ [Jkg ⁻¹ K ⁻¹]		$Cp_c = 4180$ [Jkg ⁻¹ K ⁻¹]		$\rho_h = 992$ [kg m ⁻³]	
$\mu_h = 0.652 \cdot 10^{-3}$ [Pa s]		$\mu_c = 0.932 \cdot 10^{-3}$ [Pa.s]		$k_h = 0.631$ [Wm ⁻¹ K ⁻¹]	
$\rho_c = 997.2$ [kg m ⁻³]		$kc = 0.616$ [Wm ⁻¹ K ⁻¹]			
Number	1	2	3	4	5
Q_h [m ³ s ⁻¹]	4.67E-05	4.0E-05	3.3E-05	0.25E-05	1.8E-05
Q_c [m ³ s ⁻¹]	3.0E-05	3.0E-05	3.0E-05	3.0E-05	3.0E-05
m_h [kg ³ s ⁻¹]	0.046	0.04	0.033	0.025	0.018
m_c [kg ³ s ⁻¹]	0.03	0.03	0.03	0.03	0.03
q_h [W]	1247.829	1069.568	891.306	668.48	490.218
q_c [W]	1116.06	1116.06	1116.06	1116.06	1116.06
[°C]	5.83	5.83	5.83	5.83	5.83
[°C]	8.79	8.79	8.79	8.79	8.79
Uh [W m ⁻² K ⁻¹]	890.6	763.4	636.2	477.15	349.9
Uc [W m ⁻² K ⁻¹]	528.9	528.98	528.98	528.98	528.988
$mh Cp_h$ [J K ⁻¹]	194.9	167.12	139.26	104.45	76.59
$mc Cp_c$ [J K ⁻¹]	125.4	125.4	125.4	125.4	125.4
NTU_h	1.096	1.096	1.096	1.096	1.096
NTU_c	1.01	1.01	1.01	1.012	1.012
C_R	0.64	0.75	0.90	1.20	1.63
ε_{NTU}	0.53	0.53	0.54	0.54	0.54

The scope of temperature is defined as a distribution of temperatures in individual points of the heat exchanger in a certain time (Pivarciova 2011). By plotting the graphs of temperature according to the length or flow in/of devices with different flows configuration (countercurrent or parallel), it is possible to give a basic idea of heat transfer between hot and cold streams. The Figure 3 represents the temperature change in cross length of PHE.

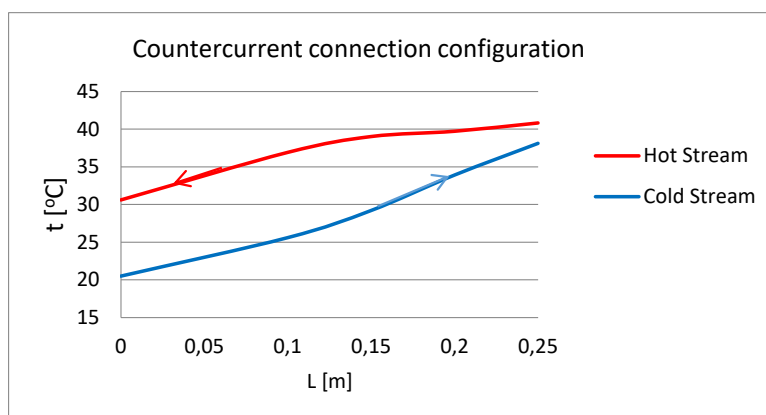


Fig. 3. Countercurrent flow connection in a PHE
Obr. 3. Pripojenie protiprúdu v PHE

To demonstrate the temperature change as function of flow a plate heat exchanger, which have done during experimental research in the laboratory of Kabul polytechnic University, the Figure 4, shows the countercurrent flow connection in PHE that the heat transfer processing is sufficient if there are a huge different between hot and cold flow of water in a PHE.

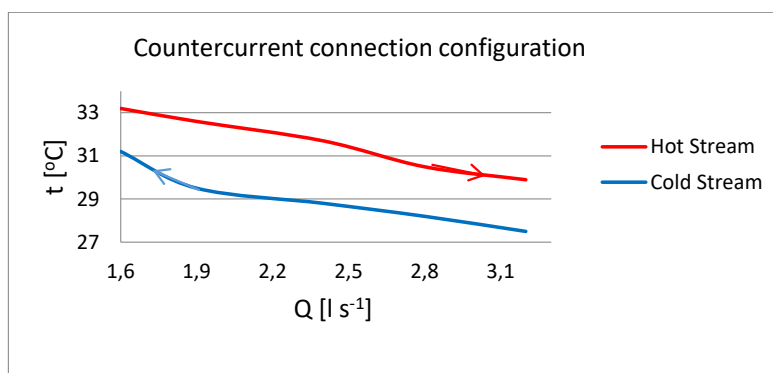


Fig. 4. Changing of temperature in a countercurrent flow of hot and cold streams
Obr. 4. Zmena teploty v protiprúde horúceho a studeného prúdu

As well for parallel flow by calculation of the average temperature of hot and cold water in the system we find the density, dynamic viscosity, specific heat capacity and thermal conductivity of water in properties table of water. For parallel flow the measured data processing according to measured data during experiment in Table 1, the calculation result are shown in Table 3.

Table 3 Measured data processing for parallel connection configuration
Tabuľka 3 Spracované údaje pre konfiguráciu paralelného pripojenia

$t_{av,h} = 41.15 [^{\circ}\text{C}]$ $t_{av,c} = 23.95 [^{\circ}\text{C}]$ $A = 0.32 [\text{m}^2]$					
$Cp_h = 4179 [\text{Jkg}^{-1}\text{K}^{-1}]$		$Cp_c = 4180 [\text{Jkg}^{-1}\text{K}^{-1}]$		$\rho_h = 992 [\text{kg m}^{-3}]$ $\rho_c = 997.2 [\text{kg m}^{-3}]$	
$\mu_h = 0.652 \cdot 10^{-3} [\text{Pa s}]$		$\mu_c = 0.932 \cdot 10^{-3} [\text{Pa s}]$		$k_h = 0.631 [\text{Wm}^{-1}\text{K}^{-1}]$ $kc = 0.616 [\text{Wm}^{-1}\text{K}^{-1}]$	
Number	1	2	3	4	5
Q_h [$\text{m}^3 \text{s}^{-1}$]	4.8E-05	4.17E-05	3.3E-05	2.67E-05	2.0E-05
Q_c [$\text{m}^3 \text{s}^{-1}$]	3.0E-05	3.0E-05	3.0E-05	3.0E-05	3.0E-05
m_h [$\text{kg}^3 \text{s}^{-1}$]	0.048	0.041	0.033	0.026	0.02
m_c [$\text{kg}^3 \text{s}^{-1}$]	0.03	0.03	0.03	0.03	0.03
q_h [W]	1231.81	1061.91	849.52	679.62	509.71
q_c [W]	815.1	815.1	815.1	815.1	815.1
[$^{\circ}\text{C}$]	7.26	7.263	7.263	7.263	7.264
[$^{\circ}\text{C}$]	8.998	8.998	8.998	8.998	8.998
Uh [$\text{W m}^{-2} \text{K}^{-1}$]	706.58	609.12	487.29	389.83	292.37
Uc [$\text{W m}^{-2} \text{K}^{-1}$]	377.4	377.42	377.42	377.42	377.42
$mh Cp_h$ [J K^{-1}]	201.93	174.08	139.26	111.41	83.56
$mc Cp_c$ [J K^{-1}]	125.4	125.4	125.4	125.4	125.4
NTU_h	0.83	0.83	0.83	0.83	0.839
NTU_c	0.72	0.72	0.722	0.722	0.722
C_R	0.62	0.72	0.90	1.12	1.50
ϵ_{NTU}	0.42	0.424	0.42	0.424	0.42

According to the separation process, the flow rate should be variable in one side and fixed in the other side (to keep constant thermal resistance) in a single test (Qian *et al.*, 2017). The Figure 5, represents the temperature change for parallel flows connection system in a PHE, which shows a huge difference between the cold and hot flow streams.

Anyway, the difference between the amount of hot and cold flow streams in a parallel flow connection system in a PHE shows the change of temperature in various amount of hot and cold flow which is indicated in Figure 6.

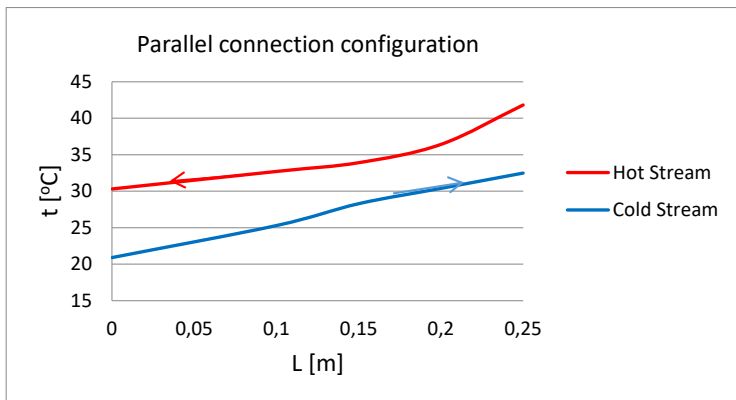


Fig. 5 Temperature changing in a parallel flow connection in a PHE
 Obr. 5 Zmena teploty v paralelnom prietokovom pripojení v PHE

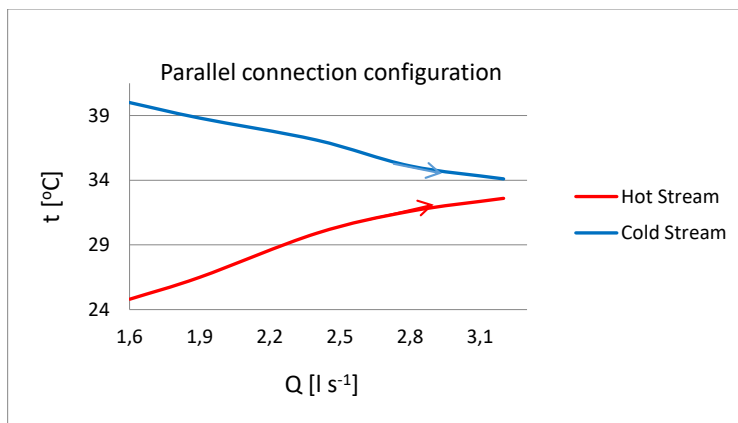


Fig. 6 Temperature change of hot and cold streams in a parallel flow connection
 Obr. 6 Zmena teploty horúceho a studeného prúdu pri paralelnom pripojení prietoku

DISCUSSION

The mentioned graphs and tables which are summarized above indicated the main conclusions from this study. Current work includes inspecting the real system in order to the effects of countercurrent and parallel flow on the heat exchanger plates for a better thermo-hydraulic performance. Results shows in a countercurrent flow the outlet temperature of the cold water can exceed then the outlet temperature of the hot fluid but this temperature increasing cannot happen in a parallel flow configuration. A heat exchanger according to the present invention is characterized by the special geometry and the particular way of assembling of pressed plates, which together make a compact, rigid heat exchanger, having only primary heat exchanging surfaces and in which counter-current operation is achieved

by means of special fluid collectors. In a heat exchanger comprising a number of plates arranged adjacent to each other and defining between them passageways for heat exchanging fluids, the plates are provided at their corner portions with openings, the fluids being transported to and from the passages via said openings.

CONCLUSION

The examined plate heat exchanger type is designed supervisory control and data acquisition software. The validate and correct results of different researches, and the performance of PHE in industrial processes has always a major goal for engineers and designers. As well the PHE allows to study global energy balance, the study of losses, the flow influence in the heat transfer, Study of the heat transfer in crosscurrent and parallel flow conditions and determination of the NTU effectiveness. The aim of the present study is to investigate application of heat transfer between hot and cold water to evaluate the influence of the flow in the heat transfer The PHE allows the heat transfer study between hot water that circulates through an internal area and cold water that flows through the annular zone between the internal and the external area. This exchanger permits to measure cold water and hot water temperatures in different points of the exchanger. This research has compared against experimental data in terms of accuracy and simulation time. The comparison of the results of this research is evaluated with the investigation other author (Nawaf H. Saeid *et al.* 2006), which they investigated thermal performance of both and counter-current and parallel flow heat exchangers. They used the effectiveness – number of transfer units method that regarded as powerful tool and easy to implement in both design and performance calculations of the heat exchangers. Their results are presented in terms of effectiveness and number of transfer units for different values of the parameters. The parameters are the NUT, the heat capacity ratios, the overall heat transfer coefficient ratio, and the inlet temperatures parameter. The experiment which we have done were classical with two-fluid flow heat exchanger but their have been done with three-fluid flow heat exchangers. Therefore the results show that the effectiveness of the three-fluid heat exchanger is always higher than that of classical two-fluid flow heat exchanger for fixed values of the parameters. The comparison of both experiment results provide confidence to the accuracy of the present numerical method to study the performance of two fluid flow and three-fluid flow heat exchangers. The rule of parameters in this case are the heat transfer coefficient parameters between the hot fluid and the cold fluids, the heat capacity ratio parameters, the inlet temperature ratio parameter in addition to the NTU.

ACKNOWLEDGMENT

Contribution has been prepared within the solving of scientific grant project of the Ministry of Education, Science, Research and Sports of the Slovak Republic within VEGA 1/0086/18: "Researching Temperature Fields in a Set of Shaped Heat Transfer Surfaces".

As well this work was done as a result of the project SAMRS/2013/ of the Slovak official development assistance supporting the cooperation between the Slovak University of Technology in Bratislava (STU) and the Kabul Polytechnic University (KPU) in Afghanistan.

REFERENCES

- BANSI, D. R., JHALA, R.L., PATEL, V. 2018. Thermal-hydraulic optimization of plate heat exchanger: A multi-objective approach. In *International Journal of Thermal Sciences*, vol. 124, pp 522–535.
- ČERNECKÝ, J., BRODNIANSKÁ, Z., BLAŠIAK, P. KONIAR, J. 2017. The research of temperature fields in the proximity of a bundle of heated pipes arranged above each other. In *Journal of heat transfer: transactions of the ASME*, vol. 139, no. 8.
- DVOŘÁK V., VÍT T. 2015. Numerical Investigation of Counter Flow Plate Heat Exchanger Original Research Article. In *Energy Procedia*, vol. 83, pp 341–349.
- DVOŘÁK, V., VÍT, T. 2017. CAE methods for plate heat exchanger design. In *Energy Procedia*, vol. 134, pp 234–243.
- GIURGIU O, PLEȘA A, SOCACIU L. 2016. Plate Heat Exchangers – Flow Analysis through Mini Channels. In *Energy Procedia*, vol. 85, pp 244–251.
- HAYDARY, J. 2013. *Chemical Engineering I*, Laboratory manual, Ministry of higher education of Afghanistan, Kabul.
- HOLGER, M. 2010. *Pressure Drop and Heat Transfer in Plate Heat Exchangers*, VDI Heat Atlas, Springer Science & Business Media.
- JACKSON, B.W., TROUPE, R.A. 1966. Plate exchanger design by e-NTU method, *Chem. Eng. Prog. Symp.*, vol. 64, no. 62, pp 185–190.
- JIN, S., HRNJAK, P. 2017. Effect of end plates on heat transfer of plate heat exchanger. *International Journal of Heat and Mass Transfer*, vol. 108, pp 740–748.
- KANDLIKAR, S. 1984. Performance Curve for Different Plate Heat Exchanger Configuration, *ASME Paper No. 84-HT-26*
- LI, Z.X. ZHANG, L.Z. 2014. Flow maldistribution and performance deteriorations in a counter flow hollow fiber membrane module for air humidification/ dehumidification. In *Internat. J. Heat Mass Transf.*, vol. 74, pp 421–430
- NAJAFI, H., NAJAFI, B. 2010. Multi-objective optimization of a plate and frame heat exchanger via genetic algorithm. In *Heat Mass Transf.*, vol. 46, pp 639–647
- NAWAF H. SAEID., SEETHARAMU, K.N. 2006. Finite element analysis for co-current and counter-current parallel flow three-fluid heat exchanger. Malaysia and Bangalore, India. *International Journal of Numerical Methods for Heat & Fluid Flow* Vol. 16 No. 3. pp. 324-337
- PIVARCIOVA, E. CERNECKY, J. 2011. Wood texture influence on temperature fields. *Annals of DAAAM for 2011 & Proceedings of the 22th International DAAAM symposium „Intelligent manufacturing & automation: Power of knowledge and creativity“*. Vienna (Austria), pp 1069–1070. ISBN 978–3–901509–83–4. ISSN 1726–9679.
- QIAN, J. LING KONG, Q. WU ZHANG, H. HONG ZHU, Z. HUANG, W.G HUI LI, W. 2017. Experimental study for shell-and-tube molten salt heat exchangers. In *Applied Thermal Engineering*, vol. 124, pp 616–623.
- SOLOTYCH, V. KIM, J. DESSIATOUN, S. V. 2015. Local heat transfer measurements within a representative plate heat exchanger geometry using infrared (IR) thermography. Maryland. *Journal of Enhanced Heat Transfer* TICC, 2014. *Practical exercises manual*, Edibon Spain
- ZHANG, Y., JIANG, C., SHOU, B., ZHOU, W., ZHANG, Z., WANG, S., BAI, B. 2018. A quantitative energy efficiency evaluation and grading of plate heat exchangers. In *Energy*, vol. 142, pp 228–233

Corresponding author:

Elena Pivarčiová, pivarciova@tuzvo.sk